



30  
31  
32  
33  
34  
35  
36  
37  
38  
39  
40  
41  
42  
43  
44  
45  
46  
47  
48  
49  
50  
51

**Abstract**  
**Genomic signatures of speciation in sympatric flying squirrels**  
**Laurelie Menelon**

Hybridization contributes to the genetic diversity and can impact speciation. This study investigates the genetic evidence of recent hybridization under climate change in sympatric populations of northern and southern flying squirrels in Ontario. Using low-coverage whole-genome sequences, my research examines the existing population structure and measures the genomic variation of the *Glaucomys* species. The global estimates of  $F_{ST}$  (0.308) and  $D_{XY}$  (0.141) are indicative of substantial differentiation between the species. Measures of genetic diversity ( $\pi$ ), differentiation ( $F_{ST}$ ), and divergence ( $D_{XY}$ ) across the genome reveal insights into the divergent selection driving speciation. Results indicate an absence of contemporary hybridization or introgression at a site with longstanding sympatry. Across both species' genomes, signatures of selection align with four different scenarios for the formation of genomic landscapes of differentiation, shedding light on the complex speciation history of these flying squirrels. These findings enhance understanding of evolutionary dynamics, adaptation, speciation, and genetic differentiation.

Keywords: Genomic differentiation, speciation, *Glaucomys volans*, *Glaucomys sabrinus*, northern flying squirrel, southern flying squirrel

## Acknowledgements

52

53 I would first like to thank my supervisors Dr. Paul Wilson and Dr. Jeff Bowman  
54 for their guidance and mentorship throughout this research. I would have not been able to  
55 complete this thesis without your support. Pursuing research in the fields of genomics and  
56 bioinformatics was a challenge, marked by a steep learning curve. I am sincerely grateful  
57 for your compassion and uplifting encouragement, especially as I hit delays in the  
58 analysis and slogged through completing the writing. You both provided me the space to  
59 overcome my own setbacks which has significantly contributed to my growth as a  
60 researcher, fostering self-reliance and resourcefulness.

61 This project would not have been possible without the guidance and feedback  
62 from my advisory committee member, Dr. Aaron Shafer. I am appreciative of your  
63 reviewing of my thesis, and providing assistance and resources whenever I sought your  
64 help by dropping into your office. The initial lab work of DNA extractions for my  
65 research would not have been possible without the training and assistance from Austin in  
66 the Wilson lab. I am grateful for your patience and kindness when teaching me the  
67 procedures and how to work with the lab equipment.

68 To the entire Bowman Lab team - thank you for being so amazing. I heard  
69 repeatedly before starting my master's that graduate research, on top of challenging, was  
70 a lonely endeavor. That was never the case here. From my first day of arriving in  
71 Peterborough, you all made me feel welcome and fast became a group of close friends to  
72 me. I would have not made it through the program without you all. You have all been an  
73 incredible support network and I hold so many fun memories with you all - from learning  
74 to rock climb, group gatherings, karaoke, winter getaways, and camping trips. I want to

75 extend a special thank you to Kirsten, as the only other genomics student in the Bowman  
76 lab, you were my lifeline in navigating bioinformatics and completing my thesis.

77 I'd also like to extend my gratitude to my roommates, friends, and family for their  
78 unwavering support, helping me maintain a semblance of sanity throughout this journey.  
79 Thank you for listening to me in my moments of complete frustration and exhaustion,  
80 even when you didn't understand what I was talking about. I would especially like to  
81 thank my parents, Sylvie and Bernard, for always supporting me in my academic  
82 pursuits, and believing in me when I didn't believe in myself.

83

84

85

86

87

88

89

90

91

92

93

94

95

96

97

98

99

TABLE OF CONTENTS

100  
101  
102 **ABSTRACT**..... II  
103 **ACKNOWLEDGEMENTS**..... III  
104 **LIST OF FIGURES** ..... VI  
105 **LIST OF TABLES**..... X  
106 CHAPTER 1: GENERAL INTRODUCTION..... 1  
107 CHAPTER 2: GENOMIC SIGNATURES OF SPECIATION IN SYMPATRIC FLYING  
108 SQUIRRELS..... 9  
109 **ABSTRACT**..... 9  
110 **INTRODUCTION**..... 10  
111 **METHODS** ..... 14  
112 **RESULTS**..... 23  
113 **DISCUSSION** ..... 40  
114 GENERAL DISCUSSION..... 49  
115 **REFERENCES**..... 54  
116 APPENDIX..... 70  
117  
118  
119  
120  
121  
122  
123  
124  
125  
126  
127  
128  
129

## List of Figures

- 130  
131 **Figure 1.** Map of sample locations and ranges for *Glaucomys* species in Ontario as  
132 delineated by IUCN (Cassola, 2016a; Cassola, 2016b).
- 133 **Figure 2.** Admixture proportions of the 114 genome sequences for  $K = 2$  of the 114  
134 genome sequences calculated with NGSAdmix.
- 135 **Figure 3.** Principal Component Analysis (PCA) of all unrelated individuals of *G.*  
136 *sabrinus* and *G. volans* (N=68).
- 137 **Figure 4.** Principal Component Analysis (PCA) of all unrelated individuals of *G.*  
138 *sabrinus* (N=23).
- 139 **Figure 5.** Principal Component Analysis (PCA) of all unrelated individuals of *G. volans*  
140 (N=45).
- 141 **Figure 6.** Ternary plot of  $K_0$ ,  $K_1$ , and  $K_2$  values from ngsRelate for *G. sabrinus* and *G.*  
142 *volans* pairwise relationships. Colored polygons represent the potential degree of relation  
143 based on the used inference criteria (see Table S2).
- 144 **Figure 7.** Phylogenetic trees constructed without (A) and with (B) bootstrap replicates,  
145 using Angsd assembled mitogenomes and IQTree (best-fit substitution model  
146 TN+F+I+R). Color assignments represent species clustering, with green representing *G.*  
147 *volans* and blue representing *G. sabrinus*. Red values in (B) indicate the confidence  
148 intervals of nodes, derived from 10 bootstrap replicates.
- 149 **Figure 8.** Inferred demographic history of *G. sabrinus* and *G. volans* using the unfolded  
150 SFS in Stairway Plot 2 assuming a mutation rate ( $\mu$ ) of  $2.0 \times 10^{-9}$  per site per year.

151 **Figure 9.** Treemix migration model with the best support ( $k=500$ ,  $m=2$ ). Both (A) and  
152 (B) yielded equal log likelihoods of 88.4539. Sympatric *G. volans* and *G. sabrinus*  
153 populations included the Kawartha Highlands and Sherborne Lake or Ganaraska  
154 respectively. The allopatric populations for *G. volans* and *G. sabrinus* in Ontario include  
155 samples from Long Point and Clear Creek, and Temagami and Roosevelt, respectively.

156 **Figure 10.** Genomic scans patterns of selection using a 50kb window and 10kb step size  
157 for nucleotide differentiation ( $F_{ST}$ ) and divergence ( $D_{XY}$ ) between northern (*G. sabrinus*)  
158 and southern (*G. volans*) flying squirrels, along with nucleotide diversity ( $\pi$ ) in *G.*  
159 *sabrinus* and *G. volans*. The red dashed line represents the 95% quartile for the fixation  
160 index ( $F_{ST}$ ).

161 **Figure 11.** Genome wide correlation for  $F_{ST}$ - $D_{XY}$  (green),  $\pi$ - $F_{ST}$  (pink), and  $\pi$ - $D_{XY}$   
162 (blue), between *G. sabrinus* and *G. volans*.

163 **Figure 12.** Correlation coefficients over divergence time for  $\pi$ - $D_{XY}$  (blue),  $F_{ST}$ - $D_{XY}$   
164 (green), and  $\pi$ - $F_{ST}$  (pink), trend lines represent a linear model. The divergence time was  
165 estimated for each pairwise population comparison using  $D_{XY}$  – mean  $\pi$  as a proxy and is  
166 represented by six comparisons of our four sampled populations.

167 **Figure S1.** Additional Principal Component Analysis (PCA) axes 2vs3 of all unrelated  
168 individuals of *G. sabrinus* and *G. volans* (N=68).

169 **Figure S2.** Additional Principal Component Analysis (PCA) axes 2vs3 of all unrelated  
170 individuals of *G. sabrinus* (N=23).

171 **Figure S3.** Additional Principal Component Analysis (PCA) axes 2vs3 of all unrelated  
172 individuals of *G. volans* (N=45).

173 **Figure S4.** Phylogenetic tree of mitogenomes assembled using GetOrganelle. Red values  
174 indicate the confidence interval of a node from 1000 iterations in IQtree, representing the  
175 uncertainty associated with the estimated branching point. Green coloring corresponds to  
176 species clustering of *G. volans*; uncolored branches in the phylogenetic tree center are *G.*  
177 *sabrinus*.

178 **Figure S5.** The 1D-SFS for *G. sabrinus* (top; N=48) and *G. volans* (bottom; N=60). The  
179 x-axis represents the derived allele frequency, while the y-axis indicates the counts of  
180 SNPs.

181 **Figure S6.** Comparison of Treemix migration models. We performed 10 iterations at k-  
182 values of 500, 1000, and 2000 for each migration model (m=0-5). The likelihood and SD  
183 values (A) and comparison of  $\Delta m$  values (B) indicate the model with 2 migrations has the  
184 best support.

185 **Figure S7.** Plotted residual fit for the maximum likelihood trees of the Treemix migration  
186 model (m=2, k=500). Positive (black) residuals indicate an underestimation of the  
187 observed covariance between population pairs and that the populations are more closely  
188 related to each other than in the best-fit tree and can be candidates for admixture events.  
189 Negative (red) residuals indicate an overestimation.

190 **Figure S8.** Genomic scan patterns of selection using a 100kb window and 50kb step size  
191 for nucleotide differentiation ( $F_{ST}$ ) and divergence ( $D_{XY}$ ) between northern flying  
192 squirrels (*G. sabrinus*) and southern flying squirrels (*G. volans*), along with nucleotide  
193 diversity ( $\pi$ ) in *G. sabrinus* and *G. volans*. The red dashed line represents the 95%  
194 quartile for the fixation index ( $F_{ST}$ ).



195 **Figure S9.** Genomic scan patterns of selection using a 10kb window and 1kb step size  
196 for nucleotide differentiation ( $F_{ST}$ ) and divergence ( $D_{XY}$ ) between northern flying  
197 squirrels (*G. sabrinus*) and southern flying squirrels (*G. volans*), along with nucleotide  
198 diversity ( $\pi$ ) in *G. sabrinus* and *G. volans*. The red dashed line represents the 95%  
199 quartile for the fixation index ( $F_{ST}$ ).

200 **Figure S10.** Genomic scans display patterns of selection using a 50kb window and 10kb  
201 step size for nucleotide differentiation ( $F_{ST}$ ) and divergence ( $D_{XY}$ ) between northern  
202 flying squirrels (*G. sabrinus*) and southern flying squirrels (*G. volans*), along with  
203 nucleotide diversity ( $\pi$ ) in *G. sabrinus* and *G. volans*. The red dashed line represents the  
204 99% quartile for the fixation index ( $F_{ST}$ ).

205

206

207

208

209

210

211

212

## List of tables

- 213
- 214 **Table 1.** Four different evolutionary models and their underlying selection with the
- 215 applied percentile thresholds for  $F_{ST}$ ,  $D_{XY}$ , and  $\pi$ .
- 216 **Table 2.** ABBA-BABA results using a 100kb block size and an ancestral file the
- 217 generated consensus fasta of *S.carolinesis* and *I.tridecemlineatus* sequences. Bold values
- 218 indicate an excess of ABBA-patterns between *Glaucomys* species. Sympatric *G. volans*
- 219 and *G. sabrinus* populations included the Kawartha Highlands and Sherborne Lake or
- 220 Ganaraska respectively. The allopatric populations for *G. volans* and *G. sabrinus* in
- 221 Ontario include samples from Long Point and Clear Creek, and Temagami and Roosevelt,
- 222 respectively.
- 223 **Table S1.** Newly generated sequences sample ID, sex, species identification in the field,
- 224 sample type, site, average mass, and capture date range for individuals captured since
- 225 2017 when sampling effort increased. For site information: CC = Clear Creek (42.52°N,
- 226 81.62°W), LP = Long Point (42.58°N, 80.38°W), KH = Kawartha Highlands (44.68°N,
- 227 78.33°W), GAN= Ganaraska (44.09°N, 78.5°W), TEM= Temagami (47.23°N, 79.77°W),
- 228 ROSV=Roosevelt Road (47.26°N, 79.71°W). When an individual was captured only as a
- 229 juvenile it is indicated with sex by “Juv”. Missing mass data is indicated by “NA”.
- 230 **Table S2.** The standard IBD relationships and inference criteria used to infer pairwise
- 231 relationships.
- 232 **Table S3.** Summary of quality control results. The percentage of reads mapped and
- 233 average coverage for each sample ID with sample type indicated. Samples marked in
- 234 bold were excluded from the analysis due to poor read mapping quality. \*The sample
- 235 appeared to be mostly blood and had gone through a freeze-thaw. Sites: APP = Algonquin

236 Provincial Park, CC = Clear Creak, GAN = Ganaraska, KH = Kawartha Highlands, LP =  
237 Long Point, ROSV = Rosevelt, SHLK = Sherborne Lake, TEM = Temagami.

238 **Table S4.** Inferred potential relationships in *G. volans* and *G. sabrinus*. Bolded values  
239 indicate the coefficients used to infer the degree of relatedness.

240

241

242

243

244

245

246

247

248

249

250

251

252

253

254

255

256

257

258

259

260

261

262 CHAPTER 1: GENERAL INTRODUCTION

263 **Species**

264 In North America, three distinct lineages of flying squirrel (*Glaucomys* spp.) have been  
265 identified, each occupying unique forest types and geographic ranges. These lineages  
266 include the northern flying squirrel (*G. sabrinus*), Humboldt's flying squirrel (*G.*  
267 *oregonensis*), and the southern flying squirrel (*G. volans*) (Arbogast, 1999). The range  
268 and habitats occupied by these lineages provide important insights into their ecological  
269 preferences and the historical biogeography of North American forests. The northern  
270 flying squirrel (*G. sabrinus*) is closely associated with boreal coniferous forests and is  
271 distributed across Alaska and Canada, with disjunct populations extending into the United  
272 States (Arbogast, 1999; Arbogast et al., 2017). In contrast, *G. oregonensis* primarily  
273 inhabits temperate rainforests and is exclusively found in the western region of North  
274 America, including the states of California, Oregon, and Washington, and extending north  
275 into British Columbia, Canada (Arbogast et al., 2017). The third lineage, *G. volans* is  
276 primarily associated with deciduous hardwood forests and is also present in mixed wood  
277 forests across the midwestern to eastern United States, with its range extending northward  
278 into southeastern Canada (Arbogast, 1999, 2007; Arbogast et al., 2005).

279 Both the northern and the southern flying squirrel lineages exhibit multiple  
280 disjunct populations in the southern reaches of their distributions. For southern flying  
281 squirrels, this includes Mesoamerican populations extending from Mexico to Honduras  
282 (Kerhoulas & Arbogast, 2010), while for northern flying squirrels, disjunct populations  
283 are found in the Appalachian Mountains, western and central states, including Utah,  
284 Montana, Wyoming, North Dakota, and South Dakota. For *G. sabrinus* disjunct

285 populations, several have been listed as endangered subspecies (ex. *G. s. californicus*, *G.*  
286 *s. fuscus*, and *G. s. coloratus*) at the state or federal level (Arbogast et al., 2005).

287         The presence of disjunct populations in both northern and southern flying  
288 squirrels suggests that these species have experienced geographic isolation and  
289 subsequent divergence. This divergence may have been driven by various factors,  
290 including habitat fragmentation, geographic barriers, and ecological differences  
291 (Arbogast et al., 2005). Interestingly, phylogenetic analyses and estimates of divergence  
292 times show that *G. volans* and the *G. sabrinus* lineages are sister taxa that have diverged  
293 from each other more recently (~1.07 Mya) than either has from the *G. oregonensis*  
294 lineage (~1.32 Mya) (Arbogast, 1999; Arbogast et al., 2017). The *G. sabrinus* and *G.*  
295 *oregonensis* lineages' geographic ranges are primarily exclusive of one another with no  
296 evidence of gene flow between them (Arbogast et al., 2017). While recent genetic  
297 evidence suggests hybridization under climate change-mediated secondary contact  
298 between the *G. sabrinus* and *G. volans* lineages (Bowman et al., 2005; Garroway et al.,  
299 2010).

### 300 **Hybridization and Speciation**

301 Hybridization can play a crucial role in speciation with different potential outcomes by  
302 driving genetic adaptation, extinction events, or the emergence of new species. It  
303 introduces genetic variation, potentially leading to selection and adaptation to distinct  
304 ecological niches (Feder et al., 2012). The outcomes of hybridization are influenced by  
305 the divergence time and degree of differentiation between species (Barton & Hewitt,  
306 1985; Servedio & Noor, 2003). Persistent hybrid zones can under opposing selective

307 forces (Barton & Hewitt, 1985) or can occur when populations are adapted to distinct  
308 habitats (Nosil et al., 2009).

309         While most hybridization events result in less fit hybrids (Barton & Hewitt,  
310 1985), some may survive and reproduce, facilitating the exchange of genetic variants  
311 through rare backcrossing with parental species (i.e., introgression; Arnold, 1992; Barton,  
312 2001). Introgression may enable the exchange of neutral or advantageous alleles between  
313 species that remain distinct despite limited gene flow. In the latter case of advantageous  
314 allele exchange, this process is referred to as adaptive introgression, and can be an  
315 important mechanism in speciation and adaptation (Abbott et al., 2013; Arnold & Kunte,  
316 2017).

317         The low fitness of hybrids, especially if they have poor survival rates or are  
318 sterile, can reduce the reproductive success of parental species. This can lead to  
319 reinforcement of reproductive barriers through selection that strengthens pre-mating  
320 isolation (Servedio & Noor, 2003). In cases where reproductive isolation fails to evolve  
321 and hybrids are not viable, there is a potential for reduced population size and an  
322 increased risk of extinction for the parental species due to wasted reproductive efforts  
323 (Adavoudi & Pilot, 2022).

324         Novel genetic combinations in hybrids can result in hybrid vigour, where hybrids  
325 exhibit greater fitness than either parental species under particular environmental  
326 conditions. This ecological success, where hybrids are better at exploiting resources and  
327 have increased survival, has the potential to lead to the formation of new ecologically  
328 specialized species (Abbott et al., 2013). This may result in the displacement of parental  
329 species, the formation of a new hybrid species with evolved reproductive isolation from

330 both parental species, or speciation reversal where hybridizing species fuse as  
331 reproductive barriers collapse under gene flow (Abbott et al., 2013; Mallet, 2005).

### 332 **Detecting Hybridization**

333         Hybridization and introgression are important processes in evolution by  
334 facilitating the exchange of genetic material between species (Abbott et al., 2013; Arnold,  
335 1992; Feder et al., 2012). Detecting hybridization and introgression is crucial for  
336 understanding the dynamics of species interactions and their evolutionary consequences  
337 (Adavoudi & Pilot, 2022; Arnold,1992). Two commonly used types of genetic markers  
338 for detecting hybridization and introgression are single nucleotide polymorphisms (SNPs)  
339 and microsatellites (Bradbury et al., 2015; Cairns et al., 2023; Hänfling et al., 2005; Li et  
340 al., 2010a; Miralles et al., 2023; Muñoz et al., 2017; Poelstra et al., 2022; Saint-Pé et al.,  
341 2019; Stroupe et al., 2022; Szatmári et al., 2021). Microsatellites are short, neutral,  
342 repetitive DNA sequences that are highly variable, whereas Single nucleotide  
343 polymorphisms (SNPs) are single base pair variations in the DNA sequence.  
344 Microsatellite and SNP data each have their advantages and limitations for detecting  
345 hybridization and introgression. Microsatellites have high allelic diversity, genotyping is  
346 relatively inexpensive, and it is well-suited for individual-level identification; however, it  
347 has limited genome coverage, higher mutation rates, and is prone to genotyping errors  
348 (Kalia et al., 2011; Pompanon et al., 2005). SNP data offer higher resolution, genome-  
349 wide coverage, and lower mutation rates, but require more resources and technical  
350 expertise (Zohren et al., 2016; Li et al., 2010a; Muñoz et al., 2016).

351         Although microsatellites are present throughout the genome, their distribution can  
352 vary across different regions (Tóth et al., 2000), potentially resulting in a biased or

353 incomplete assessment of introgression patterns (Zohren et al., 2016) and may reduce  
354 their effectiveness in detecting fine-scale genetic structure and introgression (Stroupe et  
355 al., 2022). SNPs are abundant throughout the genome, which can provide a more  
356 comprehensive and accurate measure of hybridization and introgression compared to  
357 microsatellites (Bradbury et al., 2015; Li et al., 2010b; Muñoz et al., 2017; Poelstra et al.,  
358 2022; Szatmári et al., 2021; Zimmerman et al., 2020; Zohren et al., 2016) and allows for  
359 the identification of introgression in different genomic regions (Stroupe et al., 2022).  
360 Additionally, SNPs may result in reduced errors in estimating population structure,  
361 genetic diversity, and genetic differentiation than microsatellites (Coates et al., 2009;  
362 Fischer et al., 2017; Li et al., 2010b; Saint-Pé et al., 2019; Zimmerman et al., 2020).

363         Population genetic parameters and structure show comparable patterns between  
364 microsatellite and SNP data (Zimmerman et al., 2020; Camacho-Sanchez et al., 2020).  
365 However, SNPs offer the advantage of much narrower confidence intervals around  
366 diversity measures, allowing for clearer population-level distinctions (Zimmerman et al.,  
367 2020), due to the power of having of more loci and greater distribution across the genome  
368 (Lemopoulos et al., 2019; Sunde et al., 2020). On the other hand, microsatellites excel in  
369 individual identification, making them valuable for relatedness assessment, parentage  
370 analysis, and genetic mark-recapture (Zimmerman et al., 2020).

### 371 **Measuring Variation**

372 Single nucleotide polymorphisms (SNPs) are becoming widely used to measure genetic  
373 variation. SNPs are variations in a single nucleotide at specific genomic positions, and  
374 they are abundant within populations (Kumar et al., 2012). Their prevalence, genomic  
375 distribution, reproducibility, and stability (Helyar et al., 2011) — attributed to lower



376 mutation rates and a broad representation of variations (neutral and under selection)  
377 across the genome (in coding and non-coding regions) – have made them the marker of  
378 choice to study selection, and investigate the demographic history, population structure,  
379 and genetic differentiation (Zimmerman et al., 2020).

380         The dynamics of allele frequencies and SNP variations are influenced by genetic  
381 drift, selection, and population demography (Chen et al., 2018). Analysis of these  
382 polymorphisms is often facilitated by using the site frequency spectrum (SFS) to  
383 summarize demographic parameters like effective population size, migration, and  
384 divergence times (Liu & Fu, 2020; Nielsen et al., 2012; Pickrell & Pritchard, 2012).  
385 Additionally, SNPs form the foundation for investigating selection and species  
386 divergence by assessing genetic variation between species (Cruickshank & Hahn, 2014;  
387 Han et al., 2017; Irwin et al., 2018; Shang et al., 2023). Three commonly used measures  
388 to quantify genetic differentiation, diversity, and identify selection across the genome are  
389  $F_{ST}$ ,  $D_{XY}$ , and  $\pi$ . The fixation index,  $F_{ST}$ , is a measure of genetic differentiation between  
390 populations (Wright, 1965) and has been extensively used in population genetics to  
391 understand the distribution of genetic variation frequency between populations. The other  
392 two measures,  $D_{XY}$  and  $\pi$ , measure between population variability and within population  
393 variability, respectively (Charlesworth, 1998). Genetic divergence,  $D_{XY}$ , represents the  
394 absolute nucleotide divergence between two populations. It quantifies the average  
395 number of nucleotide differences between populations (Cruickshank & Hahn, 2014; Nei  
396 & Li, 1979). This provides insight into whether populations exhibit greater or lesser  
397 diversity relative to each other (Lim et al., 2021). Lastly, nucleotide diversity,  $\pi$ , is a

398 measure of genetic variation within a population, providing valuable information about  
399 polymorphism levels within a population (Nei & Li, 1979; Tajima, 1989).

400 Genomic scans using  $F_{ST}$ ,  $D_{XY}$ , and  $\pi$  can provide insights into the selective  
401 pressures driving speciation (Cruickshank & Hahn, 2014; Han et al., 2017; Irwin et al.,  
402 2018; Shang et al., 2023). These metrics are influenced by demographic fluctuations  
403 across generations, such as effective population size (Ravinet et al., 2017). Additionally,  
404 these patterns are shaped by genomic characteristics such as recombination and mutation  
405 rates, gene density (Ravinet et al., 2017), and selection pressures (Cruickshank & Hahn,  
406 2014; Holsinger & Weir, 2009; Stephan, 2010). Considering gene flow in conjunction  
407 with these genomic variations allows us to interpret the underlying selection and  
408 speciation mechanisms that lead to the observed genome-wide patterns (Han et al., 2017;  
409 Irwin et al., 2016, 2018; Shang et al., 2023). Analyzing individual SNP values of  $F_{ST}$ ,  
410  $D_{XY}$ , and  $\pi$  alongside genome-wide correlations helps clarify signals from genome scans  
411 (Shang et al., 2023). Local patterns in high and low  $F_{ST}$ ,  $D_{XY}$ , and  $\pi$  values can be  
412 attributed to different speciation scenarios, including divergence with gene flow, selection  
413 in allopatry, recurrent selection/sweep before differentiation, and balancing selection  
414 (Irwin et al., 2018; Shang et al., 2023; Yang et al., 2020). All scenarios, except balancing  
415 selection, are expected to exhibit locally high  $F_{ST}$  and low  $\pi$  values; balancing selection  
416 will display the opposite, with low  $F_{ST}$  and high  $\pi$  values.  $D_{XY}$  measures are expected to  
417 be high for divergence with gene flow and balancing selection, average for allopatric  
418 selection, and low for recurrent selection/sweep before differentiation. Regarding  
419 genome-wide correlations, we expect average  $\pi$  and  $F_{ST}$  to be negatively correlated across  
420 all scenarios;  $F_{ST}$  and  $D_{XY}$  to be negatively correlated for recurrent selection and

421 balancing selection, uncorrelated for allopatric selection, and positively correlated for  
422 divergence with gene flow. For average  $\pi$  of the populations and  $D_{XY}$ , we expect a  
423 positive correlation for balancing selection and recurrent selection, no correlation for  
424 allopatric selection, and a negative correlation for divergence with gene flow (Shang et  
425 al., 2023).

426

427 CHAPTER 2: GENOMIC SIGNATURES OF SPECIATION IN SYMPATRIC  
428 FLYING SQUIRRELS

429 **Abstract**

430 Hybridization can be a critical mechanism in the speciation process by introducing new  
431 genetic variation into populations or promoting reproductive isolation. We examined the  
432 patterns of selection in sympatric populations of northern (*Glaucomys sabrinus*) and  
433 southern (*G. volans*) flying squirrels that have contemporary evidence of secondary  
434 contact and interbreeding. We examined population structure, admixture, and quantified  
435 genome-wide historical introgression. Additionally, we conducted scans to identify  
436 patterns in the genomic landscape, specifically examining the variations in nucleotide  
437 diversity and differentiation across the genome. We focused our investigation of genomic  
438 landscapes to within-species nucleotide diversity ( $\pi$ ) and between-species summary  
439 statistics of diversity, i.e., absolute divergence ( $D_{XY}$ ), and relative differentiation ( $F_{ST}$ ).  
440 These investigations provided insights into the speciation of between *G. sabrinus* and *G.*  
441 *volans*, and the underlying selection processes driving their divergence. Despite recent  
442 genetic evidence of hybridization and introgression, we found no evidence of current  
443 interbreeding at the sympatric site. We found evidence for limited gene flow, with  
444 signatures primarily indicating historical introgression from *G. sabrinus* to *G. volans*. The  
445 elevated  $F_{ST}$  (0.308) and  $D_{XY}$  (0.141) values we estimated indicate a significant degree of  
446 genetic differentiation between *G. sabrinus* and *G. volans*. We observed patterns across  
447 the genome that match each of the four different scenarios for the formation of genomic  
448 landscapes of differentiation investigated. However, the majority of the genome (>99%)  
449 did not display one of these selection patterns, indicating that speciation between these  
450 two lineages is likely due to genetic drift and being in allopatry.

## 451 **Introduction**

452 Hybridization has been identified across taxa at varying rates (Adavoudi & Pilot, 2022;  
453 Mallet, 2005; Taylor & Larson, 2019) and facilitates species divergence under the  
454 ecological speciation model (Cruickshank & Hahn, 2014; Nosil et al., 2009; Schluter,  
455 2009). One genetic mechanism of ecological speciation is divergence with gene flow  
456 (Feder et al., 2012; Feder & Nosil, 2010; Nosil & Feder, 2012; Nosil 2012), where  
457 ecological differences lead to divergent selection between populations, resulting in local  
458 adaptation and a decrease in gene flow between species (Schluter 2000; Rundle & Nosil  
459 2005). This process ultimately initiates population differentiation and can lead to  
460 reproductive isolation (Nosil 2012; Funk et al., 2006; Schluter 2001; Schluter 2009).

461         Divergent selection should first lead to the emergence of genomic islands, often  
462 referred to as “islands of speciation” or “islands of differentiation” (Feder et al., 2012;  
463 Quilodrán et al., 2020; Sendell-Price et al., 2020; Turner et al., 2005). These genomic  
464 regions can contain loci associated with local or global adaptations (Bay & Ruegg, 2017;  
465 Booker et al., 2021; Malinsky et al., 2015; Reifová et al., 2016; Roesti et al., 2014 ;  
466 Tavares et al., 2018) or reproductive barriers (Duranton et al., 2018; Nosil et al., 2009;  
467 Pinho & Hey, 2010; Rundle & Nosil, 2005) and display high levels of genomic  
468 differentiation ( $F_{ST}$ ) (Beaumont, 2005). However, patterns of  $F_{ST}$  are also influenced by  
469 demographic history and effective population size, and by features that vary across the  
470 genome such as recombination, mutation rate, and gene density (Ravinet et al., 2017).  
471 Furthermore, different processes that reduce genetic diversity can also create  $F_{ST}$  peaks  
472 such as genetic drift or background selection (Cruickshank & Hahn, 2014; Holsinger &  
473 Weir, 2009; Stephan, 2010). Including estimates of nucleotide diversity ( $\pi$ ) and absolute

474 divergence ( $D_{XY}$ ) can improve the interpretation of the underlying selection and  
475 speciation mechanisms; and the consideration of gene flow can provide further insight to  
476 the processes driving the formation of genomic islands (Han et al., 2017; Irwin et al.,  
477 2016, 2018; Shang et al., 2023).

478         The divergence with gene flow model involves loci contributing to reproductive  
479 isolation between differentiating populations under isolation-with-migration or secondary  
480 contact (Irwin et al., 2018; Shang et al., 2023; Yang et al., 2020). Under this model,  
481 reduced gene flow around the loci responsible for reproductive isolation results in higher  
482  $F_{ST}$  and  $D_{XY}$ , along with lower  $\pi$ ; while gene flow homogenizes the genome outside of  
483 these regions (Wu 2001) keeping  $F_{ST}$  and  $D_{XY}$  low (Irwin et al., 2016, 2018; Shang et al.,  
484 2023). In contrast, selection in allopatry involves positive or background selection on  
485 distinct genome regions to decrease  $\pi$ ; however, the average  $D_{XY}$  is maintained as it is  
486 sensitive to ancestral polymorphisms (Irwin et al., 2016, 2018; Shang et al., 2023).

487         The remaining patterns with a high  $F_{ST}$  commonly identified across the genome is one  
488 where  $D_{XY}$  and  $\pi$  are low; both the recurrent selection and the sweep before  
489 differentiation models can explain this pattern (Delmore et al., 2015; Irwin et al., 2016,  
490 2018; Shang et al., 2023). It is important to highlight that these two models differ in gene  
491 flow following the initial population split. Under recurrent selection, regions of the  
492 genome have experienced selection (positive or negative) that reduces genetic diversity in  
493 the common ancestor, consequently reducing the standing genetic variation before  
494 population divergence. These regions subsequently undergo diversity-reducing selection  
495 again in the two daughter populations, resulting in lower  $D_{XY}$  and  $\pi$  values, while the  
496 recent selection causes high  $F_{ST}$  to be observed. A critical aspect of recurrent selection is

497 that there is no gene flow between the populations. Conversely, the sweep before  
498 differentiation model accounts for reduced  $D_{XY}$  and  $\pi$  values as the outcome of  
499 advantageous alleles introduced by gene flow (e.g., through hybridization) and the  
500 subsequent rapid spread through selection across the species (Irwin et al., 2016, 2018).

501 In contrast to the other scenarios, balancing selection is characterized by patterns  
502 linked to low  $F_{ST}$ . In this scenario, ancient polymorphisms are preserved at selected sites,  
503 contributing to high  $\pi$  values, and resulting in high  $D_{XY}$  due to incomplete lineage sorting  
504 (Shang et al., 2023). Ultimately, using  $F_{ST}$ ,  $D_{XY}$ , and  $\pi$  measures allows for the  
505 identification of selection patterns against a neutral background across the genome. These  
506 scenarios are not mutually exclusive, and the speciation history between species may be  
507 complex, containing events that align with each of the models (Irwin et al., 2018).

508 Northern and southern flying squirrels are estimated to have diverged  
509 approximately 1 MYA (Wolf et al., 2022) in separate forest refugia (Arbogast, 1999).  
510 Contemporaneous expansion of *G. volans* and *G. sabrinus* lineages is reflected in the  
511 current distribution and ecological preferences of these two *Glaucomys* species. Northern  
512 and southern flying squirrels primarily inhabit parapatric ranges in North America, with  
513 their spatial separation attributed to ecological distinctions in the types of forests they  
514 occupy (Arbogast, 2007). Northern flying squirrels are predominantly associated with  
515 coniferous forests but can be found in adjacent ecotypes of mixed forests and deciduous  
516 stands (Smith, 2007; Weigl, 2007), across Alaska and Canada, with isolated populations  
517 in the southernmost part of their range extending into the United States. In contrast,  
518 southern flying squirrels inhabit deciduous forests in the midwestern to eastern United

519 States, with some populations extending northward into southeastern Canada (Arbogast,  
520 1999, 2007; Arbogast et al., 2005).

521         The two *Glaucomys* species have additional ecological differences in nesting and  
522 diet preferences. Northern flying squirrels exhibit variation in nest use type, roosting in  
523 tree cavities, dreys, and subterranean nests (Smith, 2007; Minns et al., 2024); they also  
524 display infrequent group nesting of only 3-5 individuals in the winter (O'Brien et al.,  
525 2021). In contrast, southern flying squirrels nest most often in deciduous tree cavities and  
526 use dreys less frequently; they also engage in year-round social nesting, forming larger  
527 groups of 5-25 individuals in the winter at the northern edge of their range (O'Brien et  
528 al., 2021; Minns et al., 2024). In concordance with their forest types, southern flying  
529 squirrels predominantly rely on a diet of hard mast, such as acorns (Winterrowd & Weigl,  
530 2006), while northern flying squirrels occasionally use mast but primarily subsist on  
531 fungi, lichens, buds, berries, and cones (Weigl, 2007).

532         Climatic change has contributed to the recent rapid northward expansion of the  
533 southern flying squirrel's range, leading to increased overlap with the northern flying  
534 squirrel. This range expansion has resulted in secondary contact; and genetic evidence of  
535 hybridization and introgression has been established (Garroway et al., 2010). Trapping  
536 efforts by Bowman et al. (2005) revealed southern flying squirrels 200 km north of their  
537 expected northern range limit (Stabb, 1988). This expansion was facilitated by mild  
538 winters from 1995-2004 and mediated by cold winter events and mast crop failures  
539 causing range contraction of 240km in 2004 (Bowman et al., 2005). Despite cold winters  
540 and poor mast crops limiting the southern flying squirrel range expansion, a site where



541 northern and southern flying squirrels exhibit local sympatry has persisted since at least  
542 2002 in central Ontario, Canada (22 years).

543         Here, we investigated populations of northern and southern flying squirrels at a  
544 site with long-term sympatry for ongoing hybridization and patterns of speciation. Given  
545 the history of glacial vicariance, current ecological differences, and recent genetic  
546 evidence of hybridization within the last two decades, we anticipated finding evidence of  
547 gene flow and complex patterns of selection underlying the speciation process between  
548 these two sympatric species. Specifically, considering the secondary contact and the  
549 observed ecological divergence between these species (e.g., diet, habitat, and nesting  
550 behaviors), we predicted that we would discover regions exhibiting signatures of  
551 divergence with gene flow, indicating ongoing selection associated with local adaptation.  
552 Finally, we hypothesized that adaptive introgression may be occurring, with genes from  
553 *G. sabrinus* contributing to the adaptation of *G. volans* to northern climates; we expected  
554 to identify regions in *G. volans* displaying genomic patterns with high  $F_{ST}$ , and low  $D_{XY}$   
555 and  $\pi$  values.

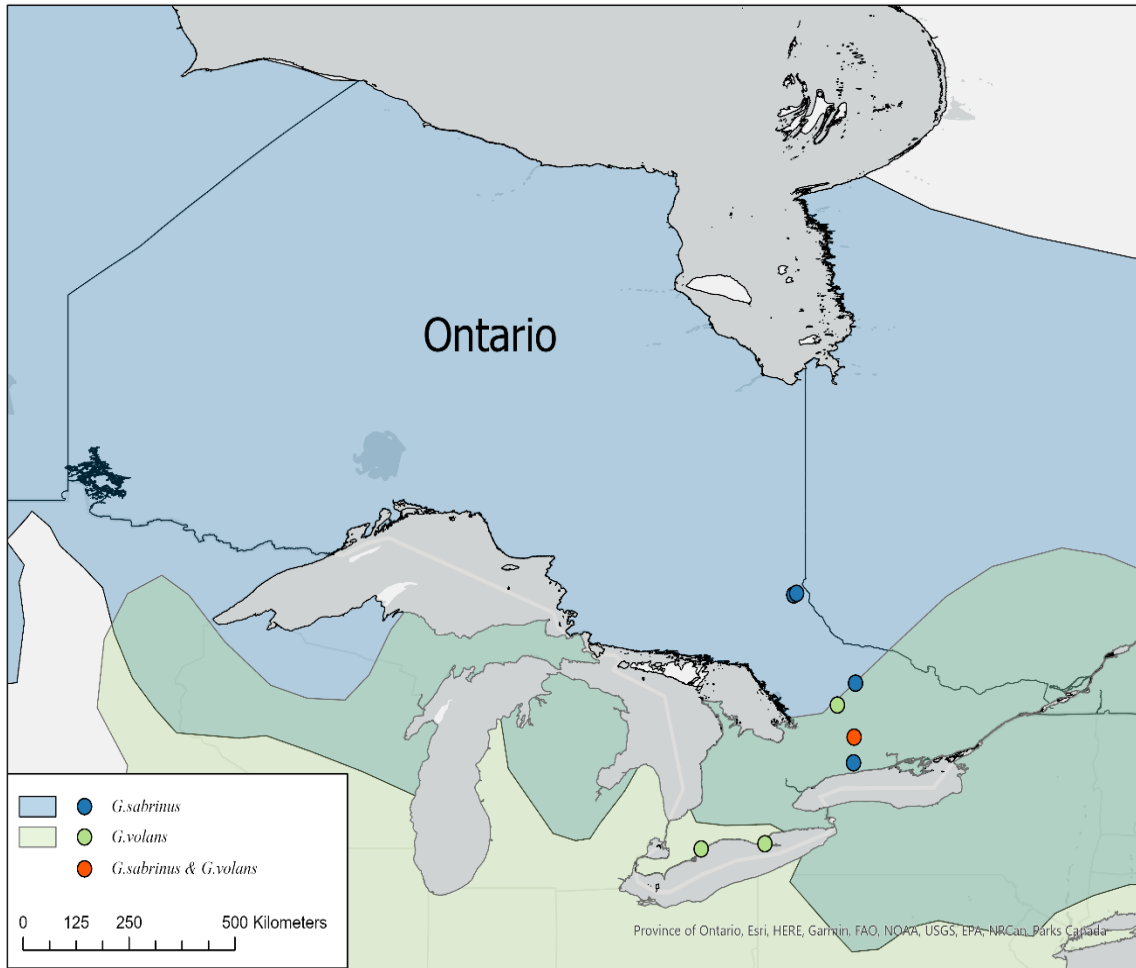
## 556 **Methods**

### 557 **Sample Collection**

558         To capture potential hybridization, we focused on sample collection at a long-term  
559 study site in the Kawartha Highlands of Ontario, Canada (44.68°N,78.33°W), where *G.*  
560 *sabrinus* and *G. volans* exhibit local sympatry (Minns et al. 2024). We collected and  
561 sequenced thirty-seven *G. sabrinus* samples and fifty-four *G. volans* samples. We  
562 selected samples based on morphology-based species assignment in the field and sex. We  
563 primarily selected adults and aimed for an equal number of male and female samples

564 within each species. An additional 27 samples were collected and sequenced from other  
565 locations in Ontario, including with allopatric populations, to help discern any population  
566 structure or genetic characteristics that were associated with hybridization at the  
567 sympatric Kawartha Highlands site. *G. volans* samples were obtained from Clear Creek  
568 (three samples; 42.52°N,81.62°W) and Long Point (ten samples; 42.58 °N,80.38°W). *G.*  
569 *sabrinus* samples were obtained from the Roosevelt Road area (four samples; 47.26°N,  
570 79.71°W), Temagami (eight samples; 47.23°N, 79.77°W), and Ganaraska (one sample;  
571 44.09°N,78.5°W). (See Supplemental Information Table S1).

572 We included four previously sampled individuals from Clear Creek (*G. volans*),  
573 Sherborne Lake (*G. volans*; 45.17°N,78.84°W), Algonquin (*G. sabrinus*;  
574 45.58°N,78.46°W), and Kawartha Highlands (*G. sabrinus*) (Wolf et al., 2022), for an  
575 initial dataset of 121 samples (Figure 1).



576  
 577 *Figure 1. Map of sample locations and ranges for Glaucomys species in Ontario as delineated by IUCN*  
 578 *(Cassola, 2016a; Cassola, 2016b).*

579 **DNA Extraction and Whole-Genome Sequencing**

580 We extracted DNA from the tissue and hair samples using the Qiagen DNeasy kit.  
 581 Extracted DNA was run on a Qubit fluorometer using the High Sensitivity Assay Kit to  
 582 ensure sufficient DNA for next-generation sequencing and on a Nanodrop ND-8000  
 583 spectrophotometer to test purity. A TrueSeq Nano library prep kit (Illumina) with PCR-  
 584 protocol was used to prepare the DNA for sequencing by The Centre for Applied  
 585 Genomics at The Hospital for Sick Children (Toronto, ON). Samples were sequenced on  
 586 an Illumina NovaSeq platform to generate 150 bp paired-end reads.

587 **Quality Control and Read Alignment**

588 The initial quality of 121 whole genome sequencing raw reads was examined using  
589 FastQC (v0.11.90; Andrews, 2010) and summarized with MultiQC (Ewels et al., 2016).  
590 We removed sequencing adaptors and low-quality bases (phred score < 30) using  
591 Trimmomatic (v0.39; Bolger et al., 2014). Trimmed reads were mapped and sorted to a  
592 scaffold-level southern flying squirrel reference genome (GenBank GCA\_020662805.1;  
593 Wolf et al., 2022) that had been concatenated with the southern flying squirrel reference  
594 mitogenome (NCBI Accession number: NC\_050026; Abreu-Jr, 2020) using bwa mem  
595 (v0.7.17; Li, 2013) and SAMtools sort (v1.15.1; Li et al., 2009). Read group information  
596 and shorter reads were marked for Picard compatibility during mapping with bwa mem.  
597 Following mapping, alignment statistics were checked using SAMtools flagstat. We then  
598 removed duplicates with GATK MarkDuplicates (Picard) (v4.2.4.0; McKenna et al.,  
599 2010). We used BamUtil clipOverlap (v1.0.14; Jun et al., 2015) default settings to hard  
600 clip overlapping read pair-end and then used Sambamba (v0.8.0; Tarasov et al., 2015) to  
601 retain only primary alignments. A local re-alignment was then performed using GATK  
602 RealignerTargetCreator and IndelRealigner (v3.8; McKenna et al., 2010). The final  
603 quality of aligned reads was examined using FastQC, summarized with multiqc, and  
604 depth coverage across each genome was calculated using SAMtools. Any genomes with a  
605 depth >3x were filtered to remove bases with mapping quality below 20 and subsampled  
606 to a depth of 2x using SAMtools.

607 **Calling Genotype Likelihoods**

608 We estimated genotype likelihoods using the SAMtools model implemented in ANGSD  
609 (v 0.939; Korneliussen et al., 2014; Li, 2011) with major and minor allele frequencies

610 inferred from allele counts (Li et al., 2010b). Bases with a quality lower than 20 and reads  
611 with mapping quality below 20 were discarded. Only proper pair reads and SNPs with a  
612 p-value  $<1e^{-6}$  were retained. Sites that had a completion of less than ~80% were  
613 discarded. We estimated linkage disequilibrium (LD) within a maximum SNP distance of  
614 100 and a maximum distance of 100kb and applied LD-pruning using ngsLD (Fox et al.,  
615 2019) to obtain a list of unlinked sites. We then calculated genotype likelihoods as  
616 described above with an additional filter to retain only unlinked sites. We generated  
617 additional Beagle genotype likelihood files using the same parameters as described above  
618 for each *Glaucomys* species for downstream analysis.

### 619 **Population Structure and Admixture Analyses**

620 To investigate population structure and identify potential hybrids, we initially examined  
621 the complete dataset consisting of 114 genomes. We utilized NGSadmix (v32; Skotte et  
622 al., 2013) to estimate population clustering and individual admixture proportions. We  
623 explored values of  $K=2-7$  (number of population clusters) with 10 replicates. To select the  
624 best support  $K$ , we used an R-script written by Bay et al. (2021) to compare log  
625 likelihood values across runs and plot the outputs. Additionally, we conducted Principal  
626 Component Analyses (PCA) using the Beagle file generated by Angsd in PCAngsd  
627 (v0.98; Meisner & Albrechtsen, 2018) and visualized the results in R to assess population  
628 structure. For each *Glaucomys* species, we performed additional Principal Component  
629 Analyses with related and inbred individuals excluded during genotype likelihood calling.  
630 Both NGSadmix and PCAngsd analyses utilized default setup and filtering parameters,  
631 retaining only SNPs with a minor allele frequency exceeding 5%.

632 **Relatedness and Inbreeding**

633 Inbreeding and relatedness were estimated within *Glaucomys* species using NgsF (v1.2.0;  
634 Vieira et al., 2013) and NgsRelate respectively (v2; Korneliussen & Moltke, 2015).  
635 Pairwise relatedness was assessed using the coefficient of kinship ( $\phi$ ) and Jacquard  
636 coefficients (Jacquard, 1974), where  $J_0=K_0$ ,  $J_1=K_1$ , and  $J_2=K_2$ . These coefficients are  
637 probabilities of sharing zero ( $K_0$ ), one ( $K_1$ ), or two alleles ( $K_2$ ) identical by descent (IBD)  
638 in the absence of inbreeding (Ackerman et al., 2017). We used the inference criteria as  
639 described by Manichaikul et al., 2010 as thresholds to assign the degree of relatedness  
640 based on the IBD probabilities for standard relationships and  $\phi$  (Table S2).

641 **Mitogenome Assembly and Species Mitogenome Assignment**

642 We used the GetOrganelle toolkit (v1.7.6.1; Jin et al., 2020; Bankevich et al., 2012;  
643 Camacho et al., 2009; Langmead & Salzberg, 2012) to assemble individual mitogenomes  
644 from trimmed reads. For the assembly seed, we used the complete *G. volans* mitogenome  
645 (NCBI Accession number: NC\_050026; de Abreu-Jr et al., 2020). We visualized the final  
646 mitogenome assembly graph using Bandage (v0.8.1; Wick et al., 2015). Additionally, we  
647 generated individual mitogenome assemblies using Angsd doFasta from the mapped  
648 BAMs by specifying the region to only the mitogenome. To test for nuclear-to-  
649 mitochondrial genome discordance, we employed two different methods to cross-check  
650 and assign the individual mitogenome species.

651 Our first method involved performing a phylogenetic tree analysis using IQ-  
652 TREE (v2.1.2; Nguyen et al., 2015; Kalyaanamoorthy et al., 2017). We created the  
653 phylogenetic tree using both the GetOrganelle assembled mitogenomes and those  
654 generated using Angsd. We initially produced a global alignment of the *Glaucomys*

655 mitogenomes to the mitogenome assembly of the grey squirrel (*S. carolinensis*) obtained  
656 from NCBI (Accession number: NC\_050012; de Abreu-Jr et al., 2020) using the multiple  
657 sequence alignment program MAFFT (v7.471; Katoh & Standley, 2013). For the  
658 GetOrganelle assembled mitogenomes, we reran the IQ-TREE phylogenetic analysis after  
659 determining the best-fit substitution model, with a bootstrap value of 1000 to assess  
660 branch support. To verify the phylogenetic tree, we used BLAST nucleotide (Camacho et  
661 al., 2009). We limited our search strategy to *Glaucomys sabrinus* and *Glaucomys volans*  
662 (taxids: 45482, 64683) and assigned the species of the mitogenome based on the best  
663 species hit for the cytochrome b (Cytb) gene, which has been sequenced for both species.

#### 664 **Site Frequency Spectrum Inference**

665 For downstream analysis of demographic history and population genetic diversity  
666 measures, we generated the site frequency spectrum (SFS). To estimate the unfolded SFS,  
667 we used an ancestral reference genome using high coverage reads for the eastern gray  
668 squirrel (*Sciurus carolinensis*) (SRA Accession: SRR17854499) and the thirteen-lined  
669 ground squirrel (*Ictidomys tridecemlineatus*) obtained from NCBI (SRA Accessions:  
670 SRR9172277- SRR9172286). These reads were mapped to the *G. volans* reference  
671 genome using the quality control and read alignment method previously described. We  
672 used the produced BAM files to generate the ancestral reference from the most common  
673 base consensus with the doFasta function in Angsd (Korneliussen et al., 2014).

674 To ensure an accurate SFS estimation, we excluded inbred individuals from the  
675 analysis. We calculated the SFS likelihood for each population, assuming Hardy-  
676 Weinberg Equilibrium, and applied the quality filters used to call genotype likelihoods.  
677 Furthermore, we included the sites flag with a file corresponding to the recovered SNPs

678 when genotype likelihoods were called with both populations, ensuring that sites with an  
679 allele fixed in one population were included. We then obtained the maximum likelihood  
680 estimate of the SFS using the Angsd program realSFS (Nielsen et al., 2012) to infer the  
681 distribution of allele frequencies within each species' population. Likewise, we used the  
682 SFS likelihoods obtained separately for *G. sabrinus* and *G. volans* populations to get the  
683 maximum likelihood estimate of the two-dimensional site frequency spectrum (2D-SFS).

684 To investigate the timing of species divergence and the effective population size  
685 of both *G. sabrinus* and *G. volans*, we utilized the one-dimensional site frequency  
686 spectrum (1D-SFS) estimated for each species as input data for Stairway Plot (v2.1.1; Liu  
687 & Fu, 2020) to infer their respective demographic histories. The analysis was performed  
688 using the default parameters for the percentage of sites and subsampling for training the  
689 model, as well as the program's suggested number of breakpoints according to our  
690 sample size. We used a mutation rate of  $2.0 \times 10^{-9}$  per site per year (Grossman et al.,  
691 2019).

692 To infer the historical relationships and gene flow between *G. sabrinus* and *G.*  
693 *volans*, we constructed evolutionary trees using Treemix (v1.13; Pickrell & Pritchard,  
694 2012) and measured historical introgression using the ABBA-BABA test. We converted  
695 the BCF output, generated by Angsd when calling genotype likelihoods without filtering  
696 linked sites, to a VCF file. We then used Stacks (v2.64; Catchen et al., 2013) to generate a  
697 format usable by Treemix for the input, converting genotype likelihoods to called  
698 genotypes. For this analysis, we grouped samples according to clustering in the PCA  
699 results where sympatric *G. volans* and *G. sabrinus* populations included the Kawartha  
700 Highlands and Sherbourne Lake or Ganaraska respectively. The allopatric *G. volans*



701 population included Long Point and Clear Creek samples, and Temagami and Roosevelt  
702 Road were used for the allopatric *G. sabrinus* population. We tested three different SNP  
703 block sizes of  $k=500$ ,  $k=1000$ , and  $k=2000$ . For each parameter setting ( $k=500$ ,  $k=1000$ ,  
704 and  $k=2000$ ), we tested evolutionary trees both with and without migration events ( $m=0$ -  
705 5) and conducted 10 iterations. We then used the OptM package in R (Fitak, 2021) to  
706 select the best-supported migration model.

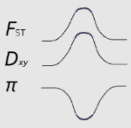
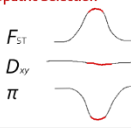
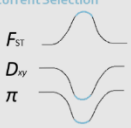

707 To measure historical gene flow, we computed the D-statistic using the Angsd  
708 ABBA-BABA multi-population test (Soraggi et al., 2018) with a SNP block size of 100  
709 kilobases and 50 kilobases, following the same population groupings utilized for Treemix  
710 and the ancestral fasta file generated to estimate unfolded SFS.

### 711 **Population Genetic Diversity Measures**

712 To detect potential regions underlying different evolutionary processes of selection and  
713 divergence, we calculated measures of genomic variation to conduct genomic scans. To  
714 measure within-population nucleotide diversity ( $\pi$ ) and population differentiation ( $F_{ST}$ ),  
715 we used Angsd for per-site and sliding window estimates (Korneliussen et al., 2013). We  
716 measured population divergence between *G. volans* and *G. sabrinus* by calculating the  
717 per-site number of nucleotide differences ( $D_{XY}$ ) using the ngsPopGen “calcDxy.R” script  
718 (by Joshua Penalba, 2018; Fumagalli et al., 2014) using each species’ allele frequency file  
719 generated when calculating the 1D-SFS with Angsd. We then used our custom R script to  
720 calculate the average  $D_{XY}$  across sliding windows. For all sliding window estimates, we  
721 used the first block as the window with the same window entries across. We calculated  
722 estimates for a window size of 100 kb with a 50 kb step and a 50 kb window size with a  
723 10 kb step. Due to the fragmentation of our scaffold-built reference genome, we also

724 calculated estimates with a window size of 10 kb and a 1 kb step. To plot the results, we  
 725 filtered to retain only windows for which we obtained estimates for all three measures.  
 726 We determined the evolutionary scenario and underlying selection mechanisms following  
 727 the descriptions provided by Irwin et al., (2018) and Shang et al., (2023) as summarized  
 728 and by the specified thresholds in Table 1.

729 *Table 1. Four different evolutionary models and their underlying selection with the applied percentile*  
 730 *thresholds for  $F_{ST}$ ,  $D_{XY}$ , and  $\pi$ .*

	Scenario Model and Type of Selection		$F_{ST}$	$D_{XY}$	$\pi$
<b>Reproductive Isolation</b> 	Divergence with Gene Flow	Loci underlying reproductive isolation	> 95%	> 95%	< 5%
<b>Allopatric Selection</b> 	Selection in Allopatry	Positive or Background Selection	> 95%	45% - 55%	< 5 %
<b>Recurrent Selection</b> 	Recurrent Selection or Sweep before Differentiation	Background, Balancing or Positive Selection	> 95%	< 5%	< 5%
<b>Balancing Selection</b> 	Balancing Selection		< 5%	> 95%	> 95%

731 We estimated Spearman's rank correlation coefficients for differentiation ( $F_{ST}$ ),  
 732  
 733 absolute divergence ( $D_{XY}$ ), and average nucleotide diversity ( $\pi$ ) across the genome using  
 734 non-overlapping 10kb windows.

## 735 **Results**

### 736 **Quality Control and Genotype Likelihoods**

737 Out of our initial 117 sequenced samples, 7 failed quality control checks either in FastQC  
 738 or SAMtools flagstat. Samples with a mapping rate of less than 85% of reads were  
 739 excluded from the dataset (Table S3). This resulted in 110 newly generated flying squirrel

740 genomes from Ontario, with an average coverage of 1.98x and a coverage range of 1.13  
 741 to 22.85x. We further subsampled the four previously sequenced high-coverage genomes  
 742 (Wolf et al., 2022), along with the newly generated sequences having a coverage greater  
 743 than 3.0x, down to 2.0x coverage. Resulting in a combined dataset of 114 genomes used  
 744 for the analysis.

745 When calling genotype likelihoods with all samples pooled, we obtained a total of  
 746 36,093,731 SNPs. After running ngsLD, we obtained a list of 10,433,403 unlinked sites  
 747 that were present in all samples. Subsequently, we removed related and inbred  
 748 individuals, resulting in 5,760,913 unlinked SNPs for all samples (N=68) in a combined  
 749 dataset, 4,544,604 unlinked SNPs for unrelated samples (N=23) of *G. sabrinus*, and  
 750 5,343,235 unlinked SNPs for unrelated samples (N=45) of *G. volans*.

### 751 Population Structure and Admixture Analyses

752 The best-supported model, with the highest log likelihood value and 100% convergence  
 753 across all 10 runs, was K=2 (Figure 2). Our analysis revealed that each species was  
 754 assigned to its own cluster, with no evidence of admixture between the species. Based on  
 755 the NGSadmix results, we identified two individuals, R6 (Roosevelt, 47.26°N, 79.71°W)

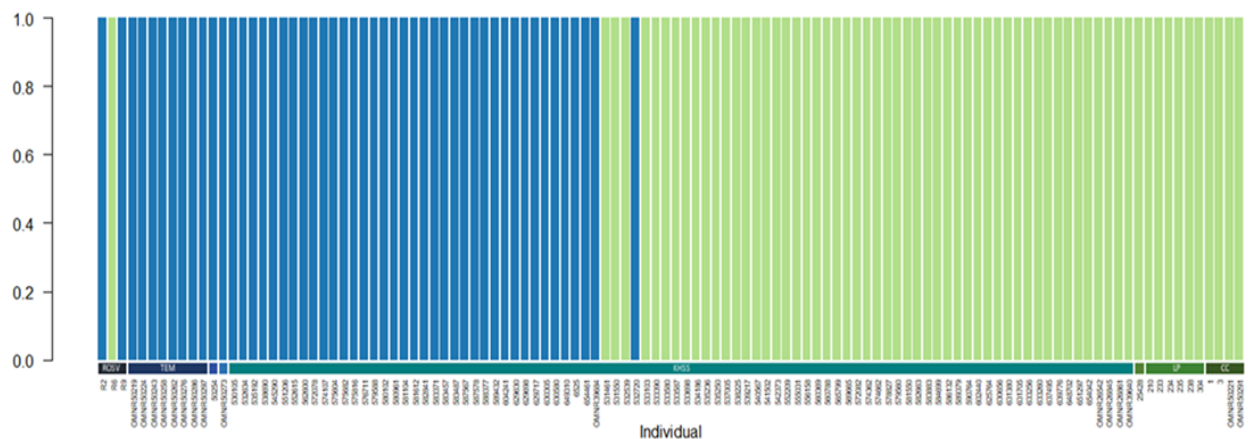
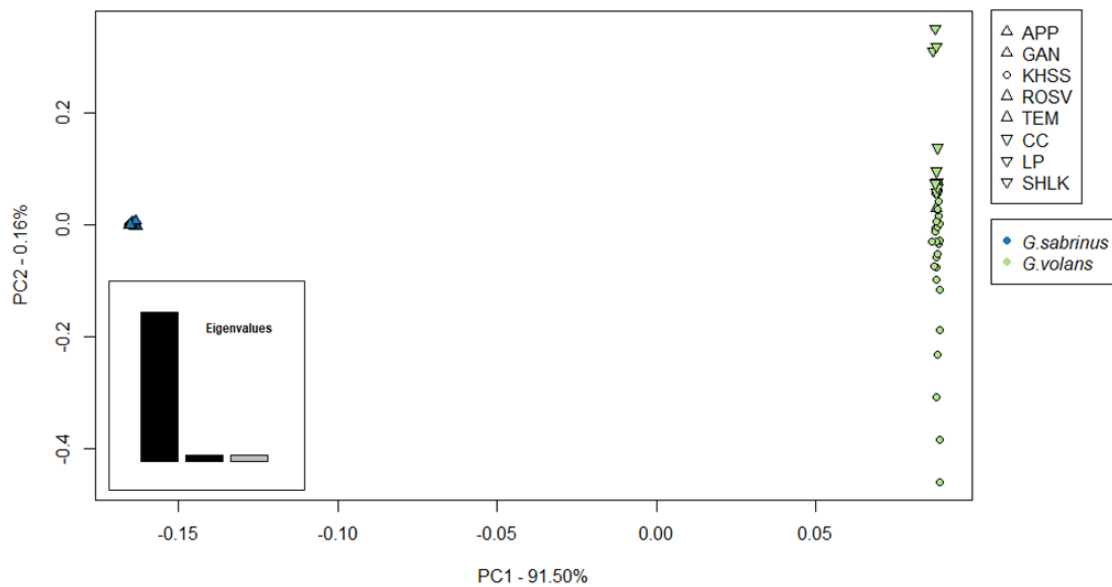


Figure 2. Admixture proportions of the 114 genomes sequences for K = 2 of the 114 genome sequences calculated with NGSAdmix.

756 and 532720 (Kawartha Highlands, 44.68°N, 78.33°W), that were incorrectly assigned  
757 species based on their morphological traits in the field.

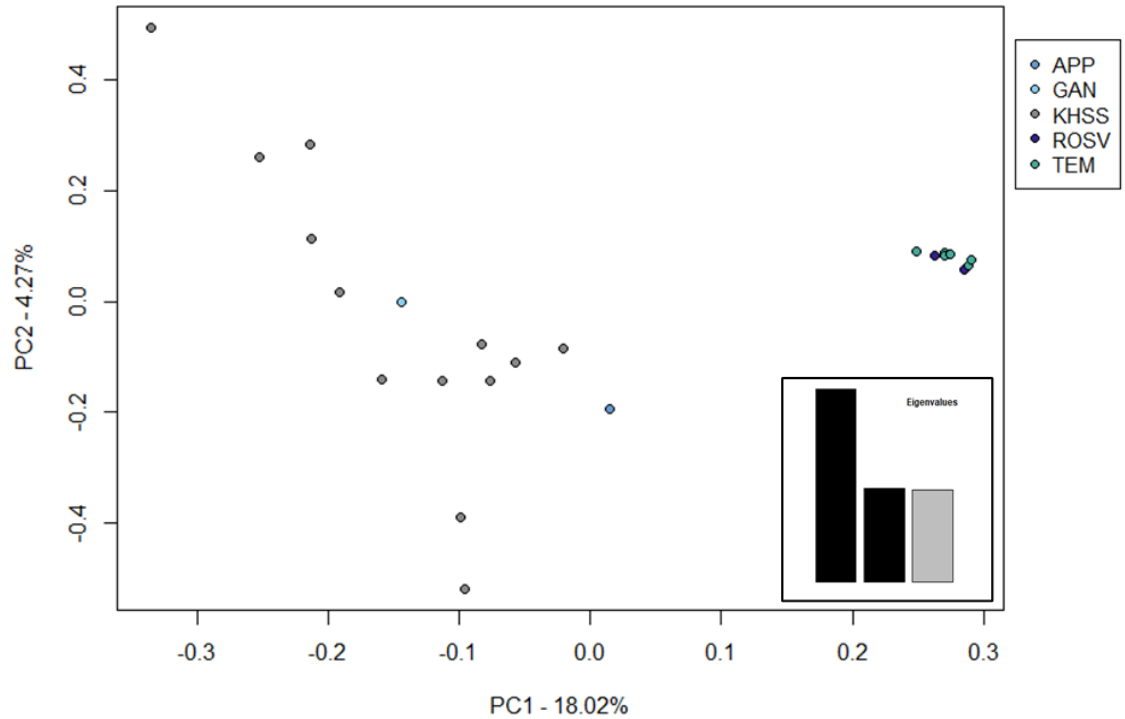
758 The Principal Component Analysis (PCA) excluded related and inbred individuals  
759 and revealed a clear separation of *G. sabrinus* and *G. volans* (Figure 3). The first  
760 principal component accounted for over 90% of the variation, while the second and third  
761 components both contributed approximately 0.16% of the total variation (Figure S1).



762

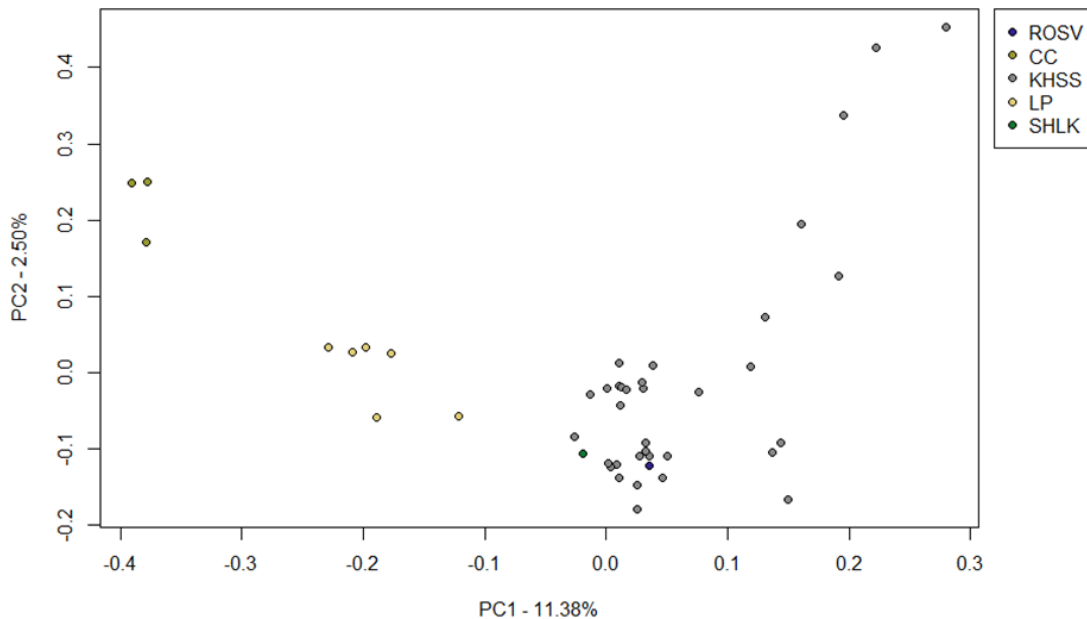
763 *Figure 3. Principal Component Analysis (PCA) of all unrelated individuals of G. sabrinus and G. volans*  
764 *(N=68).*

765 Within *G. sabrinus*, the PCA showed a distinct grouping of the more northern  
766 samples from Temagami and Roosevelt Road compared to the samples from farther south  
767 (Figure 4). The first principal component accounted for approximately 18% of the total  
768 genomic variation, while the second and third components each accounted for  
769 approximately 4% of the total variation (Figure S2).



770  
 771 *Figure 4. Principal Component Analysis (PCA) of all unrelated individuals of G. sabrinus (N=23).*

772           Similarly, within *G. volans*, the PCA revealed separation of the south-western  
 773 samples from Clear Creek and Long Point from the samples farther north (Figure 5). The  
 774 samples from Clear Creek and Long Point also clustered within each site. The first  
 775 principal component accounted for approximately 11% of the total genomic variation,  
 776 while the second and third components accounted for approximately 2% of the total  
 777 variation (Figure S3).



778

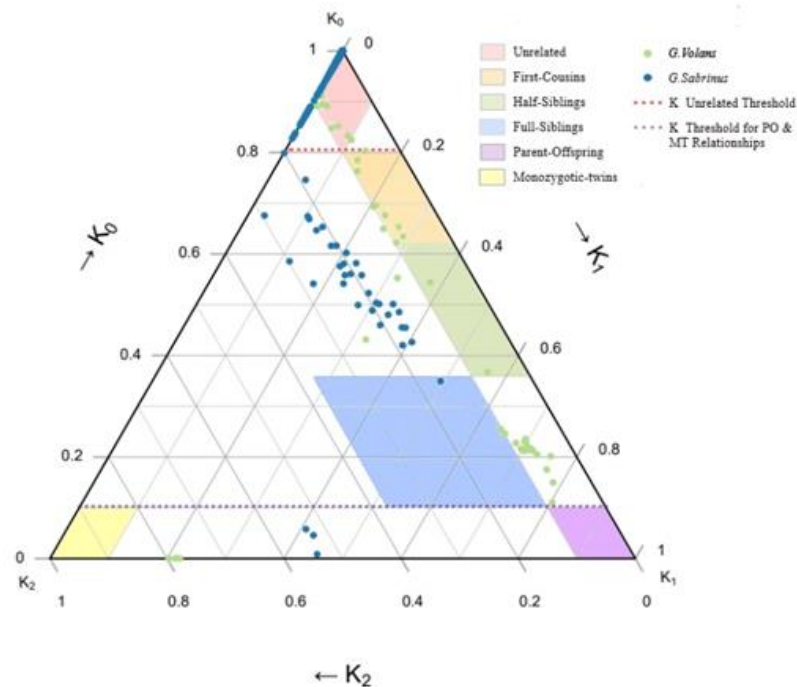
779 *Figure 5. Principal Component Analysis (PCA) of all unrelated individuals of G. volans (N=45).*

### 780 **Relatedness and Inbreeding**

781 Our ngsF results indicated no evidence of inbreeding in *G. sabrinus*, with an inbreeding  
 782 coefficient (F) value range of 0 to  $2.7 \times 10^{-4}$ . In contrast, *G. volans* exhibited a range of  
 783 inbreeding coefficients, with some individuals having elevated F values (range: 0 –  
 784 0.237). We identified one individual from *G. volans* (ID: 555031, Site: Kawartha) with a  
 785 high inbreeding coefficient of 0.237, which was subsequently removed from downstream  
 786 analysis. The remaining *G. volans* individuals had inbreeding coefficients  $< 0.07$  and were  
 787 retained in the dataset.

788 The results from ngsRelate demonstrated a higher probability of sharing two  
 789 alleles ( $K_2$ ) in *G. sabrinus* compared to *G. volans*. These elevated  $K_2$  values resulted in  
 790 pairwise relationships that deviated from the expected probabilities for standard  
 791 relationships (Figure 6). To identify potential relationships that deviated from the

792 expected probabilities, we used  $K_0$  and the coefficient of kinship ( $\phi$ ) to assigned degrees  
 793 of relatedness. After identifying potential relationships using  $K_0$  and the coefficient of  
 794 kinship ( $\phi$ ), individuals with ambiguous relationships were assessed using  $\phi$  alone to  
 795 determine the potential degree of relationship (Table S4). We subsequently removed one  
 796 individual from each pairing of potential second-degree or closer relationships. For *G.*  
 797 *sabrinus*, individuals with third-degree relationships also exhibited second-degree  
 798 relationships and were consequently excluded.



799

800 *Figure 6. Ternary plot of  $K_0$ ,  $K_1$ , and  $K_2$  values from ngsRelate for *G. sabrinus* and *G. volans* pairwise*  
 801 *relationships. Colored polygons represent the potential degree of relation based on the used inference*  
 802 *criteria (see Table S2).*

803 We observed an unexpected number of potential monozygotic twin relationships  
 804 based on  $K_0$  and  $\phi$  in both species. All cases of potential monozygotic twins were among  
 805 female flying squirrels at the Kawartha Highlands site. Among *G. volans* individuals,

806 three exhibited pairwise potential monozygotic twin relationships with each other  
807 (574362, 583833, 581550). There was an additional monozygotic twin relationship within  
808 the *G. volans* population (560788, 625764). In *G. sabrinus*, we identified three separate  
809 potential monozygotic twin relationships (574107, 575682 ; 532720, 532634 ; 552615,  
810 588377). However, in all cases of monozygotic twin relationships there were no  
811 overlapping field capture dates. To avoid possible ‘self’ cases that may have occurred  
812 from tag loss and recapture, we excluded individuals accordingly, retaining only one  
813 sample from each monozygotic twin pair for downstream analysis.

#### 814 **Mitogenome Assembly and Species Mitogenome Assignment**

815 We successfully assembled 106 complete mitogenomes and 8 mitogenomes to a contig  
816 level (IDs: 533103, 535250, 537005, 590764, 602440, 630656, 639776, OMNR50291)  
817 using GetOrganelle. For the incomplete contig assemblies, we selected the longest,  
818 unfragmented, and circular sequence as visualized in Bandage to create fasta files for  
819 downstream analysis.

820 The phylogenetic tree produced using the GetOrganelle assembled genomes did  
821 not split *G. sabrinus* and *G. volans* at a single node (Figure S4). Two distinct *G. volans*  
822 clusters were identifiable with ambiguity in the branching of *G. sabrinus* individuals.  
823 However, during the phylogenetic tree analysis of GetOrganelle assembled mitogenomes,  
824 IQ-TREE displayed a warning due sequences having >50% gaps/ambiguity and identified  
825 identical mitogenome sequences. Specifically, there were cases of identical mitogenomes  
826 between individuals that were identified as potential 3<sup>rd</sup>-degree relationships from the  
827 ngsRelate results: *G. sabrinus* (IDs: 589432, 579588) and *G. volans* (IDs: 639776,  
828 533580).



829           In contrast, when using the Angsd assembled mitogenomes, *G. sabrinus* and *G.*  
830 *volans* split at a single node into two distinct species clusters (Figure 7A). There was still  
831 uncertainty in the branching within *G. sabrinus* and *G. volans* (Figure 7B). We did not  
832 encounter any warnings related to gaps or ambiguity (range: 0.60-10.37%), and there  
833 were no identified identical mitogenomes by IQ-TREE.

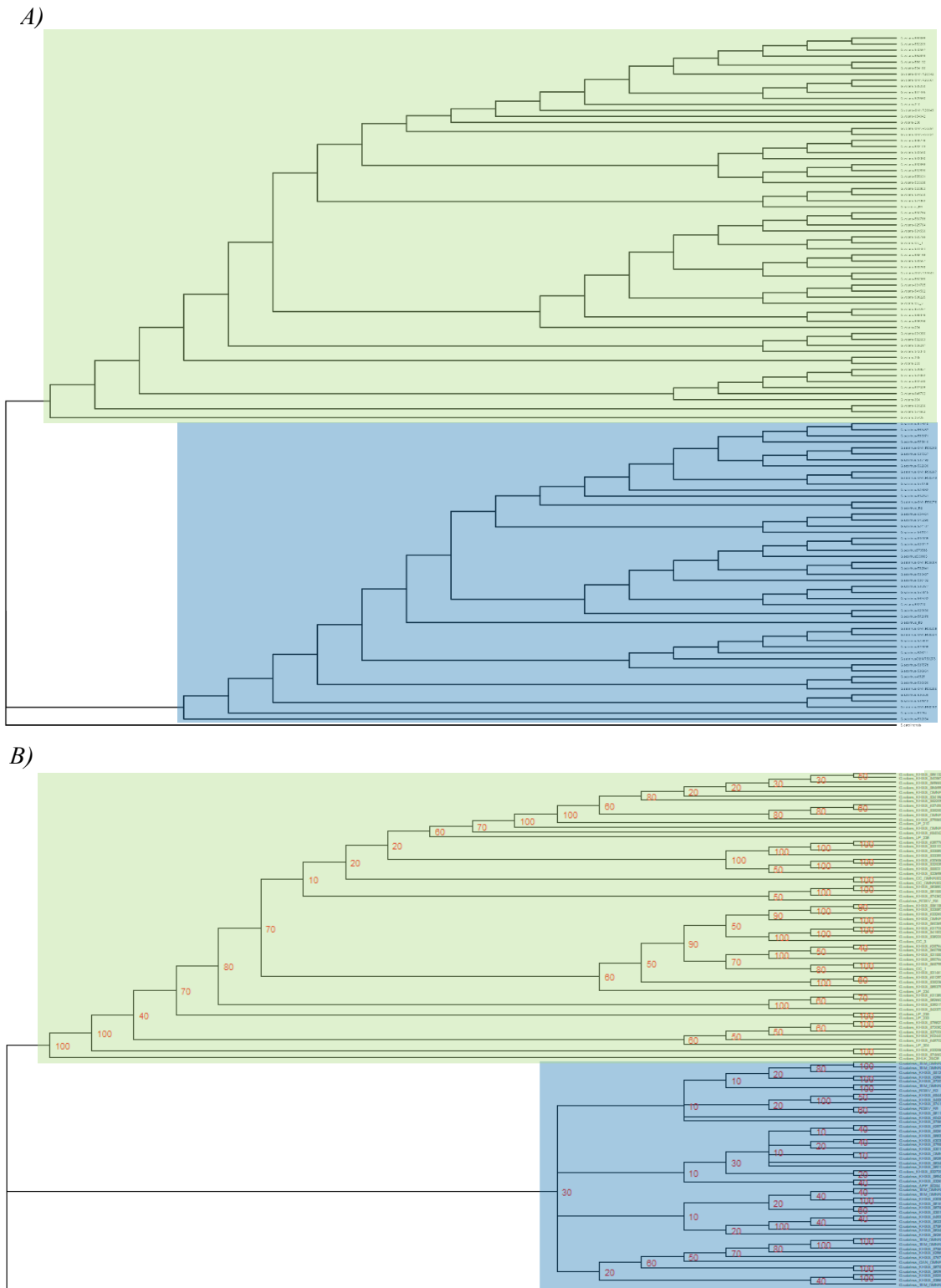
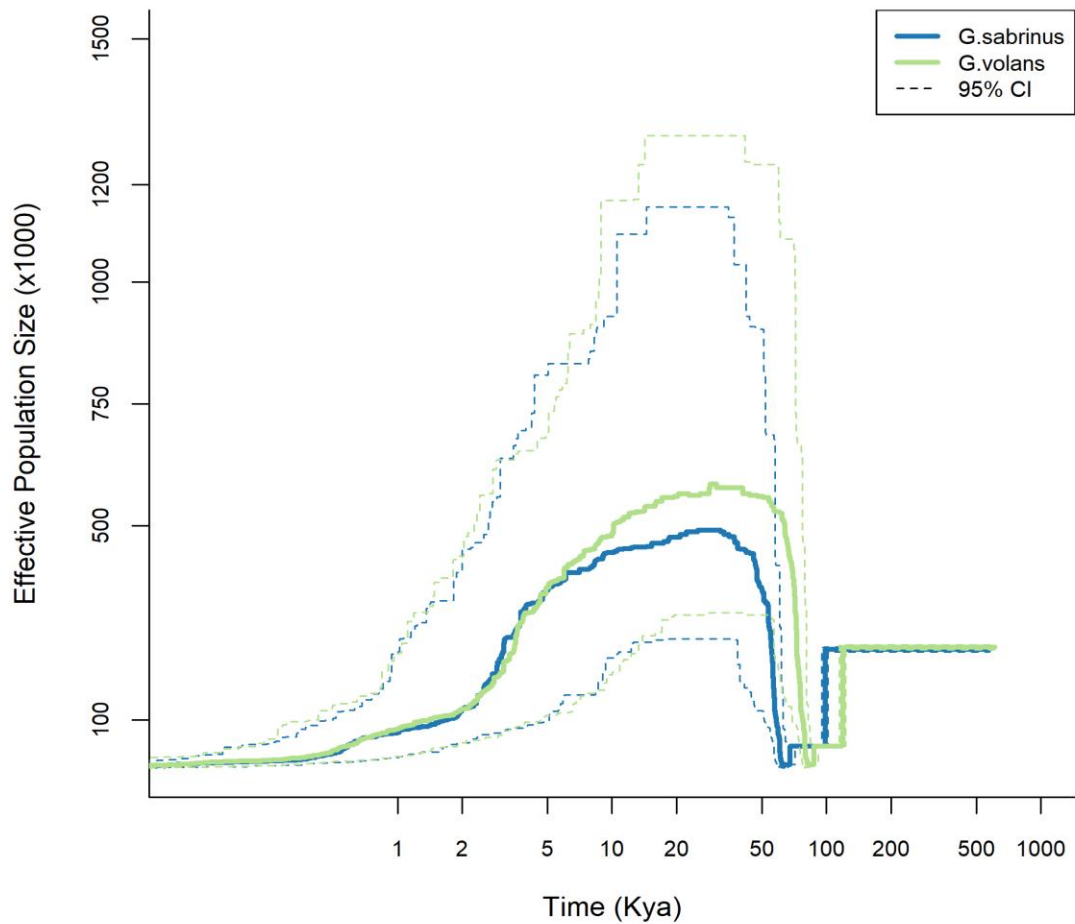


Figure 7. Phylogenetic trees constructed without (A) and with (B) bootstrap replicates, using Angsd assembled mitogenomes and IQTree (best-fit substitution model TN+F+I+R). Color assignments represent species clustering, with green representing *G. volans* and blue representing *G. sabrinus*. Red values in (B) indicate the confidence intervals of nodes, derived from 10 bootstrap replicates.

835 Our Blastn analysis showed concordance with the phylogenetic tree derived from  
836 the Angsd assembled mitogenomes. This agreement indicated a consistent relationship  
837 between the mitochondrial and nuclear genetic information, suggesting no evidence of  
838 nuclear-mitogenome discordance. Specifically, the Blastn best-hit results for the Cytb  
839 gene assigned all samples to same respective species as the nuclear genome.

#### 840 **Site Frequency Spectrum, Demographic History and Gene Flow**

841 Our Site Frequency Spectrum (SFS) results revealed similar patterns for both *Glaucomys*  
842 species (Figure S5). This is evident in the inferred demographic history by Stairway Plot  
843 where we observed similar population bottlenecks and expansions patterns for *G.*  
844 *sabrinus* and *G. volans* (Figure 8). Both species exhibit population bottlenecks and  
845 expansions that roughly coincide with 100-kyr ice sheet advancement and retreat cycle  
846 from this period of the Quaternary (Hewitt, 2000). The population bottleneck and  
847 subsequent expansion event appeared to occur first in the *G. volans* population,  
848 approximately between 140,000 – 70,000 years ago. There was a similar pattern in *G.*  
849 *sabrinus* starting with a population bottleneck approximately 100,000 – 50,000 years ago,  
850 after the bottleneck event in *G. volans*. Following these expansion events, both  
851 populations maintained relatively stable effective population sizes with some growth but  
852 beginning to decrease since the last glacial maximum (~20 Kya) and a more drastic  
853 decline since ~5 Kya.



854

855 *Figure 8. Inferred demographic history of G. sabrinus and G. volans using the unfolded SFS in Stairway*  
 856 *Plot 2 assuming a mutation rate ( $\mu$ ) of  $2.0 \times 10^{-9}$  per site per year.*

857 In addition to examining *Glaucomys* demographic history with Stairway Plots, we  
 858 used Treemix to test for gene flow between *G. volans* and *G. sabrinus*. Across all SNP  
 859 block sizes, the best-fit number of migrations edges was  $m=2$  (Figure S6). The best  
 860 supported migration models with two edges had a SNP block size of 500 (Figure 9;  
 861 Figure S7). In the first model (Figure 9A), gene flow from *G. volans* to *G. sabrinus*  
 862 originated from a basal placement, suggesting that this migration event occurred either  
 863 historically or from a closely related unsampled population. Conversely, gene flow from

864 *G. sabrinus* to *G. volans* populations in central Ontario seems to have originated from the  
865 branch tip, indicating this directional gene flow in the sampled populations. In the second  
866 model (Figure 9B), we observed evidence of gene flow from *G. sabrinus* to the central  
867 Ontario *G. volans* populations as well. However, in this case, the origin of this gene flow  
868 was situated at the node of the *G. sabrinus* population branch. Notably, unlike the model  
869 depicted in Figure 9A, there was no indication of gene flow from *G. volans* to *G.*  
870 *sabrinus* in this model. The other migration event indicated here originated from a basal  
871 placement within the *G. sabrinus* branch and extended to the northern Ontario *G.*  
872 *sabrinus* population



879 To further test historically gene flow, we conducted a genome-wide ABBA-BABA  
880 test. When employing the same population groupings as in Treemix and using the  
881 ancestral fasta sequences generated from *S. carolinensis* and *I. tridecemlineatus*, we  
882 found evidence for unidirectional gene flow between *Glaucomys* species. Specifically,  
883 both the allopatric and sympatric Ontario populations of *G. sabrinus* showed a D-statistic  
884 of approximately 0.02 for both block sizes of 100kb and 50kb tested, suggesting a limited  
885 contribution of genetic material to the central Ontario population of *G. volans* (Table 2).

Table 2. ABBA-BABA results using a 100kb block size and an ancestral file the generated consensus fasta of *S. carolinensis* and *I. tridecemlineatus* sequences. Bold values indicate an excess of ABBA-patterns between *Glaucomys* species. Sympatric *G. volans* and *G. sabrinus* populations included the Kawartha Highlands and Sherborne Lake or Ganaraska respectively. The allopatric populations for *G. volans* and *G. sabrinus* in Ontario include samples from Long Point and Clear Creek, and Temagami and Roosevelt, respectively.

D-statistic	Z-score	p-value	nABBA	nBABA	nBlocks	H1	H2	H3
<b>0.020623</b>	<b>64.217088</b>	<b>0</b>	<b>698330.6881</b>	<b>670109.59</b>	<b>59263</b>	<b><i>G. volans</i> Allopatric</b>	<b><i>G. volans</i> Sympatric</b>	<b><i>G. sabrinus</i> Sympatric</b>
<b>0.021051</b>	<b>65.705426</b>	<b>0</b>	<b>702791.7263</b>	<b>673813.465</b>	<b>60496</b>	<b><i>G. volans</i> Allopatric</b>	<b><i>G. volans</i> Sympatric</b>	<b><i>G. sabrinus</i> Allopatric</b>
0.896873	2470.337418	0	8112158.592	441033.5345	61404	<i>G. volans</i> Allopatric	<i>G. sabrinus</i> Sympatric	<i>G. sabrinus</i> Allopatric
0.896857	2533.983722	0	8112158.592	441103.099	61402	<i>G. volans</i> Allopatric	<i>G. sabrinus</i> Allopatric	<i>G. sabrinus</i> Sympatric
0.895944	2456.621934	0	8093324.915	444189.9771	61959	<i>G. volans</i> Sympatric	<i>G. sabrinus</i> Sympatric	<i>G. sabrinus</i> Allopatric
0.895968	2522.157422	0	8093324.915	444083.5092	61885	<i>G. volans</i> Sympatric	<i>G. sabrinus</i> Allopatric	<i>G. sabrinus</i> Sympatric
<b>-0.77104</b>	-1549.378399	0	698330.6881	5401696.635	61084	<i>G. volans</i> Allopatric	<i>G. sabrinus</i> Sympatric	<i>G. volans</i> Sympatric
<b>-0.770978</b>	-1567.369558	0	702791.7263	5434524.365	62141	<i>G. volans</i> Allopatric	<i>G. sabrinus</i> Allopatric	<i>G. volans</i> Sympatric
<b>-0.779272</b>	-1594.311583	0	670109.59	5401696.635	60803	<i>G. volans</i> Sympatric	<i>G. sabrinus</i> Sympatric	<i>G. volans</i> Allopatric
<b>-0.779379</b>	-1615.308127	0	673813.465	5434524.365	61753	<i>G. volans</i> Sympatric	<i>G. sabrinus</i> Allopatric	<i>G. volans</i> Allopatric
<b>-0.000079</b>	-0.180301	0.856917	441033.5345	441103.099	57183	<i>G. sabrinus</i> Sympatric	<i>G. sabrinus</i> Allopatric	<i>G. volans</i> Allopatric
<b>0.00012</b>	0.279977	0.779495	444189.9771	444083.5092	58662	<i>G. sabrinus</i> Sympatric	<i>G. sabrinus</i> Allopatric	<i>G. volans</i> Sympatric

886

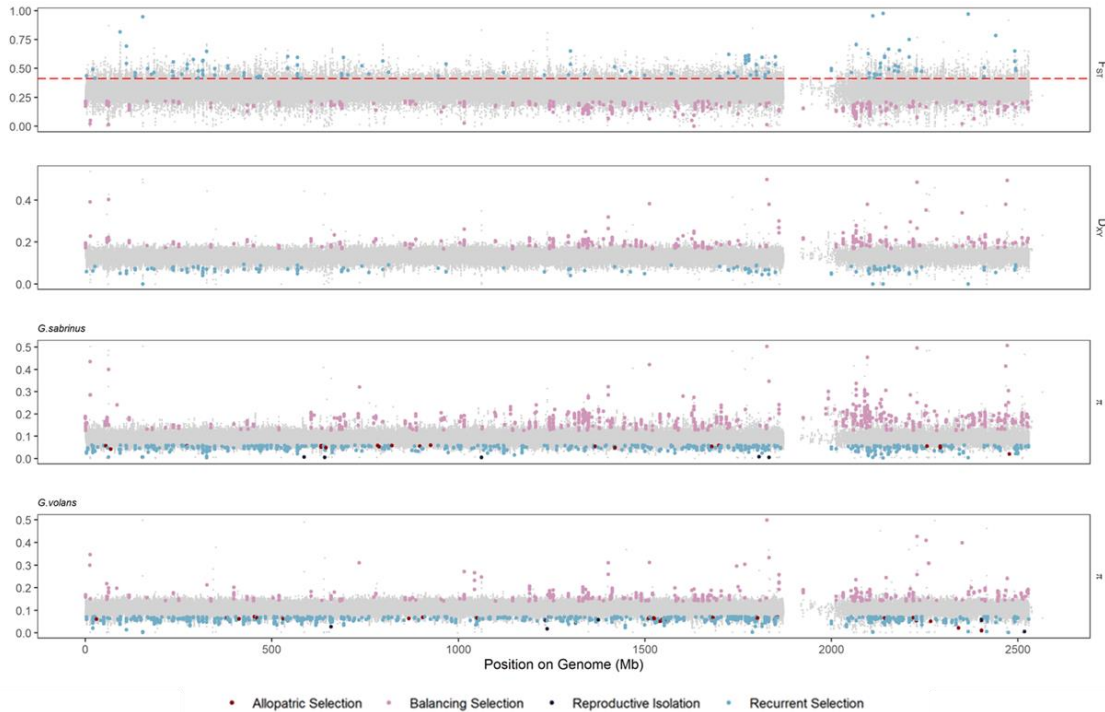
## 887 Nucleotide Diversity and Divergence Estimates

888 The global measures of genomic differentiation between *G. sabrinus* and *G. volans* were  
889 elevated (Weighted  $F_{ST} = 0.308$ ) and genomic divergence ( $D_{XY}$ ) was 0.141; genetic  
890 diversity ( $\pi$ ) was higher in *G. volans* ( $\pi = 0.115$ ) than in *G. sabrinus* ( $\pi = 0.098$ ; p-value

891  $< 2.2e^{-16}$ ). Using a 50kb window and step size of 10kb, we obtained a total of 180,554  
892 windows that had  $F_{ST}$ ,  $D_{XY}$ , and  $\pi$  estimated for both *G. sabrinus* and *G. volans* (Figure  
893 10).

894         In *G. sabrinus*, 1,504 of these windows across 591 scaffolds exhibited selection  
895 patterns consistent with one of the four evolutionary scenario models. The predominant  
896 pattern observed across the *G. sabrinus* genome was balancing selection, with 841  
897 windows distributed across 255 scaffolds, followed by recurrent selection or sweep  
898 before differentiation, which encompassed 609 windows spanning 312 scaffolds.  
899 Additionally, we found evidence for selection in allopatry, with 20 windows identified  
900 across 18 scaffolds, and divergence with gene flow, in 24 windows across only 6  
901 scaffolds.





902

Figure 10. Genomic scans display patterns of selection using a 50kb window and 10kb step size for nucleotide differentiation ( $F_{ST}$ ) and divergence ( $D_{XY}$ ) between northern (*G. sabrinus*) and southern flying squirrels (*G. volans*), along with nucleotide diversity ( $\pi$ ) in *G. sabrinus* and *G. volans*. The red dashed line represents the 95% quartile for the fixation index ( $F_{ST}$ ).

903

904

905

906

907

908

909

In *G. volans*, we identified 1,367 windows across 563 scaffolds exhibiting one of these patterns. In contrast to *G. sabrinus*, recurrent selection or sweep before differentiation was the most prevalent pattern, with 815 windows spanning 356 scaffolds, followed by balancing selection, which was observed in 508 windows across 107 scaffolds. Furthermore, we observed a greater number of sites consistent with selection in allopatry, with 30 windows over 29 scaffolds. Additionally, there were fewer sites attributed to divergence with gene flow, specifically 14 windows found on 8 scaffolds.

910

911

912

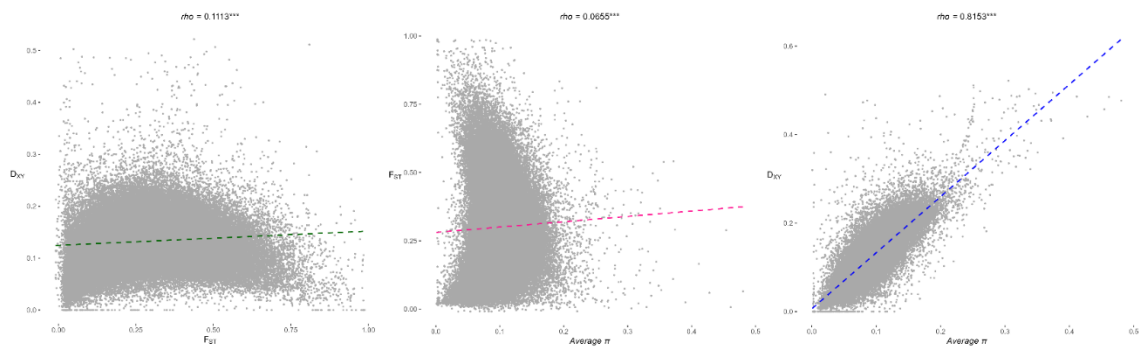
913

Differences in the selection patterns observed in each *Glaucomys* species can be attributed to the use of average  $\pi$  values calculated for each window within each species. Among the selection patterns identified for each species, 578 were shared between the two species across 238 scaffolds. Within this shared set, 435 windows distributed across

914 148 scaffolds indicated balancing selection, while the remaining 143 windows spanning  
915 90 scaffolds were suggestive of recurrent selection or sweep before differentiation.  
916 Interestingly, when we decreased the window and step size to 10kb and 1kb, we  
917 identified windows shared between *G. volans* and *G. sabrinus* consistent with selection  
918 patterns of both divergence with gene flow and selection in allopatry. Three of these  
919 windows were on two scaffolds (JAJEJO010003056.1 and JAJEJO010048944.1)  
920 displaying selection patterns indicative of divergence with gene flow. The other two  
921 windows were on scaffold JAJEJO010002268.1 and were consistent with allopatric  
922 selection (Figure S9).

923           When applying a stricter threshold of the 99% and 1% quartiles, using a 50kb  
924 window and step size of 10kb, we still detected the four different  $F_{ST}$ ,  $D_{XY}$ , and  $\pi$  patterns  
925 in both species (Figure S10). Under these refined thresholds, the dominate pattern shifted  
926 to “balancing selection” for both *G. volans* and *G. sabrinus*. Notably, while we observed  
927 the same number of windows displaying variation patterns indicative of divergence with  
928 gene flow for *G. sabrinus*, there was a reduction from 14 to 3 windows displaying this  
929 pattern in *G. volans*. Furthermore, patterns consistent with selection in allopatry were  
930 minimized to only two windows in both species.

931 Positive correlations were found across the genome for  $F_{ST}$ - $D_{XY}$ ,  $\pi$ -  $F_{ST}$ , and  $\pi$ -  
 932  $D_{XY}$  between *G. sabrinus* and *G. volans* (Figure 11). To represent divergence time, we  
 933 used the level of genetic distance between each species pair ( $D_{XY}$  – mean  $\pi$ ). We found  
 934 the same positive significant relationship between species pairs  $F_{ST}$ - $D_{XY}$  and  $\pi$ -  $F_{ST}$   
 935 correlation coefficients and divergence time ( $\rho = 0.9429$ ;  $p < 0.01$ ), and a negative  
 936 relationship for  $\pi$ -  $D_{XY}$  ( $\rho = - 0.54$ ;  $p = 0.26$ ) (Figure 12).



937 Figure 11. Genome wide correlation for  $F_{ST}$ - $D_{XY}$  (green),  $\pi$ - $F_{ST}$  (pink), and  $\pi$ - $D_{XY}$  (blue) between *G.*  
 938 *sabrinus* and *G. volans*.

## 939 Discussion

940 We sampled flying squirrels in Ontario from their range edges, with sampling effort  
 941 focused to a site where the species have documented local sympatry, and genetic  
 942 evidence for hybridization and introgression between *G. sabrinus* and *G. volans*  
 943 (Garroway et al., 2010; Lalor, 2014). Surprisingly, our findings revealed no evidence of  
 944 current hybridization or ancestral introgression between the *Glaucomys* species.  
 945 Additionally, we found no evidence of mitogenomic discordance despite previous  
 946 evidence (Lalor, 2014). Consistent with previous estimates, we found that *G. sabrinus*  
 947 and *G. volans* split over 1 MYA (Arbogast, 2007; Wolf et al., 2022). Our results indicate  
 948 however, that the speciation process between *G. sabrinus* and *G. volans* has involved  
 949 historical gene flow, specifically with genetic contribution from *G. sabrinus* to *G. volans*.

950 We found patterns across the genome consistent with all evolutionary models  
951 investigated. Under evidence of historical gene flow from *G. sabrinus* to *G. volans*,  
952 regions in *G. volans* with elevated  $F_{ST}$  and low  $D_{XY}$  values may be indicative of a longer  
953 history of adaptive introgression under a sweep before differentiation scenario. However,  
954 most of the genome does not display a pattern of selection. Given the limited gene flow  
955 indicated by our results, hybridization has likely not facilitated the speciation of *G.*  
956 *sabrinus* and *G. volans*. Instead, selection in allopatry and genetic drift best fit the  
957 divergence of these species.

### 958 **Hybridization Detection**

959 Previous studies in Ontario have reported low rates of hybridization (<5%), introgression  
960 (<3%), and mitochondrial discordance (<1%) between *G. sabrinus* and *G. volans*  
961 (Garroway et al, 2010; Lalor, 2014). Given these low rates the sample size of 114 of this  
962 study may have been insufficient to detect rare contemporary events. Alternatively,  
963 considering the already low levels of detected hybridization between *G. sabrinus* and *G.*  
964 *volans*, secondary contact driven by climatic range expansion (Bowman et al., 2005) may  
965 have rapidly reinforced partial reproductive barriers that were likely already present when  
966 sampling occurred approximately 20 years ago by Garroway et al., 2010. While this  
967 period of secondary contact is relatively short, rapid reinforcement of reproductive  
968 barriers have been found experimentally to occur within 5 generations in *Drosophila*  
969 (Matute, 2010) and Pfennig (2003) found sharp declines in hybridization rates in  
970 spadefoot toads over a period of 27 years.

971 In secondary contact sympatric populations, premating barriers are often  
972 reinforced faster than postzygotic barriers (Coyne & Orr, 1989). Previous work has found

973 willingness for heterospecific nesting between sympatric populations of flying squirrels  
974 experimentally (Olson, Bowman, & Burness, 2018). However, few instances of nest  
975 sharing were observed at our study site in 2009, and more recent investigations having  
976 found no evidence of interspecific nest interactions or sharing (O'Brien et al., 2021;  
977 Minns et al., 2024) despite these species having local sympatry and overlapping home  
978 ranges (Persad, 2023; Minns et al., 2024). Additionally, there has been little overlap in the  
979 types of winter nests used (O'Brien et al., 2021), and rare instances of both species using  
980 the same roost have been recorded only on different temporal occasions (Minns et al.,  
981 2024). This provides evidence suggesting that there may be few opportunities for  
982 interbreeding between *Glaucomys* species in late winter when the mating period begins  
983 (Stapp & Mautz, 1991; Vernes, 2004).

984         Our sampling strategy may have impacted our ability to detect contemporary  
985 hybridization between *G. sabrinus* and *G. volans* in our study. We focused our sampling  
986 efforts on a small sympatric site subject to long-term monitoring, previous, and ongoing  
987 studies examining the ecological, physiological, and behavioral dynamics of *G. sabrinus*  
988 and *G. volans* (Bowman et al., 2005; Desantis et al., 2018; Garroway et al., 2010;  
989 O'Brien et al., 2021), to provide a comprehensive understanding of the system. However,  
990 this prolonged secondary contact between the two species may have reinforced pre-  
991 zygotic reproductive barriers at the site, and we might have identified a different pattern  
992 in population structure had we sampled from the wave front of *G. volans*. Specifically,  
993 our sampling may have prevented detecting potential initial hybridization upon secondary  
994 contact at the range expansion front of *G. volans*. Additionally, our omission of broader  
995 geographic sampling for *G. volans* and *G. sabrinus* likely impeded our ability to capture

996 finer population structure between allopatric and sympatric sites. Notably, our sampled  
997 allopatric site of *G. sabrinus*, Roosevelt Road (47.26°N, 79.71°W) had an individual  
998 identified as *G. volans*, indicating this site was not truly allopatric. Broader sampling  
999 across the ranges of both *Glaucomys* species may reveal finer-scale population structures  
1000 or a cline in genetic variation associated with climate or demographic events (e.g., De La  
1001 Torre et al., 2015) we could not detect. Identifying and sampling of new sympatric sites  
1002 as *G. volans* range expands northward could provide valuable insights into the dynamics  
1003 of hybridization, offering a more comprehensive understanding of the interactions  
1004 between *Glaucomys* species and its implications on their reproductive behavior.

#### 1005 **Evidence of Limited Directional Gene Flow**

1006 Despite the absence of contemporary evidence for hybridization or backcrossing in our  
1007 data set, we found evidence of historical, and limited, gene flow from *G. sabrinus* to *G.*  
1008 *volans*. Both our ABBA-BABA and Treemix results indicate gene flow from *G. sabrinus*  
1009 populations to the central Ontario *G. volans* population (Table 2; Figure 9B). It is  
1010 important to note that the alternate Treemix model (Figure 9A) indicates the possibility of  
1011 limited gene flow, historically or from a closely related population, from *G. volans* to *G.*  
1012 *sabrinus*. However, this direction of gene flow lacked support in our ABBA-BABA test.

1013         The divergence history of North American flying squirrels likely involved cycles  
1014 of differentiation and contact periods during the glacial cycles of the Pleistocene.

1015 Previous estimates suggested that *G. sabrinus* and *G. volans* began diverging over 1 MYA  
1016 (Arbogast, 1999; Wolf et al., 2022). The Quaternary witnessed a series of glacial events  
1017 and cyclical climatic changes (Hewitt, 2000). Ultimately these environmental dynamics  
1018 shaped the evolution of several taxa by influencing genetic processes, eroding or

1019 reinforcing barriers to gene flow between these diverging species, resulting in the  
1020 accumulation of genomic differences and adaptations (Hewitt, 1996, 2011; Abbott et al.,  
1021 2013). During the Pleistocene, *G. sabrinus* and *G. volans* populations refugia were in  
1022 primarily distinct geographic regions, with *G. sabrinus* favoring boreal forests and *G.*  
1023 *volans* deciduous ecosystems (Arbogast, 1999). In separated refugia, these populations  
1024 would have started to genetically differentiate under different selective pressures and  
1025 through drift. However, the cyclical climate events during the Pleistocene and the  
1026 potential for overlapping geographic distributions of *G. sabrinus* and *G. volans*  
1027 (Arbogast, 1999), may have resulted in the limited directional historical gene flow and  
1028 genomic divergence patterns we detected in these species.

### 1029 **Genome Wide Measures of Differentiation and Selection Scans**

1030         The ecological differences in habitat preferences, diet, and nest-type use between  
1031 *G. sabrinus* and *G. volans*, have likely contributed to their genetic divergence. The  
1032 elevated  $F_{ST}$  (0.308), a measure of genetic differentiation between populations, indicates a  
1033 considerable degree of differentiation (Wright, 1965) between *G. sabrinus* and *G. volans*  
1034 populations. Additionally, genetic drift likely played a substantial role in differentiation of  
1035 these species in allopatry, given a large proportion of windows across the genome (>99%)  
1036 were not associated with one of the four selection patterns. The patterns of  $F_{ST}$ ,  $D_{XY}$ , and  
1037  $\pi$  detected across the flying squirrel genomes revealed mixed signatures of selection  
1038 underlying their speciation. Historical cycles of glaciation and forest re-expansion in  
1039 North America may have facilitated partial gene exchange (Hewitt, 1996). This historical  
1040 context likely explains the variation in selection we observed across the genomes.

1041           In both *G. sabrinus* and *G. volans*, we identified a limited number of windows  
1042 consistent with the patterns of divergence with gene flow and selection in allopatry. The  
1043 selection in allopatry patterns aligned with periods of isolation in separate refugia and  
1044 whereas periods secondary contact can explain divergence with gene flow patterns. In  
1045 isolation, strong positive or negative selection acted on different genomic regions in the  
1046 diverging species under different ecological conditions, further promoting their  
1047 differentiation. Potential periods of secondary contact during glacial retreats may have  
1048 results in gene flow further reinforced reproductive isolating loci. Reproductive isolation  
1049 is often controlled by a limited number of loci and can evolve quickly (Stanskowski &  
1050 Ravinet, 2021). The asymmetry in the local genomic patterns characterized as divergence  
1051 with gene flow, observed by more regions in *G. sabrinus* than in *G. volans*, indicates that  
1052 *G. sabrinus* may experience a more pronounced effect of gene flow promoting genetic  
1053 divergence.

1054           The predominant pattern observed in *G. sabrinus*, as well as in shared sites  
1055 between *G. sabrinus* and *G. volans*, was indicative of balancing selection. This was also  
1056 the second most common pattern observed in *G. volans*. Genes under balancing selection  
1057 are predicted to facilitate introgression (Fijarczyk et al., 2018; Grossen et al., 2014), and  
1058 introgression often proceeds from the local to invading species (Currat et al., 2008). This  
1059 would entail hybrid offspring mating with the invading *G. volans*, leading to hybrid-  
1060 mediated gene flow from *G. sabrinus* to *G. volans*. Genes under balancing selection have  
1061 been shown to be particularly susceptible to undergoing adaptive introgression. This is  
1062 because genes under balancing selection exhibit lower differentiation between species  
1063 from increased shared ancestral polymorphisms. This facilitates introgression while



1064 serving as a source of novel alleles in hybridizing species (Fijarczyk et al., 2018). The  
1065 initial stage of the sweep before differentiation model has equivalency to adaptive  
1066 introgression (Irwin et al., 2018) and has been used to explain patterns of such variation  
1067 across taxa (Grossen et al., 2014; Irwin et al., 2018; Jones et al., 2018; Whitney et al.,  
1068 2010; Zhang et al., 2016).

1069         We identified patterns characterised by high  $F_{ST}$ , and low  $D_{XY}$  and  $\pi$  values,  
1070 consistent with recurrent selection or sweep before differentiation scenarios in both *G.*  
1071 *volans* and *G. sabrinus*. Given evidence of historical gene flow from *G. sabrinus* and *G.*  
1072 *volans*, it might be that certain genomic regions in *G. volans* have undergone a longer  
1073 history of adaptive selection and introgression. In contrast, the absence of evidence for  
1074 historical gene flow from *G. volans* to *G. sabrinus* may suggest that regions experiencing  
1075 recurrent selection have driven divergent selection in isolation, acting as a mechanism for  
1076 *G. sabrinus* lineage sorting from *G. volans*.

1077         The identification of local genomic patterns aligning with divergence with gene  
1078 flow, balancing selection, recurrent selection, and adaptive introgression suggests that the  
1079 genomic landscape is driven by various selective pressures. This is supported by the  
1080 identification of significant positive correlations between  $F_{ST}$ - $D_{XY}$ ,  $\pi$ - $F_{ST}$ , and  $\pi$ - $D_{XY}$ . The  
1081 presence of these relationships implies that the genomic landscapes of *G. volans* and *G.*  
1082 *sabrinus* may be shaped by multiple selective forces. The presence of positive  
1083 correlations across all diversity measures contradicts expectations under a scenario where  
1084 divergence is solely driven by genetic drift. In the absence of selection, we would not  
1085 necessarily expect notable positive correlations among diversity measures.

1086 Rare occurrences of strong positive correlations between  $F_{ST}$ - $D_{XY}$  have been  
1087 linked to distinct patterns attributed to repeated background selection (Cruickshank &  
1088 Hahn, 2014; Ravinet et al., 2017) or to the pattern of divergence with gene flow (Shang et  
1089 al., 2023). However, the observed weak positive correlations between  $F_{ST}$ - $D_{XY}$  and  $\pi$ - $F_{ST}$   
1090 suggest that genetic differentiation and nucleotide diversity lack a strong association  
1091 across the genome between *G. sabrinus* and *G. volans*, potentially influenced by selection  
1092 factors other than background selection or divergence with gene flow. Both recurrent  
1093 selection and balancing selection exhibit a negative correlation across the whole genome,  
1094 potentially contributing to the observed weaker positive correlation between  $F_{ST}$ - $D_{XY}$ .  
1095 Additionally, the pronounced positive relationship between average  $\pi$ -  $D_{XY}$  aligns with  
1096 genome-wide patterns expected under scenarios of balancing selection or recurrent  
1097 selection/sweep before differentiation (Shang et al., 2023). This may indicate ongoing or  
1098 recent selection acting on specific genomic regions. The evidence of low rates of  
1099 hybridization (Garroway et al., 2010) and the ABBA-BABA results indicating historical  
1100 gene flow from *G. sabrinus* to *G. volans* lend support to the idea that adaptive processes  
1101 or differential selection pressures may contribute to these patterns.

1102 These findings emphasize the complexity of the evolutionary processes at play,  
1103 highlighting the need for further investigations into nuanced understanding of the  
1104 interplay between selection, gene flow, and environmental dynamics in shaping the  
1105 genetic landscape of *G. sabrinus* and *G. volans*. Overall, given the low percentage of  
1106 windows across the genome displaying one of the four selection scenario patters (<99%)  
1107 and the high  $F_{ST}$  estimate (0.308), speciation in allopatry and genetic drift likely drove the

1108 divergence of *G. sabrinus* and *G. volans*. The already high degree of divergence between  
1109 them (0.141) may have limited our ability to detect more signals of selection in allopatry.

1110         Despite the absence of recent hybridization evidence, changes in habitat, climate,  
1111 or ecological factors over the past two decades could influence hybridization dynamics  
1112 and gene flow, contributing to the genomic landscape patterns of genetic diversity and  
1113 differentiation we observed. Low rates of hybridization detected with microsatellite data  
1114 indicate that gene flow and hybridization have occurred in the recent past. Additionally,  
1115 ABBA-BABA and Treemix results indicate historical gene flow from *G. sabrinus* to *G.*  
1116 *volans*, this directionality of gene flow may be due to asymmetry in migration, or  
1117 differential adaptation to changing environments. Understanding the genetic history of *G.*  
1118 *sabrinus* and *G. volans* can inform conservation strategies for populations facing  
1119 environmental changes. Long-term monitoring and broader assessments of the genetic  
1120 diversity and population dynamics across the species ranges can provide valuable insights  
1121 into the adaptive potential and resilience of these species, and aid in the development of  
1122 targeted conservation initiatives, ensuring the preservation of both the unique genetic  
1123 makeup and the ecological roles of *G. sabrinus* and *G. volans* in the face of ongoing  
1124 environmental challenges.

1125

1126

1127

1128

1129

1130 GENERAL DISCUSSION

1131 ***Glaucomys* Hybridization under Climate Change**

1132         The complex dynamics of hybrid zones require consideration in the face of our  
1133 results. The evidence of low rates of hybridization 20 years ago with microsatellite data  
1134 suggests that gene flow between the two species was occurring, albeit at low levels, in the  
1135 recent past. It is possible that rapid changes in habitat, climate, or other ecological factors  
1136 over the past two decades, influenced the likelihood and extent of gene flow, and will  
1137 continue to do so into the future.

1138         The dynamics of hybrid zones can be influenced by factors such as selection  
1139 against hybrids, reinforcement of reproductive barriers, climate change, and changes in  
1140 the landscape affecting the likelihood of encounters between individuals from different  
1141 species (Arnold, 1992; Barton, 1979, 2001; Barton & Hewitt, 1985; Servedio & Noor,  
1142 2003; Taylor et al., 2015). Even if these sympatric populations of flying squirrels have  
1143 experienced further reinforcement of reproductive barriers in face of rare hybridization  
1144 events - climate change, range shifts and environmental changes can affect the temporal  
1145 reproductive isolation of closely related species and cause a collapse of reproductive  
1146 barriers (Canestrelli et al., 2017; Franks & Weis, 2009; Parmesan & Yohe, 2003;  
1147 Sánchez-Guillén et al., 2013; (Seehausen, 2006). Hybrid fitness can vary under climate  
1148 change (Chunco, 2014), as hybrids may adapt better to novel environmental conditions  
1149 than parental species (Abbott et al., 2013). In turn, infrequent hybrid mating can lead to  
1150 extensive introgression (Barton, 2001), potentially weakening reproductive barriers under  
1151 climate change (Owens & Samuk, 2020).

1152 **Microsatellite vs SNP data in Recent Hybridization Detection Results**

1153 While sample size, or changes to environmental and population dynamics that can  
1154 explain our lack of hybridization or introgression detection between *G. sabrinus* and *G.*  
1155 *volans*, the difference in genetic data used warrants consideration. Comparative studies  
1156 that investigate the detection of hybridization and introgression using SNP data versus  
1157 microsatellites have shown that genomic data outperforms microsatellites in identifying  
1158 genetic structure and introgressed regions (Miralles et al., 2023; Poelstra et al., 2022;  
1159 Szatmári et al., 2021). These studies indicate that the genomic SNP approach provides  
1160 more reliable and accurate results, without the false positive or false negative detections  
1161 microsatellite data is subjected to (Bradbury et al., 2015; Poelstra et al., 2022; Vähä &  
1162 Primmer, 2006).

1163         When we consider the previous rates of hybridization detection (<5%) in  
1164 *Glaucomys* species (Garroway et al., 2010; Lalor, 2014), it's possible that these detections  
1165 may have been false detections due to the performance of STRUCTURE analysis on  
1166 microsatellite data. Vähä & Primmer (2006) found that, to correctly identify over 95% of  
1167 samples with 90% accuracy, at least 12 or more loci are needed when  $F_{ST}=0.21$  to detect  
1168 hybrids and a minimum of 48 loci to detect backcrossing. Assuming a linear relationship  
1169 between  $F_{ST}$  and the number of loci required to detect hybrids, previous studies on  
1170 *Glaucomys* species using 7-10 loci (Garroway et al., 2010; Lalor, 2014; O'Brien et al.,  
1171 2021) should have been sufficient to detect hybrids, given this study's estimated global  
1172  $F_{ST}=0.308$  (e.g. Szatmári et al., 2021). We could not validate previous detections of  
1173 hybrids or introgressed individuals by Garroway et al. (2010) due to a lack of remaining  
1174 genetic material from that study. Only one sample in our study had been previously

1175 identified as a hybrid (ID: 535192) from microsatellite data and was not detected as an  
1176 admixed individual in this study. While we could not use SNP data to confirm detections  
1177 of hybridization between *G. sabrinus* and *G. volans* from approximately 20 years ago,  
1178 other studies have shown that even when employing correct methodology for  
1179 microsatellite approaches to detecting hybridization, SNP approaches perform better, and  
1180 previous conclusions based on a small number of loci should be interpreted with caution  
1181 (e.g. Miralles et al 2023).

1182         As comparative and genomic-based studies continue to be conducted, it is likely  
1183 that what was previously considered contemporary hybridization based on microsatellite  
1184 data may not be occurring or may be happening at different rates between interbreeding  
1185 populations than initially detected using microsatellites (Cairns et al., 2023; Kessler et al.,  
1186 2023; Miralles et al., 2023; Poelstra et al., 2022; Szatmári et al., 2021).

### 1187 **Limitations and Future Research**

1188 Our study encountered several limitations that warrant consideration in interpreting the  
1189 results and to guide future research efforts. The sample size in our study was limited,  
1190 totaling 114 individuals, may have impacted our ability to detect the rare hybridization  
1191 and introgression events previously identified using microsatellite genetic data. Future  
1192 research should aim for larger sample sizes to enhance statistical power and ability to  
1193 comprehensively understand population dynamics and hybridization patterns.  
1194 Furthermore, sampling primarily focused on sympatric sites, and one allopatric site  
1195 revealing unexpected species presence, indicating it did not represent a true allopatric  
1196 population. Expanding sampling efforts in future studies to cover a broader geographic  
1197 range for both species and ensuring accurate identification of allopatric sites may be  
1198 crucial for detecting finer-scale population structures, such as introgression, in sympatric

1199 populations. This will allow the consideration of population structure across multiple  
1200 scales to observe the difference in local events at smaller distances and broader dynamics,  
1201 across habitats and generations.

1202         Our sample size for each species was smaller than optimal for accurate Stairway  
1203 plot demographic history analysis which requires at least 100 individuals per population  
1204 with low-coverage sequencing data (Liu & Fu, 2020) and results are consistent with  
1205 overfitting (Lapierre et al., 2017). Our demographic history results need to be interpreted  
1206 with caution and emphasizes the need for larger sample sizes for each population to  
1207 ensure more robust and reliable demographic history reconstructions. Additionally,  
1208 including samples from the *G. oregonensis* would serve as a better outgroup for ABBA-  
1209 BABA and Treemix analyses to improve understanding of historical gene flow and  
1210 migration patterns between *G. sabrinus* and *G. volans*.

1211         Estimating recombination rates could significantly contribute to untangling the  
1212 selective forces driving speciation and understanding the degree of divergence along the  
1213 speciation continuum. Future research should incorporate methods to estimate  
1214 recombination rates across the genome and test correlation with genomic variation  
1215 measures. Lastly, improving the current reference genome assembly for *G. volans* can aid  
1216 future studies. The current reference genome assembly is fragmented, with small  
1217 scaffolds leading to gaps in the genome scan. An improved, more contiguous reference  
1218 genome assembly would enhance the accuracy of genomic analyses and provide a more  
1219 comprehensive view of the genomic landscape; and developing a gene-annotated  
1220 reference genome would allow for targeted exploration of potential genes under selection,  
1221 facilitating a more comprehensive investigation into speciation and adaptation processes.

1222           Addressing these limitations and incorporating these future research directions  
1223 will advance our understanding of genetic dynamics and inform conservation strategies  
1224 for flying squirrel populations.

## 1225 **Conclusions**

1226           Collectively, our results suggest that the speciation of these *Glaucomys* species is  
1227 the result of a complex history of geographic isolation, ecological divergence, range  
1228 expansions, inter-specific gene flow, and adaptations. Globally advantageous alleles  
1229 could have been maintained in both species following population splitting, maintaining  
1230 diversity within these genomic regions and across the genome during speciation. In  
1231 isolation, selection for ecologically adaptive traits would decrease diversity within  
1232 populations in regions under selection while increasing differentiation between these  
1233 species. During recent periods of population contact, some alleles may have been  
1234 exchanged; and alleles conferring an advantage could have sweep through the range  
1235 expanding *G. volans*. This process, potentially facilitated by the genomic regions under  
1236 balancing selection, emphasizes the intricate interplay of selection, introgression, and  
1237 adaptation in the speciation of these sympatric flying squirrels. However, the majority  
1238 genome does not display a pattern of selection, indicating that speciation in allopatry and  
1239 genetic drift were likely the main drivers of divergence of *G. sabrinus* and *G. volans*.  
1240 These findings shed light on the interplay of mechanisms driving the divergence of  
1241 closely related species in a changing environment.

1242

1243



1244 **References**

- 1245 Abbott, R., Albach, D., Ansell, S., Arntzen, J. W., Baird, S. J. E., Bierne, N., Boughman,  
1246 J., Brelsford, A., Buerkle, C. A., Buggs, R., Butlin, R. K., Dieckmann, U.,  
1247 Eroukhmanoff, F., Grill, A., Cahan, S. H., Hermansen, J. S., Hewitt, G., Hudson,  
1248 A. G., Jiggins, C., ... Zinner, D. (2013). Hybridization and speciation. *Journal of*  
1249 *Evolutionary Biology*, 26(2), 229–246. <https://doi.org/10.1111/j.1420->  
1250 [9101.2012.02599.x](https://doi.org/10.1111/j.1420-9101.2012.02599.x)
- 1251 de Abreu-Jr, E. F., Pavan, S. E., Tsuchiya, M. T. N., et al. (2020). Museomics of tree  
1252 squirrels: A dense taxon sampling of mitogenomes reveals hidden diversity,  
1253 phenotypic convergence, and the need of a taxonomic overhaul. *BMC*  
1254 *Evolutionary Biology*, 20(1), 77. <https://doi.org/10.1186/s12862-020-01639-y>
- 1255 Ackerman, M. S., Johri, P., Spitze, K., Xu, S., Doak, T. G., Young, K., & Lynch, M.  
1256 (2017). Estimating Seven Coefficients of Pairwise Relatedness Using Population-  
1257 Genomic Data. *Genetics*, 206(1), 105–118.  
1258 <https://doi.org/10.1534/genetics.116.190660>
- 1259 Adavoudi, R., & Pilot, M. (2022). Consequences of Hybridization in Mammals: A  
1260 Systematic Review. *Genes*, 13(1), Article 1.  
1261 <https://doi.org/10.3390/genes13010050>
- 1262 Andrews, S. (2010). FASTQC. A quality control tool for high throughput sequence data.  
1263 Available online at: <http://www.bioinformatics.babraham.ac.uk/projects/fastqc>
- 1264 Arbogast, B. S. (1999). Mitochondrial dna phylogeography of the new world flying  
1265 squirrels (glaucomys): implications for pleistocene biogeography. *Journal of*  
1266 *Mammalogy*, 80(1), 142-155. <https://doi.org/10.2307/1383215>
- 1267 Arbogast, B. S. (2007). A Brief History of the New World Flying Squirrels: Phylogeny,  
1268 Biogeography, and Conservation Genetics. *Journal of Mammalogy*, 88(4), 840–  
1269 849. <https://doi.org/10.1644/06-MAMM-S-322R1.1>
- 1270 Arbogast, B. S., Browne, R. A., Weigl, P. D., & Kenagy, G. J. (2005). Conservation  
1271 genetics of endangered flying squirrels (Glaucomys) from the Appalachian  
1272 mountains of eastern North America. *Animal Conservation*, 8(2), 123–133.  
1273 <https://doi.org/10.1017/S1367943004001830>

- 1274 Arnold, M. L. (1992). Natural Hybridization as an Evolutionary Process. *Annual Review*  
1275 *of Ecology and Systematics*, 23(1), 237-261.  
1276 <https://doi.org/10.1146/annurev.es.23.110192.001321>
- 1277 Arnold, M. L., & Kunte, K. (2017). Adaptive Genetic Exchange: A Tangled History of  
1278 Admixture and Evolutionary Innovation. *Trends in Ecology & Evolution*, 32(8),  
1279 601–611. <https://doi.org/10.1016/j.tree.2017.05.007>
- 1280 Bankevich, A., Nurk, S., Antipov, D., Gurevich, A. A., Dvorkin, M., Kulikov, A. S.,  
1281 Lesin, V. M., Nikolenko, S. I., Pham, S., Prjibelski, A. D., Pyshkin, A. V.,  
1282 Sirotkin, A. V., Vyahhi, N., Tesler, G., Alekseyev, M. A., & Pevzner, P. A.  
1283 (2012). SPAdes: A New Genome Assembly Algorithm and Its Applications to  
1284 Single-Cell Sequencing. *Journal of Computational Biology*, 19(5), 455–477.  
1285 <https://doi.org/10.1089/cmb.2012.0021>
- 1286 Barton, N. H. (1979). The dynamics of hybrid zones. *Heredity*, 43(3), Article 3.  
1287 <https://doi.org/10.1038/hdy.1979.87>
- 1288 Barton, N. H. (2001). The role of hybridization in evolution. *Molecular Ecology*, 10(3),  
1289 551–568. <https://doi.org/10.1046/j.1365-294x.2001.01216.x>
- 1290 Barton, N. H. & Hewitt, G. M. (1985). Analysis of hybrid zones. *Annual Review of*  
1291 *Ecology and Systematics*, 16(1), 113-148.  
1292 <https://doi.org/10.1146/annurev.es.16.110185.000553>
- 1293 Bay, R., Caplins, S., Guerra, V., & Armstrong, M. (2021). *Marine genomics, UC Davis*  
1294 *Department of Evolution and Ecology*. Available From:  
1295 [https://baylab.github.io/MarineGenomics/week9--population-structure-using-](https://baylab.github.io/MarineGenomics/week9--population-structure-using-ngsadmix.html#how-do-we-know-which-k-to-pick)  
1296 [ngsadmix.html#how-do-we-know-which-k-to-pick](https://baylab.github.io/MarineGenomics/week9--population-structure-using-ngsadmix.html#how-do-we-know-which-k-to-pick)
- 1297 Beaumont, M. A. (2005). Adaptation and speciation: What can Fst tell us? *Trends in*  
1298 *Ecology & Evolution*, 20(8), 435–440. <https://doi.org/10.1016/j.tree.2005.05.017>
- 1299 Bowman, J., Holloway, G. L., Malcolm, J. R., Middel, K. R., & Wilson, P. J. (2005).  
1300 Northern range boundary dynamics of southern flying squirrels: Evidence of an  
1301 energetic bottleneck. *Canadian Journal of Zoology*, 83(11), 1486–1494.  
1302 <https://doi.org/10.1139/z05-144>
- 1303 Bradbury, I. R., Hamilton, L. C., Dempson, B., Robertson, M. J., Bourret, V., Bernatchez,  
1304 L., & Verspoor, E. (2015). Transatlantic secondary contact in Atlantic Salmon,

1305 comparing microsatellites, a single nucleotide polymorphism array and  
1306 restriction-site associated DNA sequencing for the resolution of complex spatial  
1307 structure. *Molecular Ecology*, 24(20), 5130–5144.  
1308 <https://doi.org/10.1111/mec.13395>

1309 Cairns, K. M., Crowther, M. S., Parker, H. G., Ostrander, E. A., & Letnic, M. (2023).  
1310 Genome-wide variant analyses reveal new patterns of admixture and population  
1311 structure in Australian dingoes. *Molecular Ecology*, 32(15), 4133–4150.  
1312 <https://doi.org/10.1111/mec.16998>

1313 Camacho, C., Coulouris, G., Avagyan, V., Ma, N., Papadopoulos, J., Bealer, K., &  
1314 Madden, T. L. (2009). BLAST+: Architecture and applications. *BMC*  
1315 *Bioinformatics*, 10(1), 421. <https://doi.org/10.1186/1471-2105-10-421>

1316 Camacho-Sanchez, M., Velo-Antón, G., Hanson, J. O., Veríssimo, A., Martínez-Solano,  
1317 Í., Marques, A., Moritz, C., & Carvalho, S. B. (2020). Comparative assessment of  
1318 range-wide patterns of genetic diversity and structure with SNPs and  
1319 microsatellites: A case study with Iberian amphibians. *Ecology and Evolution*,  
1320 10(19), 10353–10363. <https://doi.org/10.1002/ece3.6670>

1321 Canestrelli, D., Bisconti, R., Chiochio, A., Maiorano, L., Zampiglia, M., & Nascetti, G.  
1322 (2017). Climate change promotes hybridisation between deeply divergent species.  
1323 *PeerJ*, 5, e3072. <https://doi.org/10.7717/peerj.3072>

1324 Catchen, J., Hohenlohe, P. A., Bassham, S., Amores, A., & Cresko, W. A. (2013). Stacks:  
1325 An analysis tool set for population genomics. *Molecular Ecology*, 22(11), 3124–  
1326 3140. <https://doi.org/10.1111/mec.12354>

1327 Charlesworth B. (1998). Measures of divergence between populations and the effect of  
1328 forces that reduce variability. *Molecular biology and evolution*, 15(5), 538–543.  
1329 <https://doi.org/10.1093/oxfordjournals.molbev.a025953>

1330 Chen, N., Jurić, I., Cosgrove, E. J., Bowman, R., Fitzpatrick, J. W., Schoech, S. J., ... &  
1331 Coop, G. (2018). Allele frequency dynamics in a pedigreed natural population.  
1332 *Proceedings of the National Academy of Sciences*, 116(6), 2158-2164.  
1333 <https://doi.org/10.1073/pnas.1813852116>

1334 Chunco, A. J. (2014). Hybridization in a warmer world. *Ecology and Evolution*, 4(10),  
1335 2019–2031. <https://doi.org/10.1002/ece3.1052>

1336 Coates, B. S., Sumerford, D. V., Miller, N. J., Kim, K. S., Sappington, T. W., Siegfried,  
1337 B. D., & Lewis, L. C. (2009). Comparative Performance of Single Nucleotide  
1338 Polymorphism and Microsatellite Markers for Population Genetic Analysis.  
1339 *Journal of Heredity*, 100(5), 556–564. <https://doi.org/10.1093/jhered/esp028>  
1340 COSEWIC. (1998). *Southern Flying Squirrel (Glaucomys volans) COSEWIC assessment*  
1341 *and status report* . Available From: [https://www.canada.ca/en/environment-](https://www.canada.ca/en/environment-climate-change/services/species-risk-public-registry/cosewic-assessments-status-reports/southern-flying-squirrel/chapter-2.html)  
1342 [climate-change/services/species-risk-public-registry/cosewic-assessments-status-](https://www.canada.ca/en/environment-climate-change/services/species-risk-public-registry/cosewic-assessments-status-reports/southern-flying-squirrel/chapter-2.html)  
1343 [reports/southern-flying-squirrel/chapter-2.html](https://www.canada.ca/en/environment-climate-change/services/species-risk-public-registry/cosewic-assessments-status-reports/southern-flying-squirrel/chapter-2.html)  
1344 Coyne, J. A., & Orr, H. A. (1989). Patterns of speciation in *Drosophila*. *Evolution*, 43(2),  
1345 362–381. <https://doi.org/10.1111/j.1558-5646.1989.tb04233.x>  
1346 Cruickshank, T. E., & Hahn, M. W. (2014). Reanalysis suggests that genomic islands of  
1347 speciation are due to reduced diversity, not reduced gene flow. *Molecular*  
1348 *Ecology*, 23(13), 3133–3157. <https://doi.org/10.1111/mec.12796>  
1349 De La Torre, A., Ingvarsson, P. K., & Aitken, S. N. (2015). Genetic architecture and  
1350 genomic patterns of gene flow between hybridizing species of *Picea*. *Heredity*,  
1351 115(2), Article 2. <https://doi.org/10.1038/hdy.2015.19>  
1352 Delmore, K. E., Hübner, S., Kane, N. C., Schuster, R., Andrew, R. L., Câmara, F., Guigó,  
1353 R., & Irwin, D. E. (2015). Genomic analysis of a migratory divide reveals  
1354 candidate genes for migration and implicates selective sweeps in generating  
1355 islands of differentiation. *Molecular Ecology*, 24(8), 1873–1888.  
1356 <https://doi.org/10.1111/mec.13150>  
1357 Desantis, L. M., Bowman, J., Vijayan, M. M., & Burness, G. (2018). Seasonal changes in  
1358 acute stressor-mediated plasma glucocorticoid regulation in New World flying  
1359 squirrels. *General and Comparative Endocrinology*, 266, 78–86.  
1360 <https://doi.org/10.1016/j.ygcen.2018.04.026>  
1361 Duranton, M., Allal, F., Fraïsse, C., Bierne, N., Bonhomme, F., & Gagnaire, P.-A.  
1362 (2018). The origin and remolding of genomic islands of differentiation in the  
1363 European sea bass. *Nature Communications*, 9. [https://doi.org/10.1038/s41467-](https://doi.org/10.1038/s41467-018-04963-6)  
1364 [018-04963-6](https://doi.org/10.1038/s41467-018-04963-6)

- 1365 Ewels, P., Magnusson, M., Lundin, S., & Källér, M. (2016). MultiQC: summarize  
1366 analysis results for multiple tools and samples in a single report. *Bioinformatics*,  
1367 32(19), 3047–3048. <https://doi.org/10.1093/bioinformatics/btw354>
- 1368 Feder, J. L., Egan, S. P., & Nosil, P. (2012). The genomics of speciation-with-gene-flow.  
1369 *Trends in Genetics: TIG*, 28(7), 342–350.  
1370 <https://doi.org/10.1016/j.tig.2012.03.009>
- 1371 Feder, J. L., & Nosil, P. (2010). The Efficacy of Divergence Hitchhiking in Generating  
1372 Genomic Islands During Ecological Speciation. *Evolution*, 64(6), 1729–1747.  
1373 <https://doi.org/10.1111/j.1558-5646.2009.00943.x>
- 1374 Fischer, M. C., Rellstab, C., Leuzinger, M., Roumet, M., Gugerli, F., Shimizu, K. K.,  
1375 Holderegger, R., & Widmer, A. (2017). Estimating genomic diversity and  
1376 population differentiation – an empirical comparison of microsatellite and SNP  
1377 variation in *Arabidopsis halleri*. *BMC Genomics*, 18(1), 69.  
1378 <https://doi.org/10.1186/s12864-016-3459-7>
- 1379 Fitak, R. R. (2021). *OptM*: Estimating the optimal number of migration edges on  
1380 population trees using *Treemix*. *Biology Methods and Protocols*, 6(1), bpab017.  
1381 <https://doi.org/10.1093/biomethods/bpab017>
- 1382 Franks, S. J., & Weis, A. E. (2009). Climate change alters reproductive isolation and  
1383 potential gene flow in an annual plant. *Evolutionary Applications*, 2(4), 481–488.  
1384 <https://doi.org/10.1111/j.1752-4571.2009.00073.x>
- 1385 Fumagalli, M., Vieira, F. G., Linderoth, T., & Nielsen, R. (2014). ngsTools: Methods for  
1386 population genetics analyses from next-generation sequencing data.  
1387 *Bioinformatics*, 30(10), 1486–1487. <https://doi.org/10.1093/bioinformatics/btu041>
- 1388 Garroway, C. J., Bowman, J., Cascaden, T. J., Holloway, G. L., Mahan, C. G., Malcolm,  
1389 J. R., Steele, M. A., Turner, G., & Wilson, P. J. (2010). Climate change induced  
1390 hybridization in flying squirrels. *Global Change Biology*, 16(1), 113–121.  
1391 <https://doi.org/10.1111/j.1365-2486.2009.01948.x>
- 1392 Garroway, C. J., Bowman, J., & Wilson, P. J. (2013). Complex social structure of  
1393 southern flying squirrels is related to spatial proximity but not kinship. *Behavioral*  
1394 *Ecology and Sociobiology*, 67(1), 113–122. [https://doi.org/10.1007/s00265-012-](https://doi.org/10.1007/s00265-012-1431-3)  
1395 1431-3

1396 Grossen, C., Keller, L., Biebach, I., Consortium, T. I. G. G., & Croll, D. (2014).  
1397 Introgression from Domestic Goat Generated Variation at the Major  
1398 Histocompatibility Complex of Alpine Ibex. *PLOS Genetics*, *10*(6), e1004438.  
1399 <https://doi.org/10.1371/journal.pgen.1004438>

1400 Gossmann, T. I., Shanmugasundram, A., Börno, S., Duvaux, L., Lemaire, C., Kuhl, H.,  
1401 Klages, S., Roberts, L. D., Schade, S., Gostner, J. M., Hildebrand, F., Vowinckel,  
1402 J., Bichet, C., Mülleder, M., Calvani, E., Zelezniak, A., Griffin, J. L., Bork, P.,  
1403 Allaine, D., ... Ralsler, M. (2019). Ice-Age Climate Adaptations Trap the Alpine  
1404 Marmot in a State of Low Genetic Diversity. *Current Biology*, *29*(10), 1712-  
1405 1720.e7. <https://doi.org/10.1016/j.cub.2019.04.020>

1406 Hänfling, B., Bolton, P., Harley, M., & Carvalho, G. R. (2005). A molecular approach to  
1407 detect hybridisation between crucian carp (*Carassius carassius*) and non-  
1408 indigenous carp species (*Carassius* spp. And *Cyprinus carpio*). *Freshwater*  
1409 *Biology*, *50*(3), 403–417. <https://doi.org/10.1111/j.1365-2427.2004.01330.x>

1410 Helyar, S. J., Hemmer-Hansen, J., Bekkevold, D., Taylor, M. I., Ogden, R., Limborg, M.  
1411 T., Cariani, A., Maes, G. E., Diopere, E., Carvalho, G. R., & Nielsen, E. E.  
1412 (2011). Application of SNPs for population genetics of nonmodel organisms:  
1413 New opportunities and challenges. *Molecular Ecology Resources*, *11*(s1), 123–  
1414 136. <https://doi.org/10.1111/j.1755-0998.2010.02943.x>

1415 Hewitt, G. (1996). Some genetic consequences of ice ages, and their role in divergence  
1416 and speciation. *Biological Journal of the Linnean Society*, *58*(3), 247–276.  
1417 <https://doi.org/10.1006/bijl.1996.0035>

1418 Hewitt, G. (2000). The genetic legacy of the Quaternary ice ages. *Nature*, *405*(6789),  
1419 907–913. <https://doi.org/10.1038/35016000>

1420 Holsinger, K. E., & Weir, B. S. (2009). Genetics in geographically structured  
1421 populations: Defining, estimating and interpreting FST. *Nature Reviews*.  
1422 *Genetics*, *10*(9), 639–650. <https://doi.org/10.1038/nrg2611>

1423 Irwin, D. E., Alcaide, M., Delmore, K. E., Irwin, J. H., & Owens, G. L. (2016). Recurrent  
1424 selection explains parallel evolution of genomic regions of high relative but low  
1425 absolute differentiation in a ring species. *Molecular Ecology*, *25*(18), 4488–4507.  
1426 <https://doi.org/10.1111/mec.13792>

- 1427 Irwin, D. E., Milá, B., Toews, D. P. L., Brelsford, A., Kenyon, H. L., Porter, A. N.,  
1428 Grossen, C., Delmore, K. E., Alcaide, M., & Irwin, J. H. (2018). A comparison of  
1429 genomic islands of differentiation across three young avian species pairs.  
1430 *Molecular Ecology*, 27(23), 4839–4855. <https://doi.org/10.1111/mec.14858>
- 1431 Jin, J.-J., Yu, W.-B., Yang, J.-B., Song, Y., dePamphilis, C. W., Yi, T.-S., & Li, D.-Z.  
1432 (2020). GetOrganelle: A fast and versatile toolkit for accurate de novo assembly  
1433 of organelle genomes. *Genome Biology*, 21(1), 241.  
1434 <https://doi.org/10.1186/s13059-020-02154-5>
- 1435 Jones, M. R., Mills, L. S., Alves, P. C., Callahan, C. M., Alves, J. M., Lafferty, D. J. R.,  
1436 Jiggins, F. M., Jensen, J. D., Melo-Ferreira, J., & Good, J. M. (2018). Adaptive  
1437 introgression underlies polymorphic seasonal camouflage in snowshoe hares.  
1438 *Science*, 360(6395), 1355–1358. <https://doi.org/10.1126/science.aar5273>
- 1439 Jun, G., Wing, M. K., Abecasis, G. R., & Kang, H. M. (2015). An efficient and scalable  
1440 analysis framework for variant extraction and refinement from population-scale  
1441 DNA sequence data. *Genome Research*, 25(6), 918–925.  
1442 <https://doi.org/10.1101/gr.176552.114>
- 1443 Kalia, R. K., Rai, M. K., Kalia, S., Singh, R., & Dhawan, A. K. (2011). Microsatellite  
1444 markers: An overview of the recent progress in plants. *Euphytica*, 177(3), 309–  
1445 334. <https://doi.org/10.1007/s10681-010-0286-9>
- 1446 Kalyaanamoorthy, S., Minh, B. Q., Wong, T. K. F., von Haeseler, A., & Jermini, L. S.  
1447 (2017). ModelFinder: Fast model selection for accurate phylogenetic estimates.  
1448 *Nature Methods*, 14(6), Article 6. <https://doi.org/10.1038/nmeth.4285>
- 1449 Katoh, K., & Standley, D. M. (2013). MAFFT Multiple Sequence Alignment Software  
1450 Version 7: Improvements in Performance and Usability. *Molecular Biology and*  
1451 *Evolution*, 30(4), 772–780. <https://doi.org/10.1093/molbev/mst010>
- 1452 Kerhoulas, N. J., & Arbogast, B. S. (2010). Molecular systematics and Pleistocene  
1453 biogeography of Mesoamerican flying squirrels. *Journal of Mammalogy*, 91(3),  
1454 654–667. <https://doi.org/10.1644/09-MAMM-A-260.1>
- 1455 Kessler, C., Wootton, E., & Shafer, A. B. A. (2023). Speciation without gene-flow in  
1456 hybridizing deer. *Molecular Ecology*, 32(5), 1117–1132.  
1457 <https://doi.org/10.1111/mec.16824>

- 1458 Korneliussen, T. S., Albrechtsen, A., & Nielsen, R. (2014). ANGSD: Analysis of Next  
1459 Generation Sequencing Data. *BMC Bioinformatics*, *15*(1), 356.  
1460 <https://doi.org/10.1186/s12859-014-0356-4>
- 1461 Korneliussen, T. S., & Moltke, I. (2015). NgsRelate: A software tool for estimating  
1462 pairwise relatedness from next-generation sequencing data. *Bioinformatics*,  
1463 *31*(24), 4009–4011. <https://doi.org/10.1093/bioinformatics/btv509>
- 1464 Korneliussen, T. S., Moltke, I., Albrechtsen, A., & Nielsen, R. (2013). Calculation of  
1465 Tajima's D and other neutrality test statistics from low depth next-generation  
1466 sequencing data. *BMC Bioinformatics*, *14*(1), 289. [https://doi.org/10.1186/1471-](https://doi.org/10.1186/1471-2105-14-289)  
1467 [2105-14-289](https://doi.org/10.1186/1471-2105-14-289)
- 1468 Kumar, S., Banks, T. W., & Cloutier, S. (2012). SNP Discovery through Next-Generation  
1469 Sequencing and Its Applications. *International Journal of Plant Genomics*, *2012*,  
1470 1–15. <https://doi.org/10.1155/2012/831460>
- 1471 Kumar, S., & Subramanian, S. (2002). Mutation rates in mammalian genomes.  
1472 *Proceedings of the National Academy of Sciences*, *99*(2), 803–808.  
1473 <https://doi.org/10.1073/pnas.022629899>
- 1474 Lalor, J.L. (2014). *Selection on functional genes across a flying squirrel (genus*  
1475 *Glaucomys) hybrid zone*. [Master's Thesis, Trent University]. Available From:  
1476 <https://digitalcollections.trentu.ca/islandora/object/etd:243>
- 1477 Langmead, B., & Salzberg, S. L. (2012). Fast gapped-read alignment with Bowtie 2.  
1478 *Nature Methods*, *9*(4), Article 4. <https://doi.org/10.1038/nmeth.1923>
- 1479 Lapierre, M., Lambert, A., & Achaz, G. (2017). Accuracy of demographic inferences  
1480 from the site frequency spectrum: the case of the yoruba population. *Genetics*,  
1481 *206*(1), 439-449. <https://doi.org/10.1534/genetics.116.192708>
- 1482 Lemopoulos, A., Prokkola, J. M., Uusi-Heikkilä, S., Vasemägi, A., Huusko, A.,  
1483 Hyvärinen, P., ... & Vainikka, A. (2019). Comparing radseq and microsatellites  
1484 for estimating genetic diversity and relatedness — implications for brown trout  
1485 conservation. *Ecology and Evolution*, *9*(4), 2106-2120.  
1486 <https://doi.org/10.1002/ece3.4905>



- 1487 Li, H. (2011). A statistical framework for SNP calling, mutation discovery, association  
1488 mapping and population genetical parameter estimation from sequencing data.  
1489 *Bioinformatics*, 27(21), 2987–2993. <https://doi.org/10.1093/bioinformatics/btr509>
- 1490 Li H. (2013). Aligning sequence reads, clone sequences and assembly contigs with  
1491 BWA-MEM. arXiv:1303.3997v2 [q-bio.GN].
- 1492 Li, S.H., Yeung, C. K.-L., Han, L., Le, M. H., Wang, C., Ding, P., & Yao, C. (2010a).  
1493 Genetic introgression between an introduced babbler, the Chinese hwamei  
1494 *Leucodioptron c. canorum*, and the endemic Taiwan hwamei *L. taewanus*: A  
1495 multiple marker systems analysis. *Journal of Avian Biology*, 41(1), 64–73.  
1496 <https://doi.org/10.1111/j.1600-048X.2009.04719.x>
- 1497 Li, Y., Vinckenbosch, N., Tian, G., Huerta-Sanchez, E., Jiang, T., Jiang, H., Albrechtsen,  
1498 A., Andersen, G., Cao, H., Korneliussen, T., Grarup, N., Guo, Y., Hellman, I., Jin,  
1499 X., Li, Q., Liu, J., Liu, X., Sparsø, T., Tang, M., ... Wang, J. (2010b).  
1500 Resequencing of 200 human exomes identifies an excess of low-frequency non-  
1501 synonymous coding variants. *Nature Genetics*, 42(11), 969–972.  
1502 <https://doi.org/10.1038/ng.680>
- 1503 Lim, M. C. W., Bi, K., Witt, C. C., Graham, C. H., & Dávalos, L. M. (2021). Pervasive  
1504 Genomic Signatures of Local Adaptation to Altitude Across Highland Specialist  
1505 Andean Hummingbird Populations. *Journal of Heredity*, 112(3), 229–240.  
1506 <https://doi.org/10.1093/jhered/esab008>
- 1507 Liu, X., & Fu, Y.-X. (2020). Stairway Plot 2: Demographic history inference with folded  
1508 SNP frequency spectra. *Genome Biology*, 21(1), 280.  
1509 <https://doi.org/10.1186/s13059-020-02196-9>
- 1510 Mallet, J. (2005). Hybridization as an invasion of the genome. *Trends in Ecology &*  
1511 *Evolution*, 20(5), 229–237. <https://doi.org/10.1016/j.tree.2005.02.010>
- 1512 Matute, D. R. (2010). Reinforcement Can Overcome Gene Flow during Speciation in  
1513 *Drosophila*. *Current Biology*, 20(24), 2229–2233.  
1514 <https://doi.org/10.1016/j.cub.2010.11.036>
- 1515 McKenna, A., Hanna, M., Banks, E., Sivachenko, A., Cibulskis, K., Kernytzky, A.,  
1516 Garimella, K., Altshuler, D., Gabriel, S., Daly, M., & DePristo, M. A. (2010). The  
1517 Genome Analysis Toolkit: A MapReduce framework for analyzing next-

1518 generation DNA sequencing data. *Genome Research*, 20(9), 1297–1303.  
1519 <https://doi.org/10.1101/gr.107524.110>

1520 Meisner, J., & Albrechtsen, A. (2018). Inferring Population Structure and Admixture  
1521 Proportions in Low-Depth NGS Data. *Genetics*, 210(2), 719–731.  
1522 <https://doi.org/10.1534/genetics.118.301336>

1523 Minns, R., Persad, R., Menelon, L., Newar, S., O’Brien, P. P., Stead, S. M., & Bowman, J.  
1524 2024. Seasonal nest selection of sympatric North American flying squirrels.  
1525 *Wildlife Research*. <https://doi.org/10.1071/WR23041>

1526 Miralles, A., Secondi, J., Pabijan, M., Babik, W., Lemaire, C., & Crochet, P.-A. (2023).  
1527 *Inconsistent estimates of hybridization frequency in newts revealed by SNPs and*  
1528 *microsatellites* [preprint]. bioRxiv. <https://doi.org/10.1101/2023.01.21.525005>

1529 Morin, P. A., Luikart, G., Wayne, R. K., & the SNP workshop group. (2004). SNPs in  
1530 ecology, evolution and conservation. *Trends in Ecology & Evolution*, 19(4), 208–  
1531 216. <https://doi.org/10.1016/j.tree.2004.01.009>

1532 Muñoz, I., Henriques, D., Jara, L., Johnston, J. S., Chávez-Galarza, J., De La Rúa, P., &  
1533 Pinto, M. A. (2017). SNPs selected by information content outperform randomly  
1534 selected microsatellite loci for delineating genetic identification and introgression  
1535 in the endangered dark European honeybee (*Apis mellifera mellifera*). *Molecular*  
1536 *Ecology Resources*, 17(4), 783–795. <https://doi.org/10.1111/1755-0998.12637>

1537 Nei, M. and Li, W. (1979). Mathematical model for studying genetic variation in terms of  
1538 restriction endonucleases. *Proceedings of the National Academy of Sciences*,  
1539 76(10), 5269-5273. <https://doi.org/10.1073/pnas.76.10.5269>

1540 Newar, S. L., & Bowman, J. (2020). Think Before They Squeak: Vocalizations of the  
1541 Squirrel Family. *Frontiers in Ecology and Evolution*, 8, 193.  
1542 <https://doi.org/10.3389/fevo.2020.00193>

1543 Nguyen, L.-T., Schmidt, H. A., von Haeseler, A., & Minh, B. Q. (2015). IQ-TREE: A  
1544 Fast and Effective Stochastic Algorithm for Estimating Maximum-Likelihood  
1545 Phylogenies. *Molecular Biology and Evolution*, 32(1), 268–274.  
1546 <https://doi.org/10.1093/molbev/msu300>

1547 Nielsen, R., Korneliussen, T., Albrechtsen, A., Li, Y., & Wang, J. (2012). SNP Calling,  
1548 Genotype Calling, and Sample Allele Frequency Estimation from New-

1549           Generation Sequencing Data. *PLoS ONE*, 7(7), e37558.  
1550           <https://doi.org/10.1371/journal.pone.0037558>

1551   Nosil, P., & Feder, J. L. (2012). Genomic divergence during speciation: Causes and  
1552           consequences. *Philosophical Transactions of the Royal Society B: Biological*  
1553           *Sciences*, 367(1587), 332–342. <https://doi.org/10.1098/rstb.2011.0263>

1554   Nosil, P., Harmon, L. J., & Seehausen, O. (2009). Ecological explanations for  
1555           (incomplete) speciation. *Trends in Ecology & Evolution*, 24(3), 145–156.  
1556           <https://doi.org/10.1016/j.tree.2008.10.011>

1557   O'Brien, P. P., Bowman, J., Coombs, A. B., Newar, S. L., & Garroway, C. J. (2021).  
1558           Winter nest trees of sympatric northern ( *Glaucomys sabrinus* ) and southern ( *Glaucomys volans* ) flying squirrels: A test of reinforcement in a hybrid zone.  
1559           *Canadian Journal of Zoology*, 99(10), 859–866. [https://doi.org/10.1139/cjz-2021-](https://doi.org/10.1139/cjz-2021-0086)  
1561           0086

1562   Olson, M. N., Bowman, J., & Burness, G. (2017). Seasonal energetics and torpor use in  
1563           north american flying squirrels. *Journal of Thermal Biology*, 70, 46-53.  
1564           <https://doi.org/10.1016/j.jtherbio.2017.10.006>

1565   Owens, G. L., & Samuk, K. (2020). Adaptive introgression during environmental change  
1566           can weaken reproductive isolation. *Nature Climate Change*, 10(1), Article 1.  
1567           <https://doi.org/10.1038/s41558-019-0628-0>

1568   Parmesan, C., & Yohe, G. (2003). A globally coherent fingerprint of climate change  
1569           impacts across natural systems. *Nature*, 421(6918), 37–42.  
1570           <https://doi.org/10.1038/nature01286>

1571   Penalba, J. (22 October, 2016). calcDxy.R. Retrieved October 6, 2023, from  
1572           <https://github.com/mfumagalli/ngsPopGen/blob/master/scripts/calcDxy.R>

1573   Persad, R. (2023). *Home range size, habitat selection, and mycophagy of sympatric North*  
1574           *American flying squirrels*. [Master's Thesis, Trent University].

1575   Pfennig, K. S. (2003). A TEST OF ALTERNATIVE HYPOTHESES FOR THE  
1576           EVOLUTION OF REPRODUCTIVE ISOLATION BETWEEN SPADEFOOT  
1577           TOADS: SUPPORT FOR THE REINFORCEMENT HYPOTHESIS. *Evolution*,  
1578           57(12), 2842–2851. <https://doi.org/10.1111/j.0014-3820.2003.tb01525.x>

- 1579 Pickrell, J. K., & Pritchard, J. K. (2012). Inference of Population Splits and Mixtures  
1580 from Genome-Wide Allele Frequency Data. *PLoS Genetics*, 8(11), e1002967.  
1581 <https://doi.org/10.1371/journal.pgen.1002967>
- 1582 Pinho, C., & Hey, J. (2010). Divergence with Gene Flow: Models and Data. *Annual*  
1583 *Review of Ecology, Evolution, and Systematics*, 41(1), 215–230.  
1584 <https://doi.org/10.1146/annurev-ecolsys-102209-144644>
- 1585 Poelstra, J. W., Montero, B. K., Lüdemann, J., Yang, Z., Rakotondranary, S. J.,  
1586 Hohenlohe, P., Stetter, N., Ganzhorn, J. U., & Yoder, A. D. (2022). RADseq data  
1587 reveal a lack of admixture in a mouse lemur contact zone contrary to previous  
1588 microsatellite results. *Proceedings. Biological sciences*, 289(1980), 20220596.  
1589 <https://doi.org/10.1098/rspb.2022.0596>
- 1590 Pompanon, F., Bonin, A., Bellemain, E., & Taberlet, P. (2005). Genotyping errors:  
1591 Causes, consequences and solutions. *Nature Reviews Genetics*, 6(11), Article 11.  
1592 <https://doi.org/10.1038/nrg1707>
- 1593 Quilodrán, C. S., Ruegg, K., Sendell-Price, A. T., Anderson, E. C., Coulson, T., & Clegg,  
1594 S. M. (2020). The multiple population genetic and demographic routes to islands  
1595 of genomic divergence. *Methods in Ecology and Evolution*, 11(1), 6–21.  
1596 <https://doi.org/10.1111/2041-210X.13324>
- 1597 Ravinet, M., Faria, R., Butlin, R. K., Galindo, J., Bierne, N., Rafajlović, M., Noor, M. A.  
1598 F., Mehlig, B., & Westram, A. M. (2017). Interpreting the genomic landscape of  
1599 speciation: A road map for finding barriers to gene flow. *Journal of Evolutionary*  
1600 *Biology*, 30(8), 1450–1477. <https://doi.org/10.1111/jeb.13047>
- 1601 Rundle, H. D., & Nosil, P. (2005). Ecological speciation. *Ecology Letters*, 8(3), 336–352.  
1602 <https://doi.org/10.1111/j.1461-0248.2004.00715.x>
- 1603 Saint-Pé, K., Leitwein, M., Tissot, L., Poulet, N., Guinand, B., Berrebi, P., Marselli, G.,  
1604 Lascaux, J.-M., Gagnaire, P.-A., & Blanchet, S. (2019). Development of a large  
1605 SNPs resource and a low-density SNP array for brown trout (*Salmo trutta*)  
1606 population genetics. *BMC Genomics*, 20(1), 582. [https://doi.org/10.1186/s12864-](https://doi.org/10.1186/s12864-019-5958-9)  
1607 [019-5958-9](https://doi.org/10.1186/s12864-019-5958-9)
- 1608 Sánchez-Guillén, R. A., Muñoz, J., Rodríguez-Tapia, G., Arroyo, T. P. F., & Córdoba-  
1609 Aguilar, A. (2013). Climate-Induced Range Shifts and Possible Hybridisation

1610 Consequences in Insects. *PLOS ONE*, 8(11), e80531.  
1611 <https://doi.org/10.1371/journal.pone.0080531>

1612 Schluter, D. (2009). Evidence for Ecological Speciation and Its Alternative. *Science*,  
1613 323(5915), 737–741. <https://doi.org/10.1126/science.1160006>

1614 Seehausen, O. (2006). Conservation: Losing Biodiversity by Reverse Speciation. *Current*  
1615 *Biology*, 16(9), R334–R337. <https://doi.org/10.1016/j.cub.2006.03.080>

1616 Sendell-Price, A. T., Ruegg, K. C., Anderson, E. C., Quilodrán, C. S., Van Doren, B. M.,  
1617 Underwood, V. L., Coulson, T., & Clegg, S. M. (2020). The Genomic Landscape  
1618 of Divergence Across the Speciation Continuum in Island-Colonising Silvereyes  
1619 (*Zosterops lateralis*). *G3: Genes|Genomes|Genetics*, 10(9), 3147–3163.  
1620 <https://doi.org/10.1534/g3.120.401352>

1621 Servedio, M. R., & Noor, M. A. F. (2003). The Role of Reinforcement in Speciation:  
1622 Theory and Data. *Annual Review of Ecology, Evolution, and Systematics*, 34(1),  
1623 339–364. <https://doi.org/10.1146/annurev.ecolsys.34.011802.132412>

1624 Shang, H., Field, D. L., Paun, O., Rendón-Anaya, M., Hess, J., Vogl, C., Liu, J.,  
1625 Ingvarsson, P. K., Lexer, C., & Leroy, T. (2023). Drivers of genomic landscapes  
1626 of differentiation across a *Populus* divergence gradient. *Molecular Ecology*,  
1627 32(15), 4348–4361. <https://doi.org/10.1111/mec.17034>

1628 Skotte, L., Korneliussen, T. S., & Albrechtsen, A. (2013). Estimating Individual  
1629 Admixture Proportions from Next Generation Sequencing Data. *Genetics*, 195(3),  
1630 693–702. <https://doi.org/10.1534/genetics.113.154138>

1631 Soraggi, S., Wiuf, C., & Albrechtsen, A. (2018). Powerful Inference with the D-Statistic  
1632 on Low-Coverage Whole-Genome Data. *G3 Genes|Genomes|Genetics*, 8(2), 551–  
1633 566. <https://doi.org/10.1534/g3.117.300192>

1634 Stapp, P., & Mautz, W. W. (1991). Breeding Habits and Postnatal Growth of the  
1635 Southern Flying Squirrel (*Glaucomys volans*) in New Hampshire. *The American*  
1636 *Midland Naturalist*, 126(1), 203–208. <https://doi.org/10.2307/2426165>

1637 Stephan, W. (2010). Genetic hitchhiking versus background selection: The controversy  
1638 and its implications. *Philosophical Transactions: Biological Sciences*, 365(1544),  
1639 1245–1253.

- 1640 Stroupe, S., Forgacs, D., Harris, A., Derr, J. N., & Davis, B. W. (2022). Genomic  
1641 evaluation of hybridization in historic and modern North American Bison (Bison  
1642 bison). *Scientific Reports*, *12*(1), Article 1. [https://doi.org/10.1038/s41598-022-](https://doi.org/10.1038/s41598-022-09828-z)  
1643 [09828-z](https://doi.org/10.1038/s41598-022-09828-z)
- 1644 Sunde, J., Yıldırım, Y., Tibblin, P., & Forsman, A. (2020). Comparing the Performance  
1645 of Microsatellites and RADseq in Population Genetic Studies: Analysis of Data  
1646 for Pike (*Esox lucius*) and a Synthesis of Previous Studies. *Frontiers in Genetics*,  
1647 *11*. <https://www.frontiersin.org/articles/10.3389/fgene.2020.00218>
- 1648 Szatmári, L., Cserkés, T., Laczkó, L., Lanszki, J., Pertoldi, C., Abramov, A. V.,  
1649 Elmeros, M., Ottlecz, B., Hegyeli, Z., & Sramkó, G. (2021). A comparison of  
1650 microsatellites and genome-wide SNPs for the detection of admixture brings the  
1651 first molecular evidence for hybridization between *Mustela eversmanii* and  
1652 *M. putorius* (Mustelidae, Carnivora). *Evolutionary Applications*, *14*(9), 2286–  
1653 2304. <https://doi.org/10.1111/eva.13291>
- 1654 Tajima, F. (1989). Statistical method for testing the neutral mutation hypothesis by DNA  
1655 polymorphism. *Genetics*, *123*(3), 585–595.  
1656 <https://doi.org/10.1093/genetics/123.3.585>
- 1657 Taylor, S. A., & Larson, E. L. (2019). Insights from genomes into the evolutionary  
1658 importance and prevalence of hybridization in nature. *Nature Ecology &*  
1659 *Evolution*, *3*(2), Article 2. <https://doi.org/10.1038/s41559-018-0777-y>
- 1660 Taylor, S. A., Larson, E. L., & Harrison, R. G. (2015). Hybrid zones: Windows on  
1661 climate change. *Trends in Ecology & Evolution*, *30*(7), 398–406.  
1662 <https://doi.org/10.1016/j.tree.2015.04.010>
- 1663 Tóth, G., Gáspári, Z., & Jurka, J. (2000). Microsatellites in Different Eukaryotic  
1664 Genomes: Survey and Analysis. *Genome Research*, *10*(7), 967–981.  
1665 <https://doi.org/10.1101/gr.10.7.967>
- 1666 Turner, T. L., Hahn, M. W., & Nuzhdin, S. V. (2005). Genomic Islands of Speciation in  
1667 *Anopheles gambiae*. *PLoS Biology*, *3*(9), e285.  
1668 <https://doi.org/10.1371/journal.pbio.0030285>
- 1669 Vähä, J.-P., & Primmer, C. R. (2006). Efficiency of model-based Bayesian methods for  
1670 detecting hybrid individuals under different hybridization scenarios and with

1671 different numbers of loci. *Molecular Ecology*, 15(1), 63–72.  
1672 <https://doi.org/10.1111/j.1365-294X.2005.02773.x>

1673 Vernes, K. (2004). Breeding Biology and Seasonal Capture Success of Northern Flying  
1674 Squirrels (*Glaucomys sabrinus*) and Red Squirrels (*Tamiasciurus hudsonicus*) in  
1675 Southern New Brunswick. *Northeastern Naturalist*, 11(2), 123–136.

1676 Vieira, F. G., Fumagalli, M., Albrechtsen, A., & Nielsen, R. (2013). Estimating  
1677 inbreeding coefficients from NGS data: Impact on genotype calling and allele  
1678 frequency estimation. *Genome Research*, 23(11), 1852–1861.  
1679 <https://doi.org/10.1101/gr.157388.113>

1680 Weigl, P. D. (2007). The Northern Flying Squirrel (*Glaucomys sabrinus*): A  
1681 Conservation Challenge. *Journal of Mammalogy*, 88(4), 897–907.  
1682 <https://doi.org/10.1644/06-MAMM-S-333RR.1>

1683 Whitney, K. D., Randell, R. A., & Rieseberg, L. H. (2010). Adaptive introgression of  
1684 abiotic tolerance traits in the sunflower *Helianthus annuus*. *The New Phytologist*,  
1685 187(1), 230–239. <https://doi.org/10.1111/j.1469-8137.2010.03234.x>

1686 Wick, R. R., Schultz, M. B., Zobel, J., & Holt, K. E. (2015). Bandage: Interactive  
1687 visualization of de novo genome assemblies. *Bioinformatics*, 31(20), 3350–3352.  
1688 <https://doi.org/10.1093/bioinformatics/btv383>

1689 Winterrowd, M. F., & Weigl, P. D. (2006). Mechanisms of Cache Retrieval in the Group  
1690 Nesting Southern Flying Squirrel (*Glaucomys volans*). *Ethology*, 112(11), 1136–  
1691 1144. <https://doi.org/10.1111/j.1439-0310.2006.01268.x>

1692 Wolf, J. F., Bowman, J., Keobouasone, S., Taylor, R. S., & Wilson, P. J. (2022). A de  
1693 novo genome assembly and annotation of the southern flying squirrel (*Glaucomys*  
1694 *volans*). *G3 Genes|Genomes|Genetics*, 12(1), jkab373.  
1695 <https://doi.org/10.1093/g3journal/jkab373>

1696 Wright, S. (1965). The Interpretation of Population Structure by F-Statistics with Special  
1697 Regard to Systems of Mating. *Evolution*, 19(3), 395–420.  
1698 <https://doi.org/10.2307/2406450>

1699 Yang, W., Feiner, N., Laakkonen, H., Sacchi, R., Zuffi, M. A. L., Scali, S., While, G. M.,  
1700 & Uller, T. (2020). Spatial variation in gene flow across a hybrid zone reveals

1701 causes of reproductive isolation and asymmetric introgression in wall lizards.  
1702 *Evolution*, 74(7), 1289–1300. <https://doi.org/10.1111/evo.14001>

1703 Zhang, W., Dasmahapatra, K. K., Mallet, J., Moreira, G. R. P., & Kronforst, M. R.  
1704 (2016). Genome-wide introgression among distantly related *Heliconius* butterfly  
1705 species. *Genome Biology*, 17(1), 25. <https://doi.org/10.1186/s13059-016-0889-0>

1706 Zimmerman, S. J., Aldridge, C. L., & Oyler-McCance, S. J. (2020). An empirical  
1707 comparison of population genetic analyses using microsatellite and SNP data for a  
1708 species of conservation concern. *BMC Genomics*, 21(1), 382.  
1709 <https://doi.org/10.1186/s12864-020-06783-9>

1710 Zohren, J., Wang, N., Kardailsky, I., Borrell, J. S., Joecker, A., Nichols, R. A., & Buggs,  
1711 R. J. A. (2016). Unidirectional diploid–tetraploid introgression among British  
1712 birch trees with shifting ranges shown by restriction site-associated markers.  
1713 *Molecular Ecology*, 25(11), 2413–2426. <https://doi.org/10.1111/mec.13644>

1714  
1715  
1716  
1717  
1718  
1719  
1720  
1721  
1722  
1723  
1724  
1725  
1726  
1727



## Appendix

Table S1. Newly generated sequences sample ID, sex, species identification in the field, sample type, site, average mass, and capture dates range for individuals captured since 2017 when sampling effort increased. For site information: CC = Clear Creek (42.52°N,81.62°W), LP = Long Point (42.58°N,80.38°W), KH = Kawartha Highlands (44.68°N,78.33°W), GAN= Ganaraska (44.09°N,78.5°W), TEM= Temagami (47.23°N, 79.77°W), ROSV=Roosevelt (47.26°N, 79.71°W). When individual was captured only as a juvenile it is indicated with sex by "Juv". Missing mass data is indicated by "NA".

Sample ID	Site	Species	Sex	Mass (g)	Capture Dates
OMNR50221	CC	<i>G. volans</i>	F	71	2008
OMNR50291	CC	<i>G. volans</i>	M (Juv)	49	2008
CC3SFS	CC	<i>G. volans</i>	F	NA	2008
210	LP	<i>G. volans</i>	F	81	2000
233	LP	<i>G. volans</i>	F (Juv)	42	2000
234	LP	<i>G. volans</i>	M	78	2000
235	LP	<i>G. volans</i>	F	75	2000
238	LP	<i>G. volans</i>	F (Juv)	39	2000
239	LP	<i>G. volans</i>	M	58	2000
284	LP	<i>G. volans</i>	M	NA	2000
299	LP	<i>G. volans</i>	M	NA	2000
304	LP	<i>G. volans</i>	M	NA	2000
305	LP	<i>G. volans</i>	M	NA	2000
531461	KH	<i>G. volans</i>	F	82	21 Jun 2018
531550	KH	<i>G. volans</i>	M	59.5	13 Aug 2018 - 16 Aug 2021
532315	KH	<i>G. volans</i>	F	67.5	2014
532539	KH	<i>G. volans</i>	F	80	15 Jan 2020 - 15 Aug 2020
532720	KH	<i>G. volans</i>	F (Juv)	43	21 Jun 2018 - 31 Aug 2018
533103	KH	<i>G. volans</i>	F	69	16 Aug 2017 - 2023
533390	KH	<i>G. volans</i>	F	59	5 Nov 2020 - 3 Aug 2021
533580	KH	<i>G. volans</i>	F	59	30 Nov 2017 - 4 Jul 2018
533587	KH	<i>G. volans</i>	F	64	21 Jun 2018
533698	KH	<i>G. volans</i>	M	68	15 Jan 2020 - 9 Sep 2021
534186	KH	<i>G. volans</i>	F	74	20-21 Jun 2018
535236	KH	<i>G. volans</i>	F	62	15 Jan 2020
535250	KH	<i>G. volans</i>	M	67	21 Jun 2018 - 15 Aug 2019
537005	KH	<i>G. volans</i>	M	71	2015 - 2017
538225	KH	<i>G. volans</i>	F	79	2016
539217	KH	<i>G. volans</i>	F	72	22 Jul 2020 - 1 Jun 2021
540567	KH	<i>G. volans</i>	M	73	15 Jan 2020
541502	KH	<i>G. volans</i>	F	NA	28 Nov 2019 - 14 Jan 2020
542373	KH	<i>G. volans</i>	F	65	2015-2016
552209	KH	<i>G. volans</i>	F (Juv)	46	26 Aug 2021
555031	KH	<i>G. volans</i>	F	70	20 Sep 2021 - 14 Dec 2022
556158	KH	<i>G. volans</i>	M	66	27 May 2021 - 30 Jun 2021
560369	KH	<i>G. volans</i>	M	61	29 Mar 2021 - 12 May 2022

560788	KH	<i>G. volans</i>	F	76.5	5 Apr 2022 - 13 Jun 2022
565799	KH	<i>G. volans</i>	M	52	2 Apr 2019
569665	KH	<i>G. volans</i>	F	76	15 - 17 Jan 2020
572082	KH	<i>G. volans</i>	F (Juv)	66	20 Oct 2021
574362	KH	<i>G. volans</i>	F	80	29 Apr 2022
574662	KH	<i>G. volans</i>	M	66	13 May 2021 - 1 Jun 2021
578827	KH	<i>G. volans</i>	M	58.5	29 Sept 2021
579560	KH	<i>G. volans</i>	F	71	2-13 Jun 2022
581550	KH	<i>G. volans</i>	F	66	29 Mar 2022
582663	KH	<i>G. volans</i>	F	61	29 Mar 2021 - 9 Aug 2021
583883	KH	<i>G. volans</i>	F	68.5	18 Oct 2021
584699	KH	<i>G. volans</i>	F	63.5	13-14 Oct 2021
586132	KH	<i>G. volans</i>	F	57	3 Mar 2021 - 17 May 2022
589379	KH	<i>G. volans</i>	M (Juv)	56	3 - 16 Aug 2021
590764	KH	<i>G. volans</i>	M	63	12 Mar 2021 - 20 Oct 2021
602440	KH	<i>G. volans</i>	M	75	29 Mar 2021 - 17 May 2022
625764	KH	<i>G. volans</i>	F	79	29 Mar 2022
630656	KH	<i>G. volans</i>	M (Juv)	46	15 Aug 2019
631380	KH	<i>G. volans</i>	F	60	15 Jan 2020 - 17 Oct 2021
631705	KH	<i>G. volans</i>	M	60.5	2014-2019
633256	KH	<i>G. volans</i>	M	65	2016
633260	KH	<i>G. volans</i>	F	67	15 Jan 2020 - 12 Aug 2021
637495	KH	<i>G. volans</i>	M	63	17 Aug 2017- 20 Jul 2018
639776	KH	<i>G. volans</i>	M (Juv)	38	20 Jun 2018
648702	KH	<i>G. volans</i>	M	103	09 Aug 2022
651297	KH	<i>G. volans</i>	M (Juv)	56	19 Jul 2021 - 15 Aug 2021
654042	KH	<i>G. volans</i>	M	64.5	3 Mar 2021 - 12 May 2022
OMNR26542	KH	<i>G. volans</i>	F	76	4 Apr 2021 - 10 Nov 2021
OMNR26845	KH	<i>G. volans</i>	M	NA	30 Mar 2021
OMNR26861	KH	<i>G. volans</i>	M	72.5	4 Apr 2021 - 9 May 2021
OMNR39640	KH	<i>G. volans</i>	M	69	29 Mar 2021 - 6 May 2022
530105	KH	<i>G. sabrinus</i>	M	90	9 Jan 2020 - 14 May 2021
532634	KH	<i>G. sabrinus</i>	F	98	30 Nov 2017 - 5 Nov 2018
535192	KH	<i>G. sabrinus</i>	M	76	17 Jan 2020 - 2 Dec 2021
538690	KH	<i>G. sabrinus</i>	F	60	2013
545290	KH	<i>G. sabrinus</i>	F	96	17 Jun 2020
551206	KH	<i>G. sabrinus</i>	M	90	23 Nov 2021 - 17 May 2022
552615	KH	<i>G. sabrinus</i>	Unk (Juv)	70	6-10 Jul 2021
560490	KH	<i>G. sabrinus</i>	M	86	16 Apr - 6 May 2021
562600	KH	<i>G. sabrinus</i>	M	99	6 May 2021 - 2 Jun 2022
572078	KH	<i>G. sabrinus</i>	M	128	17 May 2022 - 2 Jun 2022
574107	KH	<i>G. sabrinus</i>	F	96.5	13 Oct 2021 - 12 Apr 2022
575604	KH	<i>G. sabrinus</i>	M	82.5	2015

575682	KH	<i>G. sabrinus</i>	M	92	27 May 2021 - 15 Jun 2021
575816	KH	<i>G. sabrinus</i>	F	113	28 Sept 2022
576711	KH	<i>G. sabrinus</i>	M	102.5	20 Sep 2021 - 21 Dec 2021
579588	KH	<i>G. sabrinus</i>	F	106	7 Aug 2020 - 2 Dec 2021
580102	KH	<i>G. sabrinus</i>	M	95	8 Dec 2020 - 16 May 2022
580961	KH	<i>G. sabrinus</i>	M	87.5	13 Oct 2021 - 25 May 2022
581104	KH	<i>G. sabrinus</i>	F (Juv)	85.5	13 Oct 2021
581612	KH	<i>G. sabrinus</i>	M	85	31 May 2021 - 21 Dec 2021
582841	KH	<i>G. sabrinus</i>	F (Juv)	80	27 Sep 2021 - 2 Dec 2021
583371	KH	<i>G. sabrinus</i>	F (Juv)	74.5	11 Aug 2022
583457	KH	<i>G. sabrinus</i>	F	97	2 Dec 2021 - 12 Apr 2022
583487	KH	<i>G. sabrinus</i>	F (Juv)	73	9 Aug 2022
587567	KH	<i>G. sabrinus</i>	M	96	3-17 Jun 2021
587578	KH	<i>G. sabrinus</i>	M	97	2 Sep 2021 - 14 Dec 2021
588377	KH	<i>G. sabrinus</i>	F (Juv)	NA	23 Jul 2021
589432	KH	<i>G. sabrinus</i>	F	100	25 Nov 2020 - 2 Dec 2021
604241	KH	<i>G. sabrinus</i>	M	100	4 Mar 2021 - 7 May 2021
629630	KH	<i>G. sabrinus</i>	M	75	2014
629698	KH	<i>G. sabrinus</i>	Unk	80	16 Oct 2018
629717	KH	<i>G. sabrinus</i>	F	84	9 Jan 2020 - 28 Sept 2022
630305	KH	<i>G. sabrinus</i>	F	102	2015
630580	KH	<i>G. sabrinus</i>	M	70	14 Aug 2019
649310	KH	<i>G. sabrinus</i>	F (Juv)	74.5	11 Aug 2022
654461	KH	<i>G. sabrinus</i>	M	96	26 Apr 2021
OMNR39684	KH	<i>G. sabrinus</i>	F	106	7 Aug 2020 - 2 Dec 2021
OMNR50273	GAN	<i>G. sabrinus</i>	F (Juv)	54	2008
OMNR50219	TEM	<i>G. sabrinus</i>	F	92	2008
OMNR50224	TEM	<i>G. sabrinus</i>	F	91	2008
OMNR50243	TEM	<i>G. sabrinus</i>	F	98	2008
OMNR50258	TEM	<i>G. sabrinus</i>	M (Juv)	76	2008
OMNR50262	TEM	<i>G. sabrinus</i>	M (Juv)	85	2008
OMNR50276	TEM	<i>G. sabrinus</i>	F	93	2008
OMNR50286	TEM	<i>G. sabrinus</i>	M	88	2008
OMNR50297	TEM	<i>G. sabrinus</i>	M	93	2008
R2	ROSV	<i>G. sabrinus</i>	M	NA	2008
R4	ROSV	<i>G. sabrinus</i>	Unk	NA	2008
R6	ROSV	<i>G. sabrinus</i>	F	NA	2008
R9	ROSV	<i>G. sabrinus</i>	Unk	NA	2008

1729

1730

1731

Table S2. The standard IBD relationships and inference criteria used to infer pairwise relationships.

Relationship	$\phi$	Inference Criteria	$K_0$	Inference Criteria	$K_1$	Inference Criteria	$K_2$	Inference Criteria
<b>Monozygotic-twins</b>	$1/2$	$> \frac{1}{2^{3/2}}$	<b>0</b>	$< 0.1$	<b>0</b>	$< 0.1$	<b>1</b>	$> 1 - \frac{1}{2^{5/2}}$
<b>Parent-offspring</b>	$1/4$	$(\frac{1}{2^{5/2}}, \frac{1}{2^{3/2}})$	<b>0</b>	$< 0.1$	<b>1</b>	$> 1 - \frac{1}{2^{5/2}}$	<b>0</b>	$< 0.1$
<b>Full-Siblings</b>	$1/4$	$(\frac{1}{2^{5/2}}, \frac{1}{2^{3/2}})$	$1/4$	(0.1,0.365)	$1/2$	$(0.365, 1 - \frac{1}{2^{3/2}})$	$1/4$	(0.1,0.365)
<b>Half-siblings</b>	$1/8$	$(\frac{1}{2^{7/2}}, \frac{1}{2^{5/2}})$	$1/2$	$(0.365, 1 - \frac{1}{2^{3/2}})$	$1/2$	$(0.365, 1 - \frac{1}{2^{3/2}})$	<b>0</b>	$< 0.1$
<b>First-Cousins</b>	$1/16$	$(\frac{1}{2^{9/2}}, \frac{1}{2^{7/2}})$	$3/4$	$(1 - \frac{1}{2^{3/2}}, 1 - \frac{1}{2^{5/2}})$	$1/4$	(0.1,0.365)	<b>0</b>	$< 0.1$
<b>Unrelated</b>	<b>0</b>	$< \frac{1}{2^{9/2}}$	<b>1</b>	$> 1 - \frac{1}{2^{5/2}}$	<b>0</b>	$< 0.1$	<b>0</b>	$< 0.1$

Table S3. Summary of quality control results. The percentage of reads mapped and average coverage for each sample ID with sample type indicated. Samples marked in bold were excluded from the analysis due to poor read mapping quality. \*Sample appeared to be mostly blood and had gone through a freeze-thaw. Sites: APP = Algonquin Provincial Park, CC = Clear Creek, GAN = Ganaraska, KH = Kawartha Highlands Signature Site, LP = Long Point, ROSV = Roosevelt, SHLK = Sherborne Lake, TEM = Temagami.

Sample ID	Site	Species	Sample Type	% Reads Mapped	Coverage
50254	APP	<i>G. sabrinus</i>	Tissue (carcass)	99.16%	20.880
CC3SFS	CC	<i>G. volans</i>	Tissue (ear clipping) - extracted in or prior to 2020	99.54%	1.782
CC1	CC	<i>G. volans</i>	Tissue (carcass)	99.45%	16.680
OMNR50221	CC	<i>G. volans</i>	Tissue (ear clipping) - extracted in or prior to 2020	99.58%	1.800
OMNR50291	CC	<i>G. volans</i>	Tissue (ear clipping) - extracted in or prior to 2020	99.16%	1.505
OMNR50273	GAN	<i>G. sabrinus</i>	Tissue (ear clipping) - extracted in or prior to 2020	99.43%	1.533
6525	KH	<i>G. sabrinus</i>	Tissue (carcass)	99.25%	17.330
530105	KH	<i>G. sabrinus</i>	Tissue (ear clipping) - extracted in or prior to 2020	99.32%	2.039
532634	KH	<i>G. sabrinus</i>	Tissue (ear clipping) - extracted in or prior to 2020	99.30%	1.724
535192	KH	<i>G. sabrinus</i>	Tissue (ear clipping) - extracted in or prior to 2020	99.34%	1.707
538690	KH	<i>G. sabrinus</i>	Tissue (ear clipping)	99.42%	1.983
545290	KH	<i>G. sabrinus</i>	Tissue (ear clipping) - extracted in or prior to 2020	99.41%	1.429
551206	KH	<i>G. sabrinus</i>	Tissue (ear clipping)	99.42%	2.563
552615	KH	<i>G. sabrinus</i>	Tissue (ear clipping)	99.51%	1.884
<b>560490</b>	<b>KH</b>	<b><i>G. sabrinus</i></b>	<b>Tissue (ear clipping)</b>	<b>15.03%</b>	
562600	KH	<i>G. sabrinus</i>	Tissue (ear clipping)	98.96%	1.688
572078	KH	<i>G. sabrinus</i>	Tissue (ear clipping)	99.40%	7.292
574107	KH	<i>G. sabrinus</i>	Tissue (ear clipping)	99.48%	2.553
575604	KH	<i>G. sabrinus</i>	Tissue (ear clipping)	99.15%	2.128

575682	KH	<i>G. sabrinus</i>	Tissue (ear clipping)	99.33%	2.271
575816	KH	<i>G. sabrinus</i>	Tissue (ear clipping)	99.48%	1.748
576711	KH	<i>G. sabrinus</i>	Tissue (ear clipping)	99.32%	1.583
579588	KH	<i>G. sabrinus</i>	Tissue (ear clipping)	98.57%	1.847
580102	KH	<i>G. sabrinus</i>	Tissue (ear clipping)	99.35%	1.758
580961	KH	<i>G. sabrinus</i>	Tissue (ear clipping)	99.17%	1.619
581104	KH	<i>G. sabrinus</i>	Tissue (ear clipping)	99.41%	1.365
581612	KH	<i>G. sabrinus</i>	Tissue (ear clipping)	98.99%	1.550
582841	KH	<i>G. sabrinus</i>	Tissue (ear clipping)	99.48%	2.588
583371	KH	<i>G. sabrinus</i>	Tissue (ear clipping)	99.50%	1.578
583457	KH	<i>G. sabrinus</i>	Tissue (ear clipping)	96.26%	1.429
583487	KH	<i>G. sabrinus</i>	Tissue (ear clipping)	99.51%	1.414
587567	KH	<i>G. sabrinus</i>	Tissue (ear clipping)	99.44%	1.811
587578	KH	<i>G. sabrinus</i>	Tissue (ear clipping)	99.43%	1.535
588377	KH	<i>G. sabrinus</i>	Tissue (ear clipping)	99.52%	2.186
589432	KH	<i>G. sabrinus</i>	Tissue (ear clipping)	98.72%	1.816
604241	KH	<i>G. sabrinus</i>	Tissue (ear clipping)	99.30%	22.850
629630	KH	<i>G. sabrinus</i>	Tissue (ear clipping)	99.16%	2.305
629698	KH	<i>G. sabrinus</i>	Tissue (ear clipping) - extracted in or prior to 2020	95.82%	1.247
629717	KH	<i>G. sabrinus</i>	Tissue (ear clipping) - extracted in or prior to 2020	99.40%	1.516
630305	KH	<i>G. sabrinus</i>	Tissue (ear clipping)	98.98%	4.623
630580	KH	<i>G. sabrinus</i>	Tissue (ear clipping) - extracted in or prior to 2020	99.39%	1.258
649310	KH	<i>G. sabrinus</i>	Tissue (ear clipping)	99.45%	2.482
654461	KH	<i>G. sabrinus</i>	Tissue (ear clipping)	99.40%	1.627
OMNR39684	KH	<i>G. sabrinus</i>	Tissue (ear clipping)	99.28%	1.347
531461	KH	<i>G. volans</i>	Tissue (ear clipping) - extracted in or prior to 2020	97.31%	1.516
531550	KH	<i>G. volans</i>	Tissue (ear clipping) - extracted in or prior to 2020	98.02%	1.428
<b>532315</b>	<b>KH</b>	<b><i>G. volans</i></b>	<b>Tissue (ear clipping) - extracted in or prior to 2020*</b>	<b>4.25%</b>	
532539	KH	<i>G. volans</i>	Tissue (ear clipping)	99.53%	1.367
532720	KH	<i>G. volans</i>	Tissue (ear clipping) - extracted in or prior to 2020	99.32%	3.460
533103	KH	<i>G. volans</i>	Tissue (ear clipping)	99.57%	4.442
533390	KH	<i>G. volans</i>	Tissue (ear clipping)	99.54%	1.846
533580	KH	<i>G. volans</i>	Tissue (ear clipping)	99.45%	2.222
533587	KH	<i>G. volans</i>	Tissue (ear clipping) - extracted in or prior to 2020	94.86%	1.710
533698	KH	<i>G. volans</i>	Tissue (ear clipping) - extracted in or prior to 2020	99.57%	1.401
534186	KH	<i>G. volans</i>	Tissue (ear clipping)	98.08%	1.652
535236	KH	<i>G. volans</i>	Tissue (ear clipping) - extracted in or prior to 2020	99.56%	1.714
535250	KH	<i>G. volans</i>	Tissue (ear clipping)	99.47%	2.061
537005	KH	<i>G. volans</i>	Tissue (ear clipping)	99.50%	1.520
538225	KH	<i>G. volans</i>	Tissue (ear clipping)	99.52%	2.655
539217	KH	<i>G. volans</i>	Tissue (ear clipping) - extracted in or prior to 2020	99.56%	1.610
540567	KH	<i>G. volans</i>	Tissue (ear clipping) - extracted in or prior to 2020	99.44%	1.507
541502	KH	<i>G. volans</i>	Tissue (ear clipping)	99.56%	1.597

542373	KH	<i>G. volans</i>	Tissue (ear clipping)	99.47%	1.773
552209	KH	<i>G. volans</i>	Tissue (ear clipping)	99.50%	1.554
555031	KH	<i>G. volans</i>	Tissue (ear clipping)	99.57%	1.758
556158	KH	<i>G. volans</i>	Tissue (ear clipping)	99.46%	1.513
560369	KH	<i>G. volans</i>	Tissue (ear clipping)	99.52%	1.613
560788	KH	<i>G. volans</i>	Tissue (ear clipping)	99.60%	1.593
565799	KH	<i>G. volans</i>	Tissue (ear clipping) - extracted in or prior to 2020	99.12%	1.521
569665	KH	<i>G. volans</i>	Tissue (ear clipping)	99.57%	1.624
572082	KH	<i>G. volans</i>	Tissue (ear clipping)	99.46%	1.059
574362	KH	<i>G. volans</i>	Tissue (ear clipping)	98.96%	1.637
574662	KH	<i>G. volans</i>	Tissue (ear clipping)	99.42%	1.639
578827	KH	<i>G. volans</i>	Tissue (ear clipping)	99.52%	1.491
579560	KH	<i>G. volans</i>	Tissue (ear clipping)	99.52%	1.545
581550	KH	<i>G. volans</i>	Tissue (ear clipping)	99.55%	1.860
582663	KH	<i>G. volans</i>	Tissue (ear clipping)	98.88%	1.690
583883	KH	<i>G. volans</i>	Tissue (ear clipping)	99.56%	1.647
584699	KH	<i>G. volans</i>	Tissue (ear clipping)	99.45%	1.423
586132	KH	<i>G. volans</i>	Tissue (ear clipping)	99.54%	1.730
589379	KH	<i>G. volans</i>	Tissue (ear clipping)	99.54%	1.647
590764	KH	<i>G. volans</i>	Tissue (ear clipping)	99.52%	1.619
602440	KH	<i>G. volans</i>	Tissue (ear clipping)	99.52%	1.611
625764	KH	<i>G. volans</i>	Tissue (ear clipping)	99.62%	1.750
630656	KH	<i>G. volans</i>	Tissue (ear clipping) - extracted in or prior to 2020	99.49%	1.595
631380	KH	<i>G. volans</i>	Tissue (ear clipping) - extracted in or prior to 2020	99.49%	1.658
631705	KH	<i>G. volans</i>	Tissue (ear clipping)	99.43%	1.595
633256	KH	<i>G. volans</i>	Tissue (ear clipping)	99.43%	1.692
633260	KH	<i>G. volans</i>	Tissue (ear clipping) - extracted in or prior to 2020	99.57%	1.489
637495	KH	<i>G. volans</i>	Tissue (ear clipping)	99.39%	1.307
639776	KH	<i>G. volans</i>	Tissue (ear clipping) - extracted in or prior to 2020	99.49%	2.016
648702	KH	<i>G. volans</i>	Tissue (ear clipping)	99.49%	1.416
651297	KH	<i>G. volans</i>	Tissue (ear clipping)	99.21%	0.736
654042	KH	<i>G. volans</i>	Tissue (ear clipping)	99.48%	1.519
OMNR26542	KH	<i>G. volans</i>	Tissue (ear clipping)	99.57%	1.463
OMNR26845	KH	<i>G. volans</i>	Tissue (ear clipping)	99.52%	1.316
OMNR26861	KH	<i>G. volans</i>	Tissue (ear clipping)	99.53%	1.524
OMNR39640	KH	<i>G. volans</i>	Tissue (ear clipping)	99.51%	1.360
210	LP	<i>G. volans</i>	Hair	95.46%	1.438
233	LP	<i>G. volans</i>	Hair	95.59%	1.333
234	LP	<i>G. volans</i>	Hair	94.79%	1.513
235	LP	<i>G. volans</i>	Hair	95.36%	1.499
238	LP	<i>G. volans</i>	Hair	93.33%	1.444
<b>239</b>	<b>LP</b>	<b><i>G. volans</i></b>	<b>Hair</b>	<b>62.49%</b>	
<b>284</b>	<b>LP</b>	<b><i>G. volans</i></b>	<b>Hair</b>	<b>62.30%</b>	

<b>299</b>	<b>LP</b>	<i>G. volans</i>	<b>Hair</b>	<b>71.96%</b>	
304	LP	<i>G. volans</i>	Hair	86.81%	1.155
<b>305</b>	<b>LP</b>	<i>G. volans</i>	<b>Hair</b>	<b>58.02%</b>	
R2	ROSV	<i>G. sabrinus</i>	Tissue (carcass)	99.45%	1.419
<b>R4</b>	<b>ROSV</b>	<i>G. sabrinus</i>	<b>Tissue (carcass)</b>	<b>80.81%</b>	
R6	ROSV	<i>G. sabrinus</i>	Tissue (carcass)	99.53%	1.496
R9	ROSV	<i>G. sabrinus</i>	Tissue (carcass)	99.44%	1.616
25428	SHLK	<i>G. volans</i>	Tissue (carcass)	99.31%	19.020
OMNR50219	TEM	<i>G. sabrinus</i>	Tissue (ear clipping) - extracted in or prior to 2020	99.44%	1.637
OMNR50224	TEM	<i>G. sabrinus</i>	Tissue (ear clipping) - extracted in or prior to 2020	99.39%	1.550
OMNR50243	TEM	<i>G. sabrinus</i>	Tissue (ear clipping) - extracted in or prior to 2020	99.32%	1.643
OMNR50258	TEM	<i>G. sabrinus</i>	Tissue (ear clipping) - extracted in or prior to 2020	99.18%	1.614
OMNR50262	TEM	<i>G. sabrinus</i>	Tissue (ear clipping) - extracted in or prior to 2020	99.33%	1.637
OMNR50276	TEM	<i>G. sabrinus</i>	Tissue (ear clipping) - extracted in or prior to 2020	99.39%	1.717
OMNR50286	TEM	<i>G. sabrinus</i>	Tissue (ear clipping) - extracted in or prior to 2020	99.37%	1.305
OMNR50297	TEM	<i>G. sabrinus</i>	Tissue (ear clipping) - extracted in or prior to 2020	99.16%	1.653

1733

1734 *Table S4. Inferred potential relationships in G. volans and G. sabrinus. Bolded values indicate the*  
1735 *coefficients used to infer degree of relatedness.*

<i>Glaucomys volans</i>						
Individual a	Individual b	$\phi$	$K_0$	$K_1$	$K_2$	Potential Relationship
<b>KH</b>						
538225	631705	<b>0.062</b>	0.825	0.102	0.073	Third Degree
533580	639776	0.064	<b>0.803</b>	<b>0.137</b>	<b>0.060</b>	First-Cousins
631705	633260	0.074	<b>0.785</b>	<b>0.133</b>	<b>0.082</b>	First-Cousins
534186	586132	0.083	<b>0.763</b>	<b>0.144</b>	<b>0.093</b>	First-Cousins
569665	OMNR26542	0.100	<b>0.696</b>	<b>0.208</b>	<b>0.096</b>	First-Cousins
533587	572082	0.102	<b>0.693</b>	<b>0.207</b>	<b>0.100</b>	First-Cousins
533587	578827	0.103	<b>0.676</b>	<b>0.235</b>	<b>0.089</b>	First-Cousins
533390	540567	0.106	<b>0.653</b>	<b>0.269</b>	<b>0.077</b>	First-Cousins
534186	540567	0.111	<b>0.635</b>	<b>0.286</b>	<b>0.079</b>	First-Cousins
552209	OMNR26542	<b>0.114</b>	0.650	0.245	0.105	Second Degree
572082	631380	<b>0.119</b>	<b>0.622</b>	0.281	0.097	Second Degree
582663	637495	0.133	<b>0.544</b>	<b>0.378</b>	<b>0.078</b>	Half-Siblings
533390	533580	0.175	<b>0.367</b>	<b>0.564</b>	<b>0.069</b>	Half-Siblings
572082	578827	<b>0.203</b>	0.431	0.324	0.245	First Degree
533390	OMNR39640	<b>0.209</b>	<b>0.235</b>	0.695	0.070	First-Degree
533103	639776	<b>0.210</b>	<b>0.202</b>	0.755	0.044	First-Degree
531550	625764	<b>0.211</b>	<b>0.228</b>	0.699	0.072	First-Degree
531550	560788	<b>0.211</b>	<b>0.230</b>	0.696	0.074	First-Degree
540567	OMNR39640	0.212	<b>0.255</b>	<b>0.643</b>	<b>0.102</b>	Full Siblings
602440	630656	<b>0.213</b>	<b>0.246</b>	0.654	0.100	First-Degree
586132	OMNR26542	<b>0.213</b>	<b>0.216</b>	0.713	0.070	First-Degree
631705	639776	<b>0.214</b>	<b>0.220</b>	0.706	0.074	First-Degree
578827	631380	<b>0.214</b>	<b>0.212</b>	0.719	0.069	First-Degree

---

---

*Glaucomys volans*

---

---

Individual a	Individual b	$\Phi$	K <sub>0</sub>	K <sub>1</sub>	K <sub>2</sub>	Potential Relationship
533103	533390	<b>0.215</b>	<b>0.205</b>	0.730	0.065	First-Degree
552209	586132	<b>0.215</b>	<b>0.214</b>	0.711	0.075	First-Degree
534186	OMNR26542	<b>0.216</b>	<b>0.227</b>	0.682	0.090	First-Degree
534186	569665	<b>0.218</b>	<b>0.216</b>	0.697	0.087	First-Degree
532539	630656	<b>0.218</b>	<b>0.212</b>	0.704	0.084	First-Degree
533103	533580	<b>0.222</b>	<b>0.175</b>	0.761	0.064	First-Degree
539217	582663	<b>0.229</b>	<b>0.150</b>	0.785	0.066	First-Degree
574362	583883	<b>0.445</b>	<b>0.000</b>	0.222	0.778	Monozygotic Twins
581550	583883	<b>0.446</b>	<b>0.000</b>	0.214	0.786	Monozygotic Twins
574362	581550	<b>0.446</b>	<b>0.000</b>	0.216	0.783	Monozygotic Twins
560788	625764	<b>0.449</b>	<b>0.000</b>	0.203	0.797	Monozygotic Twins
<b>CC</b>						
OMNR50221	OMNR50291	<b>0.244</b>	<b>0.110</b>	0.802	0.087	First-Degree

---

1736

---

---

*Glaucomys sabrinus*

---

---

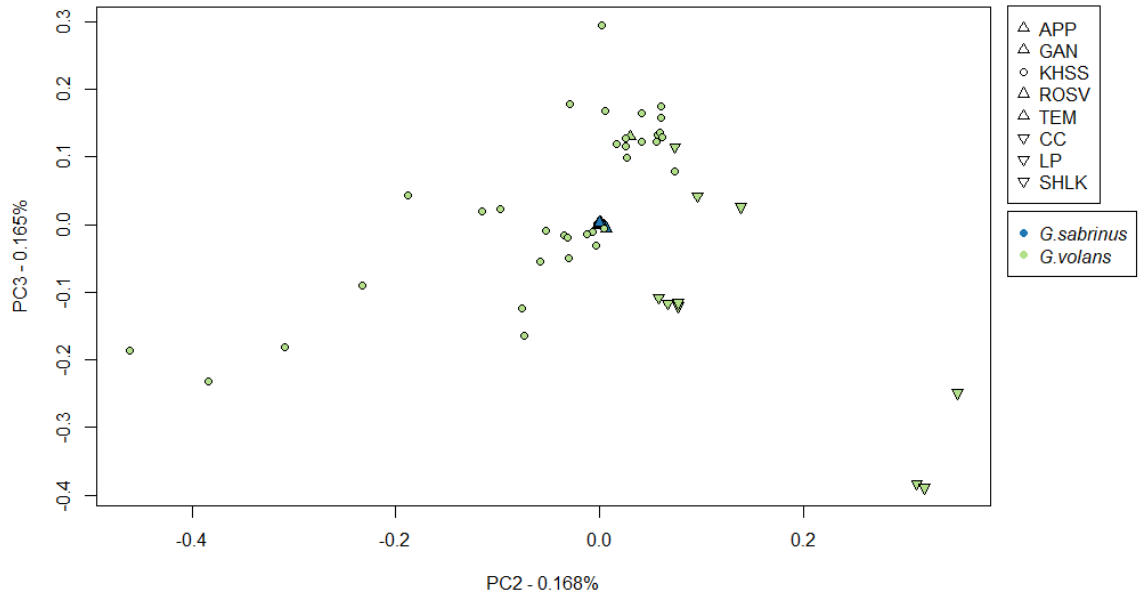
Individual a	Individual b	$\Phi$	K <sub>0</sub>	K <sub>1</sub>	K <sub>2</sub>	Potential Relationship
<b>KH</b>						
532634	583487	<b>0.055</b>	0.890	0.000	0.110	Third Degree
629717	630580	<b>0.055</b>	0.889	0.000	0.111	Third Degree
580102	629717	<b>0.057</b>	0.887	0.000	0.113	Third Degree
532720	583487	<b>0.057</b>	0.886	0.000	0.114	Third Degree
575816	583371	<b>0.059</b>	0.882	0.000	0.118	Third Degree
530105	629717	<b>0.060</b>	0.880	0.000	0.120	Third Degree
582841	630305	<b>0.060</b>	0.880	0.000	0.120	Third Degree
583371	649310	<b>0.060</b>	0.879	0.000	0.121	Third Degree
552615	604241	<b>0.062</b>	0.876	0.000	0.124	Third Degree
532634	582841	<b>0.063</b>	0.874	0.000	0.126	Third Degree
588377	604241	<b>0.064</b>	0.872	0.000	0.128	Third Degree
579588	589432	<b>0.064</b>	0.872	0.000	0.128	Third Degree
532720	582841	<b>0.065</b>	0.869	0.000	0.131	Third Degree
579588	581612	<b>0.067</b>	0.866	0.000	0.134	Third Degree
530105	580102	<b>0.069</b>	0.861	0.000	0.139	Third Degree
545290	574107	<b>0.071</b>	0.859	0.000	0.141	Third Degree
575816	583487	<b>0.072</b>	0.856	0.000	0.144	Third Degree
583487	649310	<b>0.073</b>	0.853	0.000	0.146	Third Degree
552615	587578	<b>0.081</b>	0.839	0.000	0.161	Third Degree
587578	588377	<b>0.082</b>	0.835	0.000	0.164	Third Degree
530105	579588	<b>0.084</b>	0.833	0.000	0.167	Third Degree
581612	589432	<b>0.086</b>	0.828	0.000	0.172	Third Degree
630305	OMNR39684	<b>0.100</b>	0.799	0.001	0.201	Second Degree
545290	575682	<b>0.111</b>	0.746	0.064	0.190	Second Degree
583487	629717	<b>0.137</b>	0.674	0.103	0.222	Second Degree
532634	629717	<b>0.139</b>	0.669	0.108	0.223	Second Degree

---



*Glaucomys sabrinus*

Individual a	Individual b	$\Phi$	$K_0$	$K_1$	$K_2$	Potential Relationship
579588	629717	<b>0.139</b>	0.653	0.139	0.208	Second Degree
532720	629717	<b>0.144</b>	0.647	0.132	0.221	Second Degree
589432	629717	<b>0.146</b>	<b>0.616</b>	0.181	0.202	Second Degree
552615	579588	<b>0.148</b>	<b>0.602</b>	0.205	0.192	Second Degree
581612	629717	<b>0.149</b>	<b>0.616</b>	0.172	0.212	Second Degree
579588	588377	<b>0.151</b>	<b>0.582</b>	0.232	0.186	Second Degree
581612	630580	<b>0.155</b>	0.676	0.029	0.296	Second Degree
530105	532634	<b>0.157</b>	<b>0.581</b>	0.211	0.208	Second Degree
580961	583487	<b>0.158</b>	<b>0.558</b>	0.253	0.188	Second Degree
532634	580102	<b>0.160</b>	<b>0.576</b>	0.208	0.217	Second Degree
532720	530105	<b>0.161</b>	<b>0.561</b>	0.233	0.206	Second Degree
532720	580102	<b>0.165</b>	<b>0.558</b>	0.225	0.217	Second Degree
579588	604241	<b>0.165</b>	<b>0.501</b>	0.336	0.163	Second Degree
562600	589432	<b>0.168</b>	<b>0.523</b>	0.283	0.194	Second Degree
530105	604241	<b>0.169</b>	<b>0.486</b>	0.354	0.161	Second Degree
552615	572078	<b>0.171</b>	<b>0.502</b>	0.312	0.187	Second Degree
575816	583457	<b>0.171</b>	<b>0.542</b>	0.231	0.228	Second Degree
575816	580961	<b>0.172</b>	<b>0.504</b>	0.306	0.191	Second Degree
572078	588377	<b>0.175</b>	<b>0.480</b>	0.338	0.182	Second Degree
574107	575682	0.202	<b>0.350</b>	<b>0.492</b>	<b>0.158</b>	Full Siblings
580102	582841	<b>0.178</b>	0.455	0.380	0.165	First Degree
580961	649310	<b>0.179</b>	0.455	0.374	0.171	First Degree
583457	649310	<b>0.179</b>	0.489	0.307	0.205	First Degree
583371	583457	<b>0.181</b>	0.499	0.277	0.224	First Degree
582841	OMNR39684	<b>0.186</b>	0.426	0.405	0.168	First Degree
572078	587578	<b>0.186</b>	0.460	0.334	0.206	First Degree
538690	6525	<b>0.192</b>	0.420	0.392	0.188	First Degree
532720	532634	<b>0.369</b>	<b>0.058</b>	0.408	0.534	Monozyotic Twin
552615	588377	<b>0.370</b>	<b>0.046</b>	0.427	0.527	Monozyotic Twin
575816	649310	<b>0.383</b>	<b>0.008</b>	0.452	0.539	Monozyotic Twin
<b>TEM</b>						
OMNR50219	OMNR50262	<b>0.184</b>	0.541	0.179	0.279	First Degree
OMNR50243	OMNR50297	<b>0.178</b>	0.586	0.116	0.298	First Degree



1737

Figure S1. Additional Principal Component Analysis (PCA) axes 2vs3 of all unrelated individuals of *G. sabrinus* and *G. volans* (N=68)

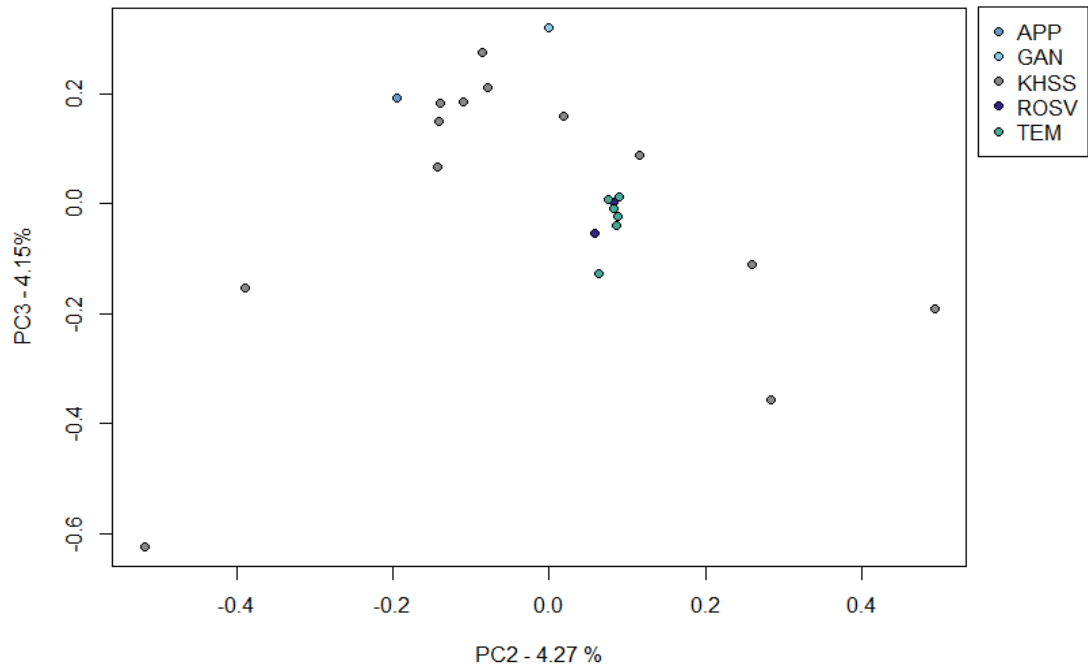


Figure S2. Additional Principal Component Analysis (PCA) axes 2vs3 of all unrelated individuals of *G. sabrinus* (N=23).

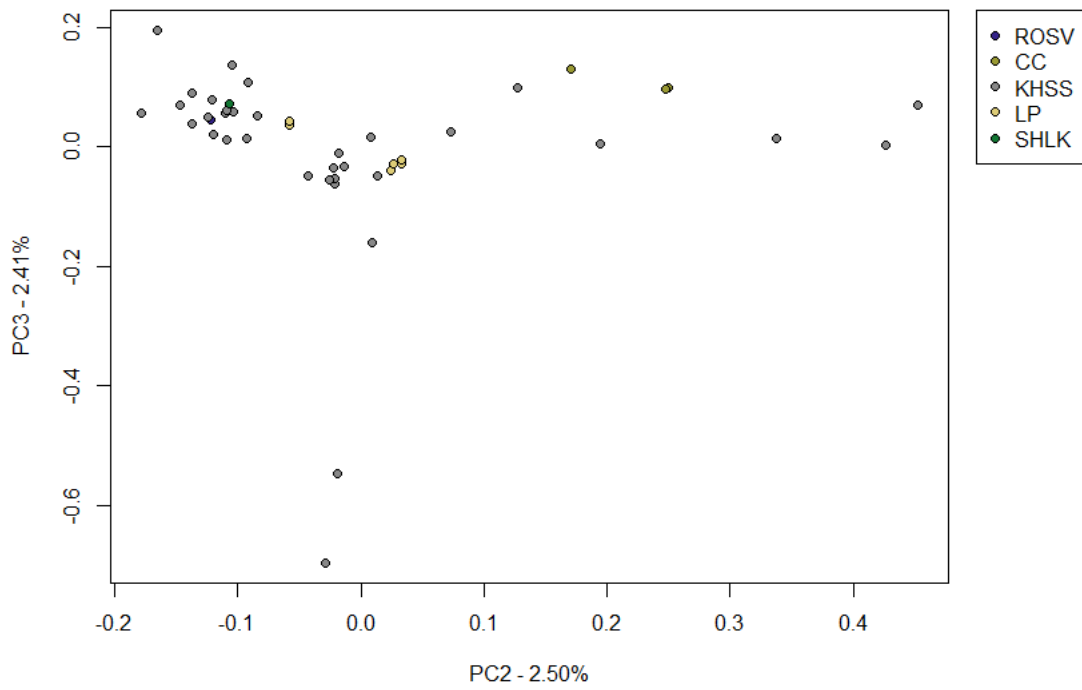


Figure S3. Additional Principal Component Analysis (PCA) axes 2vs3 of all unrelated individuals of *G. volans* (N=45).

1739

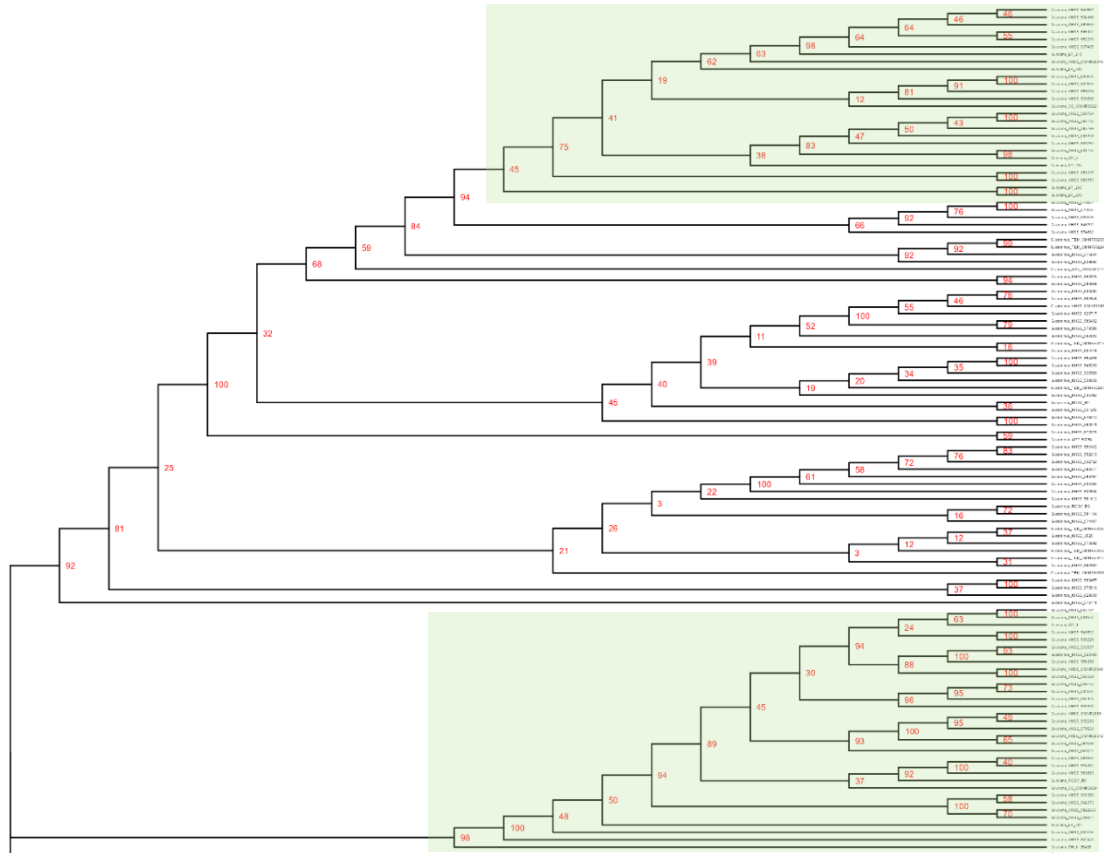
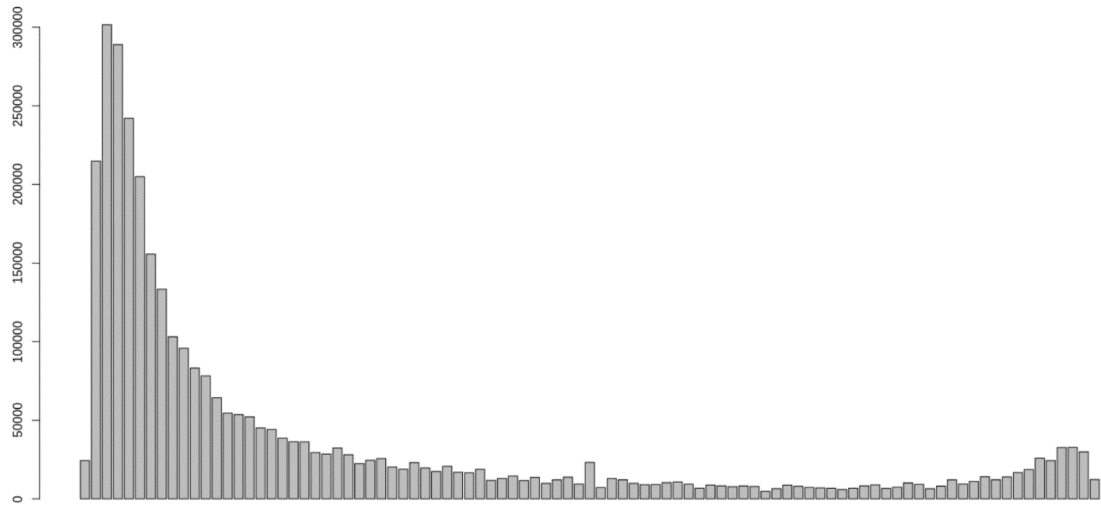
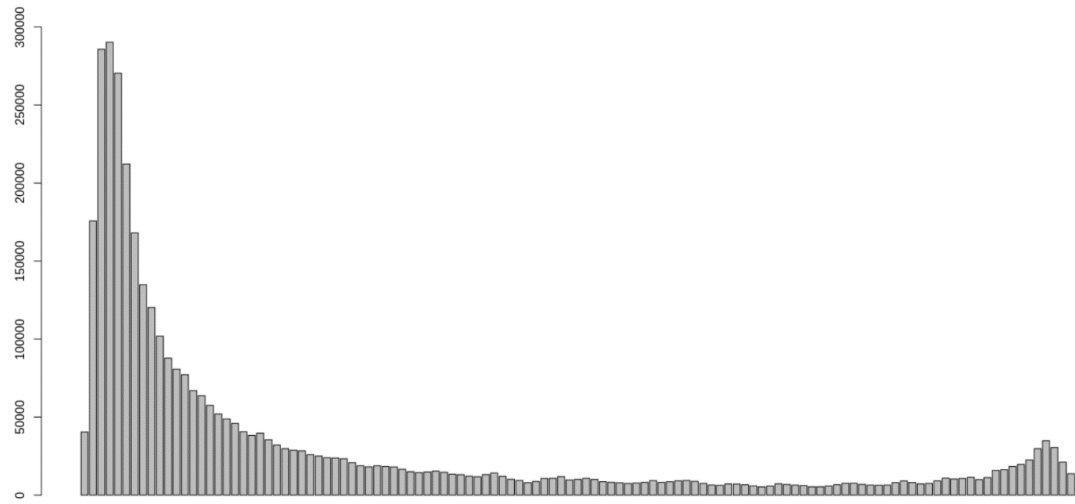


Figure S4. Phylogenetic tree of mitogenomes assembled using GetOrganelle. Red values indicate the confidence interval of a node from 1000 iterations in IQtree, representing the uncertainty associated with the estimated branching point. Green coloring correspond to species clustering of *G. volans*; uncolored branches in the phylogenetic tree center are *G. sabrinus*.



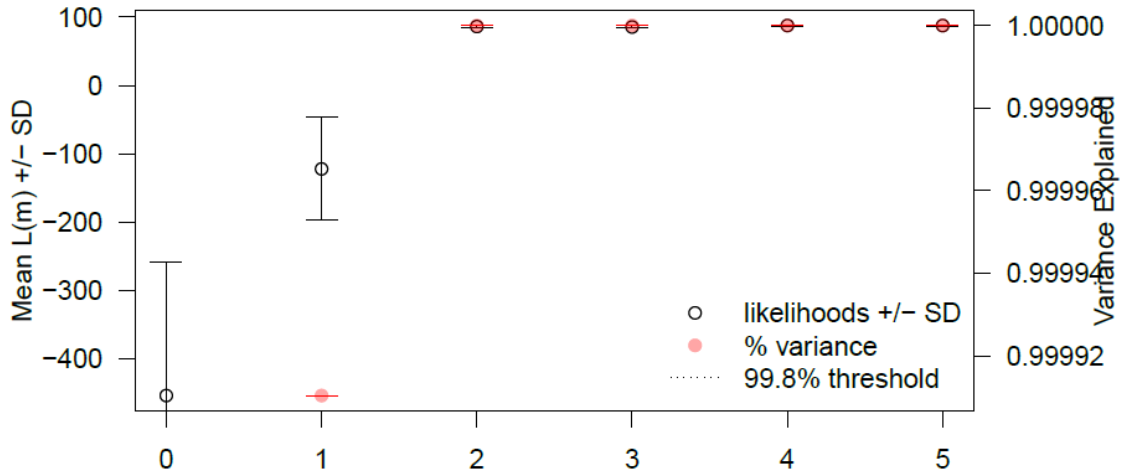
1740



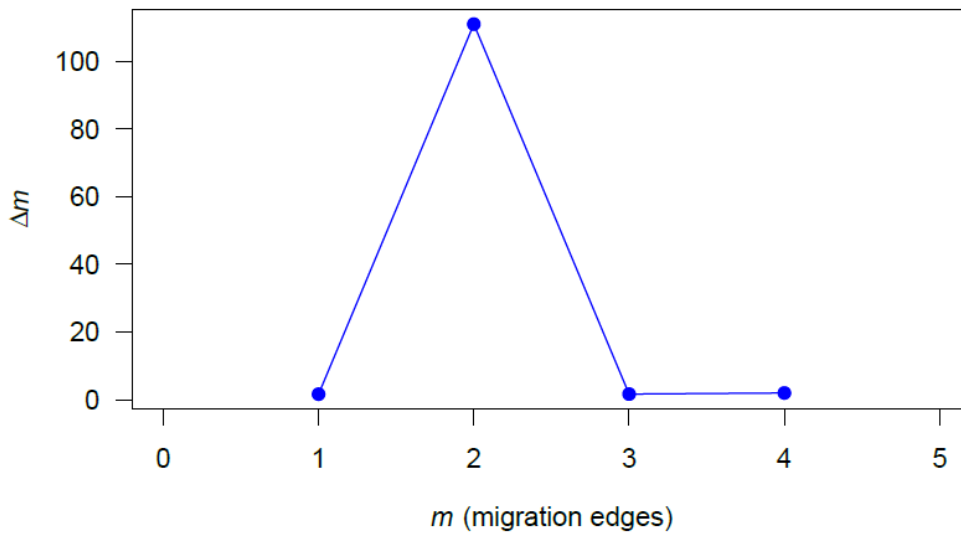
1741

1742 *Figure S5. The 1D-SFS for G. sabrinus (top; N=48) and G. volans (bottom; N=60). The x-axis represents*  
 1743 *the derived allele frequency, while the y-axis indicates the counts of SNPs.*

1744 **A)**



**B)**

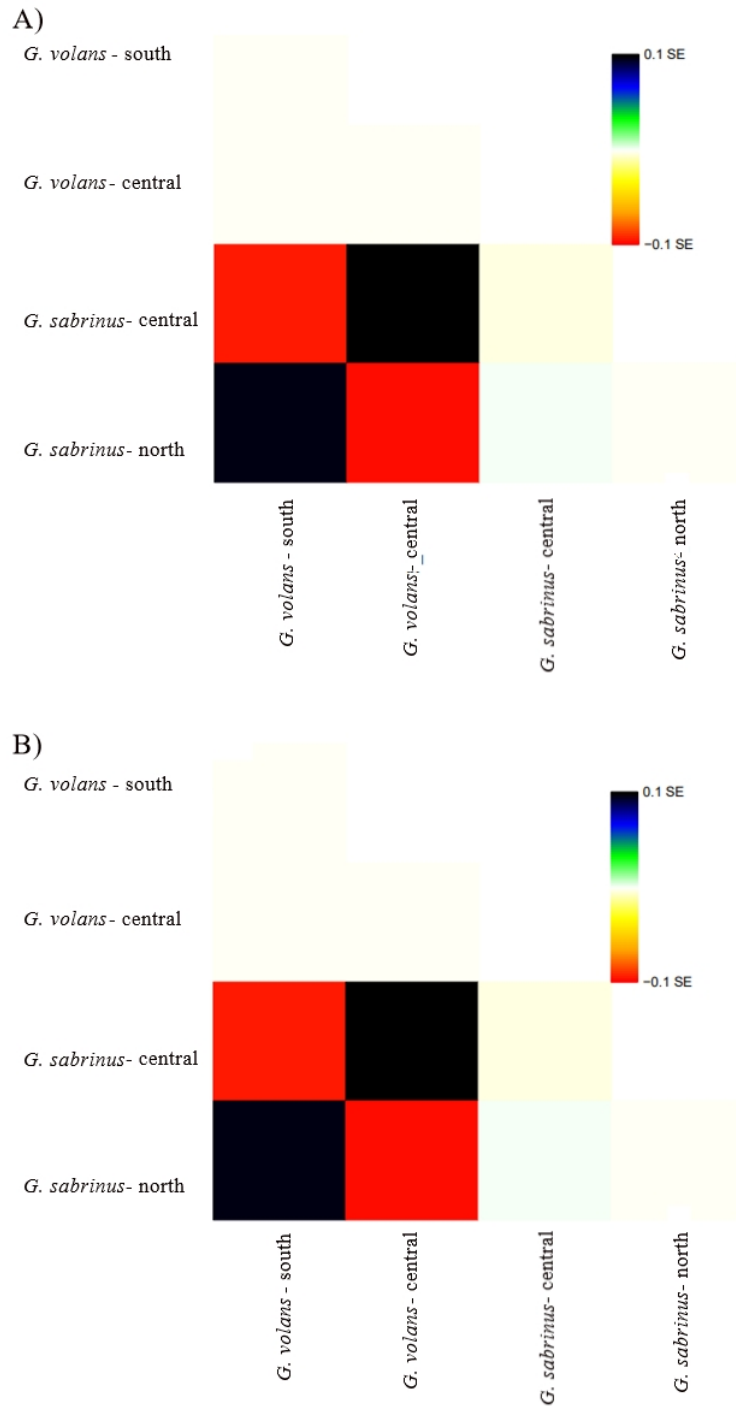


1745

1746 *Figure S6. Comparison of Treemix migration models. We performed 10 iterations at k-values of 500, 1000,*  
1747 *and 2000 for each migration model (m=0-5). The likelihood and SD values (A) and comparison of  $\Delta m$*   
1748 *values (B) indicate the model with 2 migrations has the best support.*

1749

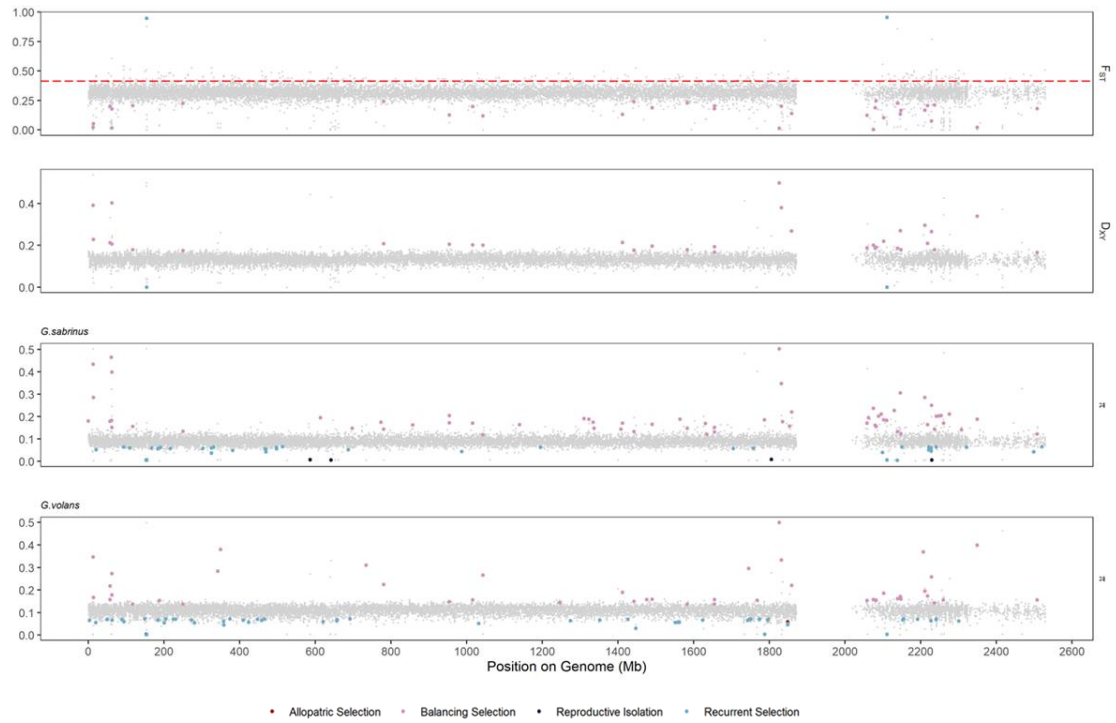
1750



1751

Figure S7. Plotted residual fit for the maximum likelihood trees of the Treemix migration model ( $m=2$ ,  $k=500$ ). Positive (black) residuals indicate an underestimation of the observed covariance between population pairs and that the populations are more closely related to each other than in the best-fit tree and can be candidates for admixture events. Negative (red) residuals indicate an overestimation.

1752



1753

Figure S8. Genomic scans display patterns of selection using a 100kb window and 50kb step size for nucleotide differentiation ( $F_{ST}$ ) and divergence ( $D_{XY}$ ) between northern flying squirrels (*G. sabrinus*) and southern flying squirrels (*G. volans*), along with nucleotide diversity ( $\pi$ ) in *G. sabrinus* and *G. volans*. The red dashed line represents the 95% quartile for the fixation index ( $F_{ST}$ ).

1754

1755

1756

1757

1758

1759

1760

1761

1762



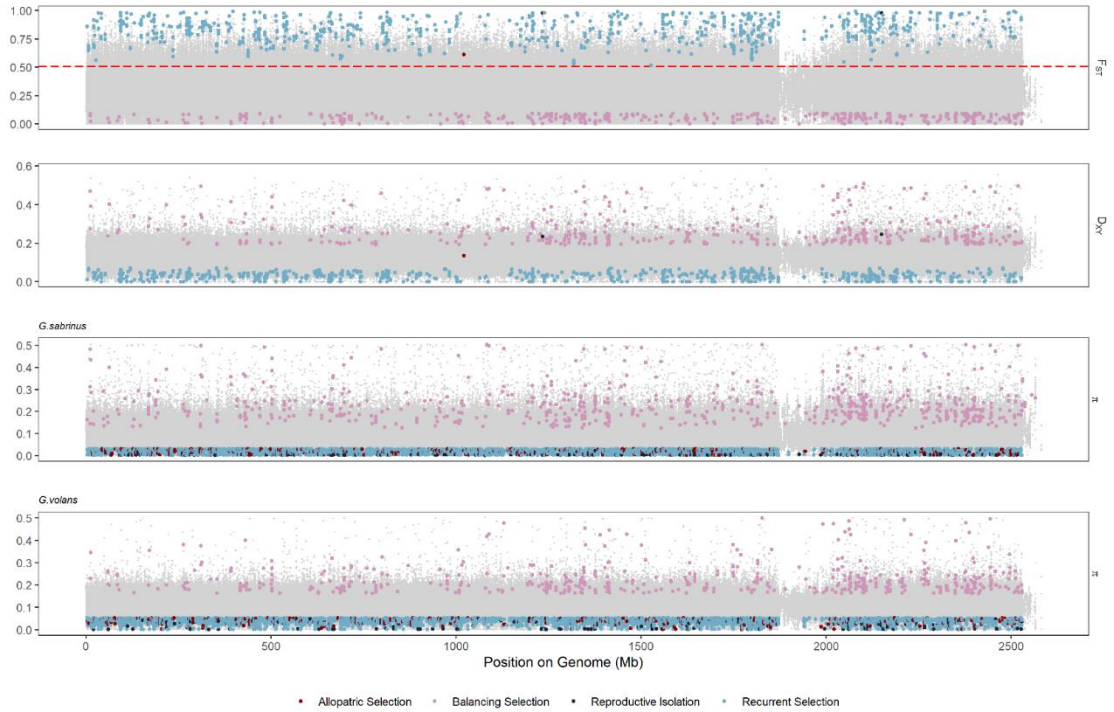


Figure S9. Genomic scans display patterns of selection using a 10kb window and 1kb step size for nucleotide differentiation ( $F_{ST}$ ) and divergence ( $D_{XY}$ ) between northern flying squirrels (*G. sabrinus*) and southern flying squirrels (*G. volans*), along with nucleotide diversity ( $\pi$ ) in *G. sabrinus* and *G. volans*. The red dashed line represents the 95% quartile for the fixation index ( $F_{ST}$ ).

1763

1764

1765

1766

1767

1768

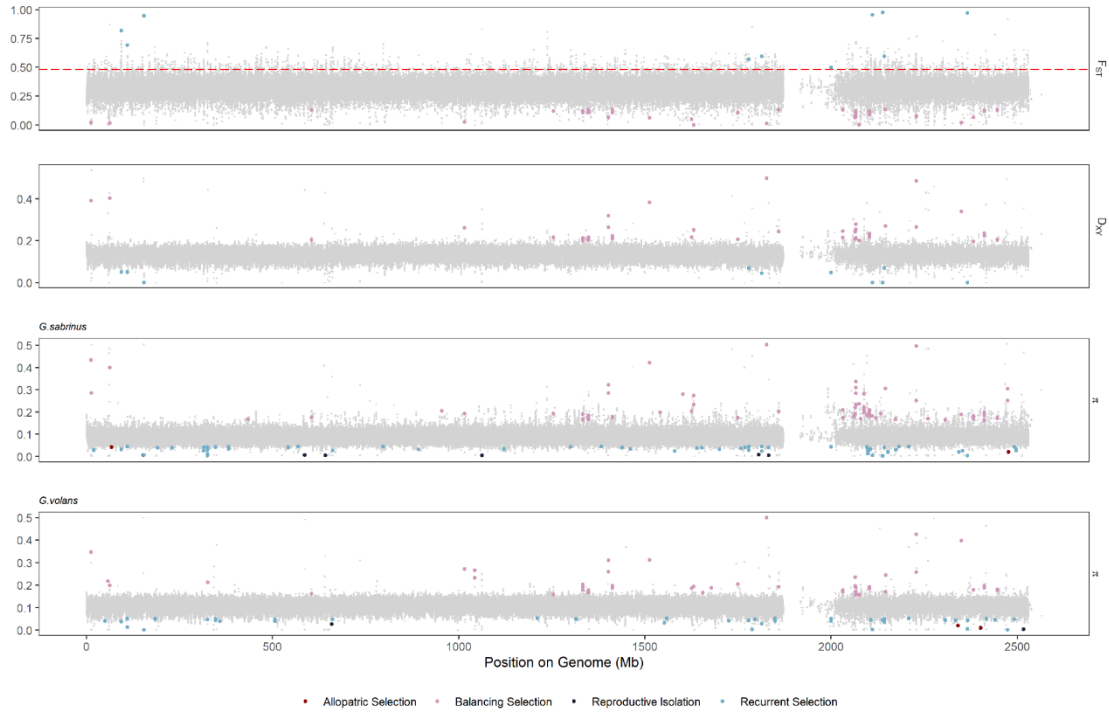


Figure S10. Genomic scans display patterns of selection using a 50kb window and 10kb step size for nucleotide differentiation ( $F_{ST}$ ) and divergence ( $D_{XY}$ ) between northern flying squirrels (*G. sabrinus*) and southern flying squirrels (*G. volans*), along with nucleotide diversity ( $\pi$ ) in *G. sabrinus* and *G. volans*. The red dashed line represents the 99% quartile for the fixation index ( $F_{ST}$ ).

1769